

**Master Thesis in Geodynamics**

**Seismotectonics in Central Sudan and Local Site Effects  
in Western Khartoum**



**Alrasheed Warage**

**Department of Earth Science  
University of Bergen, Norway**

**March, 2008**



# Table of content

Abstract.....	5
1 Introduction .....	7
1.1 Background.....	9
1.1.1 Previous seismological studies in central Sudan .....	9
1.1.2 Topography of the study area .....	10
1.2 The present study and its objectives.....	10
1.3 Seismicity.....	11
1.3.1 Regional seismicity.....	11
1.3.2 Local seismicity .....	12
1.4 Tectonics and stress conditions .....	14
1.5 Geology of Central Sudan.....	19
1.5.1 Regional geology of the Central Sudan .....	19
1.5.2 Local geology of the area around Khartoum .....	21
1.6 Geological structures.....	27
1.7 Other environmental conditions .....	28
2 Relocation of earlier events and focal mechanisms in Central Sudan .....	29
2.1 Analysis methods and results.....	29
2.1.1 Relocation of earlier events.....	29
2.1.2 Relocation using master event .....	36
2.1.3 Intensity.....	38
2.1.4 Magnitude .....	42
2.1.5 Length of fault rupture.....	44
2.1.6 Focal mechanisms.....	45
2.2 Discussion of the seismotectonics.....	52
3 Local site effects in Western Khartoum .....	55

3.1	Methods and data for empirical estimation of the site effects .....	56
3.1.1	Methods.....	56
3.1.2	Description of the two sets of data.....	64
3.2	Analysis and results.....	73
3.2.1	Analysis of H/V ratio of ambient noise data.....	73
3.2.2	Analysis of earthquake data for estimating local site effects.....	100
3.3	Discussion of the local site effects .....	114
3.3.1	Description of the H/V ratio results with respect to geological units .....	114
3.3.2	Description of the H/V ratio result with respect to subsurface layers .....	118
3.3.3	Description of the H/V ratio and Standard Spectral Ratio result using earthquake data .....	121
4	Conclusions and future perspectives.....	125
4.1	Conclusions on the seismotectonics of Central Sudan .....	125
4.2	Conclusions on the local site effect study applied in Western Khartoum .....	125
5	Acknowledgements.....	127
6	References .....	129
 Appendixes		
A	H/V ratio for ambient noise .....	iii
B	H/V ratio with subsurface layers .....	v
C	Standard Spectral Ratio and H/V ratio using local earthquake records .....	xxi

# Abstract

The central part of Sudan is tectonically significant and thus needs to be studied. In recent years, the central part has grown economically and the population has increased. This results in growing interest to estimate the seismic hazard through tectonic and seismological studies. In the present work we have carried out two studies. We have used earthquake data to analyze the seismotectonics of the area and conducted a local site effects study in the western part of Khartoum.

The first part discusses the seismicity and tectonics of central Sudan. Five significant earthquakes are used to constraint mechanism of the seismic sources in the area. Earthquakes are relocated and the focal mechanism of the 1966 earthquake is made. We observed that all the events are associated with normal and strike-slip faulting. Focal mechanism of the 1966 earthquake in the southern part of central Sudan is interpreted as a left lateral strike-slip fault. It has similar focal mechanism as the 1993 earthquake in the northern part of central Sudan. Both of them are conformable with the same stress regimes in that area. However, they do not fit with the orientation of the stress tensor dominated by the Red Sea and East African Rift Systems.

In the second part of this work, we have surveyed the site effects in western part of Khartoum city (Omdurman and western Khartoum town). The H/V spectral ratio method is used to calculate the fundamental site frequencies and amplification factors in different sites. The geological conditions of these sites are different, which contain basement rocks, mainly granite, exposed at the boundaries of the area and covered by Cretaceous and Quaternary sediments in the central part. In the study area, we observed that the agreement of the fundamental site frequencies and the amplification factors with the underlying geology was good. The method itself is known to be less reliable for the estimation of the exact amplification factor. Therefore the standard spectral ratio method was tried with earthquake data to estimate the amplification factors in the Khartoum area. However, the earthquake locations did not satisfy the far-field criteria and hence the results were not useful. In spite of this, we observed that the H/V ratio and the standard spectral method gave reasonably good correlation for the fundamental sites frequencies.

Both methods show good agreement between the sites response and the underlying geology. Furthermore, the H/V spectral ratio results are similar to the analytical studies conducted by Mohamedzein et al (2006) in central Khartoum. We believe that the present work highlights the importance of local site effects in Khartoum and needs to be taken into account in estimating the earthquake hazard in the area.

# 1 Introduction

Most of Sudan is classified as an area of low seismic activity and is tectonically stable since the area is an intraplate region (Figure 1.1). Only the southern Sudan and the Red Sea have high seismic activity. These areas have experienced large earthquakes due to their proximity to the plate boundary. Generally central Sudan is an area characterised with low seismicity, but the area has experienced many infrequent moderate earthquakes; the largest one was in October, 1966 ( $M_s = 5.6$ ) and located close to Jebel Dumbeir area (Qureshi and Sadig, 1967). The earthquake in August, 1993 ( $M_s = 5.5$ ) was located near Khartoum city and it named 080193A on map (Figure 1.1). Central Sudan is of special interest, because the area is located in a relatively stable part of the African land mass away from the East Africa Rift system and Red Sea. The influence of stress condition represented by the focal mechanism of Khartoum earthquake in 1993 (Figure 1.3) is opposite to the stress condition represented from the spreading of the Red Sea and East African rift system. Past and recent events are concentrated around Khartoum earthquake area. They have caused damage in Khartoum town and this event was located more than 150 km from the town. Therefore this study is significant in both a regional and local scale. Also it is an economically important area because of the high population density and industry.

Recently, after the installation of the Sudanese's Seismological Network (SSN) in 2003, new and better information about seismic activity in parts of central Sudan has become available. In addition, geophysical studies are being carried out to investigate the tectonics of that area.

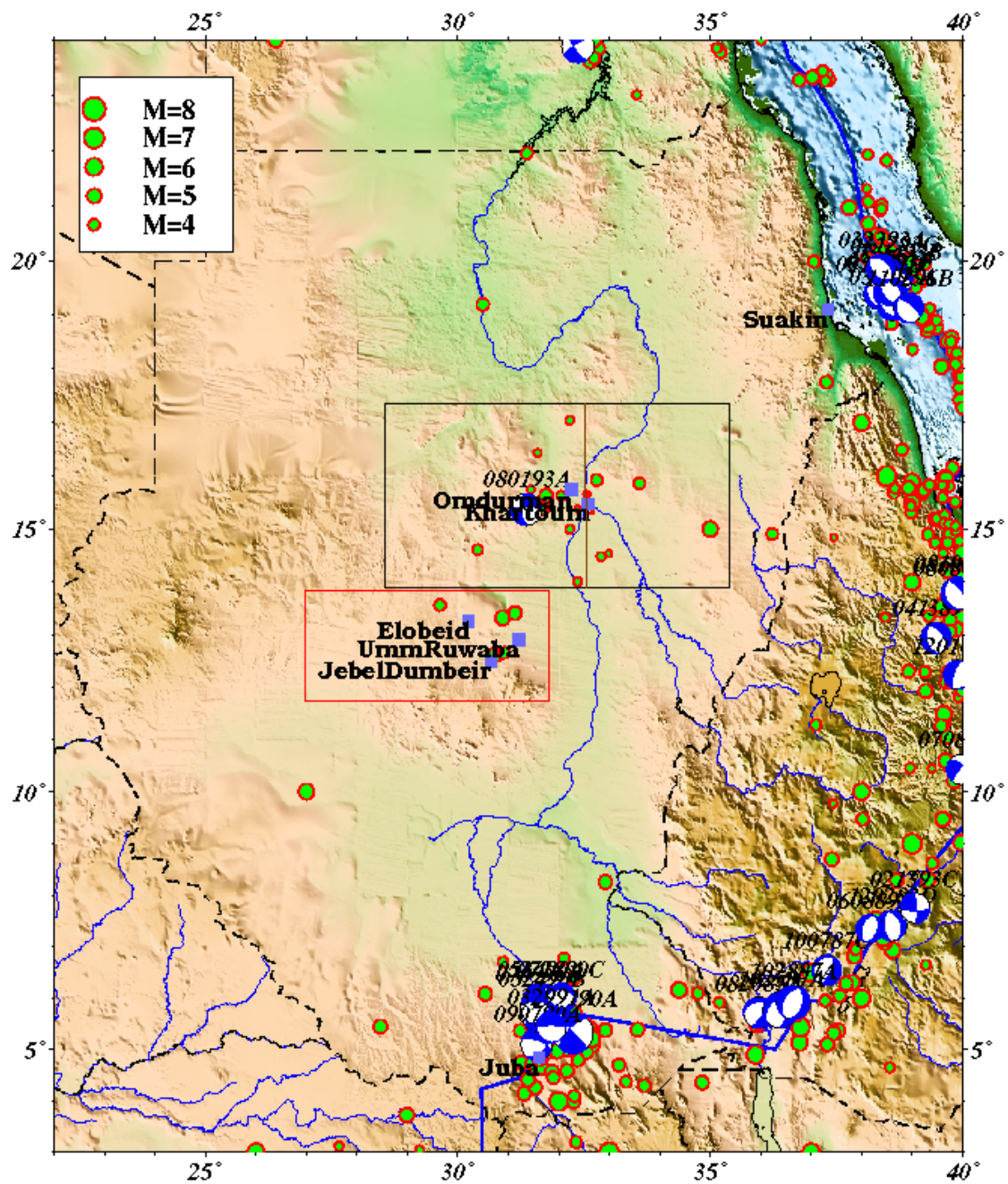


Figure 1.1: Seismicity map of Sudan, the two color rectangles mark the two study areas. Upper and Lower rectangles showing Part II and Part I respectively. The upper left corner the legend for event magnitudes is shown. All focal mechanisms are collected from CMT (Larson, 2006). The data are compiled from International Seismological Centre (ISC) and SSN.



## 1.1 Background

In general the seismicity inside the plate (Intraplate seismicity) is less than the area along the boundaries of plate (Interplate seismicity). That it has longer recurrence times implies a higher stress drop than in an interplate seismic active area. There are two factors that can produce the intraplate earthquake; first is local stress, which the earthquakes are often associated with extensional faulting deep within the continental crust where the early stage rifting was started (Stein and Wysession, 2003). Second is regional stress, it is made by influence of the stress condition represented by plate boundaries into the continental crust with area has weak faults (Clark and Browne, 1987). In central Sudan these two mechanisms of the earthquake generation as mentioned above can exist. Hence the central Sudan area has many rifting and it is occupied between the spreading at Red Sea and rifting extension in Ethiopia. Therefore it seems to be difficult to interpret the mechanism of those earthquakes are associated with low seismicity in intraplate area. In following sections, the previous and recent work in seismology and tectonic are discussed.

### 1.1.1 Previous seismological studies in central Sudan

Due to the small magnitude of the events few seismological and geophysical studies such as gravity and resistivity has been carried out in central Sudan (Abdalla, 2006; Mohammed et al., 2002). Since the SSN was started operation after 2003.

Qureshi and Sadig (1967) were the first to describe the October 1966 earthquake using primary methods as intensity data and surface rupture observations. This event showed that fault has a sinistral strike -slip motion, which trend of  $20^{\circ}$ N. Ambrasey and Adam (1986) reviewed historic seismicity; they suggested that a structure where earthquake are located in this intraplate region is responsible for producing medium magnitudes earthquake. A focal mechanism solution was made by using the relative amplitude method of 06:48 GMT ( $M_b$  5.1) in 1966 earthquake (Clark and Browne, 1987). The seismic hazard estimated in Sudan is built on an earthquake recurrence model (Eltahir, 2001). Eltahir (2001) produced the probabilistic analysis of exceeding a specified ground motion level within a specified time. The analytical studies of site response and earthquake design for central Khartoum town conducted by Mohamedzein

et al (2006). This study is based on shear modulus, damping and shear wave velocity. It is calculated from pertinent cyclic soil and it integrates those parameters with worldwide strong- motion records at different places to calculate the local soil condition.

### 1.1.2 Topography of the study area

In the present study two areas has been investigated. The first area covers most of the south Kordofan State and is characterised by different tectonic settings including the sediment basin Bara, metamorphic rocks exposed in the Nuba Mountain, the Tertiary volcanic in Jebel Marra in the western part of Sudan and the basement rock complex exposed at Dumbeir hills (Figure 1.1). Two big towns, El Obeid, Umm Ruwaba and several villages are scattered on a large agricultural area, and a small natural stream called El Rahid crosses the area and flows into the White Nile. The second area is around Omdurman and the western part of Khartoum town and is characterised by a flat topography flat wide few hills in the surrounding of the northern part of Omdurman town.

## 1.2 The present study and its objectives

In order to demonstrate the seismotectonics and local site effect in central Sudan we should first understand the mechanism of the moderate earthquakes sources in this area. Therefore, the present study is divided into two parts.

The first part concerns the reassessment of the seismicity and tectonics of southern part of the central Sudan. Data compiled from <http://www.isc.ac.uk> and ISC bulletin in 1966 are used. We will describe the relocation of the events, the macro seismic observations, the magnitudes, the intensity information and the focal mechanisms and also we will try to determine the length of surface rupture. However, the results will be evaluated in the context of the general tectonics of central Sudan. The intention is to obtain better location of the events and study the earthquake in 1966 in detail.

The second part focus on the local site effects in western part of Khartoum city. The eastern and western parts of the central Sudan have high moderate seismicity and many earthquakes damage the towns of Khartoum and El Obeid in 1993 and 1966 respectively. The western part of the area has higher seismicity and intensity than the

eastern part. Accounting for local site effects is therefore essential in earthquake risk mitigation. The expected local site effects are empirically evaluated. Two methods with two different datasets are used to calculate the local site response. H/V spectral ratio and Standard Spectral Ratio methods are conducted by using ambient seismic noise and local earthquakes recorded by SSN respectively. The objectives of this second part study are;

- Determine the site response at different sites in western Khartoum city, which is underlain by different geological formations. The aim of that is to map the fundamental frequency and amplification factors at each site for various sedimentary deposits.
- Evaluate the local site effects in Khartoum basin using both ambient noise records and earthquake data as weak motion to obtain the fundamental frequency and amplification factors.

## 1.3 Seismicity

### 1.3.1 Regional seismicity

A catalogue of the seismicity in internal Sudan is compiled from the following sources: historical data represented by Ambraseys and Adams (1986), East African Seismological catalogue (EAF), Preliminary Determinations of Epicenters (PDE), USGS, and (SSN). In total 1160 events are compiled and plotted in figure (1.2). The areas are located at plate boundaries characterised by active seismicity such as the East African Rift system and the Red Sea (Figure 1.1). The earthquake of the 20 May 1990 ( $M_s = 7.1 - 7.4$ ), one of the largest earthquakes occurred in Africa in the last century was located near the town of Juba (south Sudan) was probably related to movements of the east Africa rift system. The main event was followed by several after-shocks of which the largest one had magnitude of  $M_s = 7.0$  (Giardini and Beranzoli, 1992). Local earthquakes have been reported frequently around Rejaf (4.7 N, 31.5 E), villages close to Juba town. Another earthquake whose effect caused damage was the May 12, 1938 ( $M_s = 5.8$ ), which located near the Suakin town on western coast of the Red Sea. Both events are associated with the active rifting areas along the western Red Sea and one of the East African Rift system (EARS). The central Sudan area has experienced many infrequent moderate earthquakes.

Two areas of seismic activity are delineated in central Sudan (Figure 1.1). The southern group includes the earthquake of 1966 which caused strong shaking including the Khartoum city. The northern group has experienced occasionally low to moderate magnitude events that can produce extreme damage in the surrounding towns. We divided the seismicity of the northern part of Central Sudan into two groups based on the location and on the tectonic province. One group is in eastern area of Khartoum and the other is in the western part of Khartoum. The western group exhibits higher intensity and activity than the eastern part. Before the Sudanese Seismological Network started in 2003, the area had three strong earthquakes located in the southern and western part of the study area. Examples, the March 1974 earthquake and the July 1996 earthquake, located close to Ed-Dueim -southern of Khartoum town.

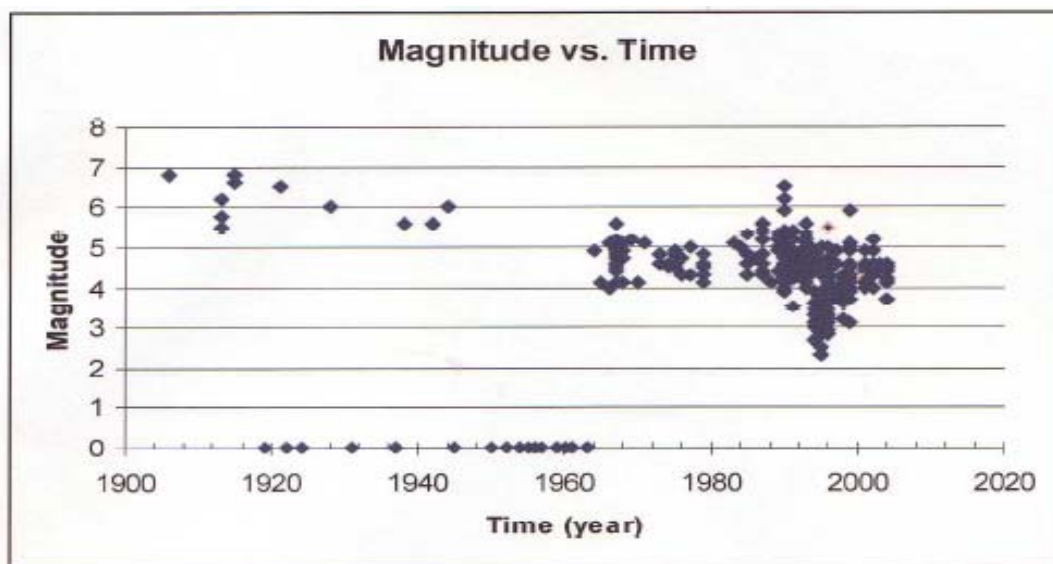


Figure 1.2: Magnitude distribution of the compiled catalogue of the Sudan area. The catalogue compiled from the period from 1910 to 2007. Data collected from ISC, EAF, PDE, Ambraseys & Adams (1986) and SSN.

### 1.3.2 Local seismicity

As mentioned in the previous section the regional seismicity of the central Sudan the area around Khartoum has experienced infrequent moderate earthquakes. Recently, 22 local events were located by SSN during the three years from November 2003 to September 2007. Most of them have been located in the eastern and western part of the

Khartoum area like the earthquake at Abo Dulige November 2004 ( $M_s = 4.5$ ) was located about 149 km east of the Khartoum. This event was followed by three aftershocks with short surface cracks observed (Ayad et al., 2004). About 60% of local events take place in the western part. Both of these groups may represent the sources of earthquakes that affect part of Khartoum town.

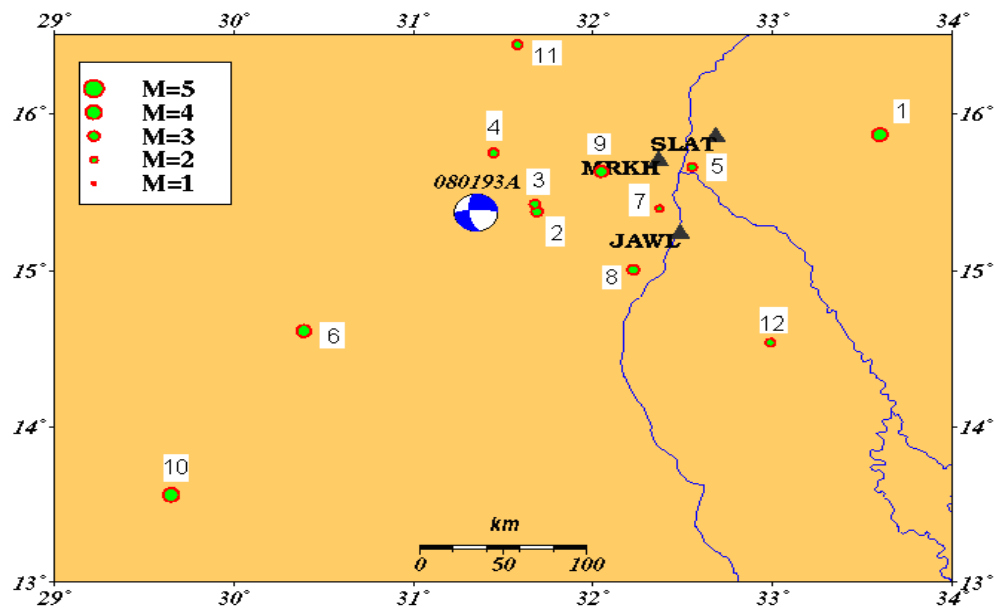


Figure 1.3: Local seismicity map of Khartoum area shows the distribution of the events recorded with stations named MRKH, SLAT and JAWL. Events are recorded during the period from November 2003 to April 2007. The upper left corner the legend for event magnitudes is shown. At western part of the Khartoum area show the focal mechanism of the earthquake in 1993 is compiled from Harvard moment tensor solution databases (CMT). The number of each event is given in Table 3.2. These data are compiled from SSN.

However, most of the local events recorded are found close to the epicenter of the Khartoum earthquakes in August 1993. Based on the seismological data a fault plane solution associated with a strike slip fault trending NE (Figure 1.1) might be related with these earthquakes. The majority of the focal mechanisms of events located near Khartoum region have no focal mechanisms. All events occur at shallow depths from 5 to 22 km, with magnitudes ( $M_c$ ) 1.8 to 3.6. In the eastern part of Khartoum area the earthquake in November 2004 was associated with strike slip fault trending NW. This interpretation have been done by using geological, geophysical (gravity and resistivity measurement) and remote sensing evidences(Mula et al., 2006).

The temporal distribution of earthquakes detected by SSN is given in (Figure 1.4B) for the period from November 2003 to April 2007 is plotted in figure 1.3. The number of events gradually decreased during 2005, while the network continued increasing as the same rate as before 2005 (Figure 1.4B). This indicates that many events were missed, probably due to technical problems of the SSN stations themselves or to the inadequate distribution of the stations.

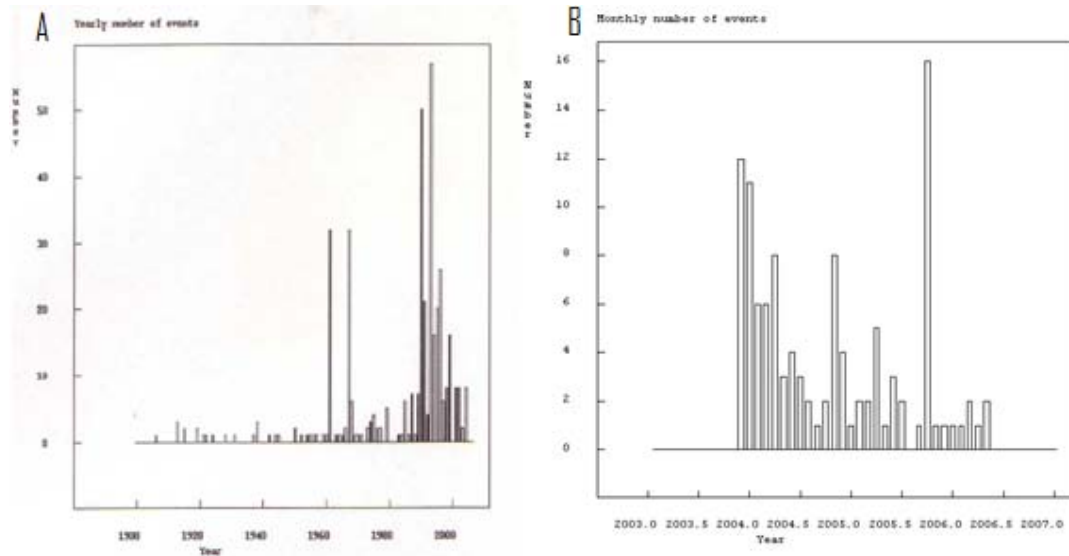


Figure 1.4: Two Histograms show the distribution of event for two different databases. Histogram A show the data come from ISC for the period 1900 to 2003 in Sudan area. Increase the number of events during the 1990 to 1992 due to aftershock events of earthquake in 1990,  $M_s=7.4$ . Histogram B shows the distribution of earthquakes detected by SSN data for the period from November 2003 to April 2007 in central Sudan around Khartoum area.

## 1.4 Tectonics and stress conditions

During early Cambrian times, immediately after the Pan African orogeny, the NE African continental plate was subjected of various episodes of intercontinental deformation.

However, in Sudan the stresses imposed during the break up of Gondwana land from the late Triassic to the present were resolved along existing trend NW –SE; this is represented by extensions E-W orientation (Figure 1.5). As a result a number of rifts have been formed, some of which appear to have been originated in the early Mesozoic basin while others date only from Tertiary (Salama, 1985), extending from the western boundaries of Sudan to the eastern borders. The Sudanese's Cenozoic rift systems over a

large area include (a) Bahr el Arab rift (b) White Nile Rift (c) Blue Nile Rift, (d) River Atbara Rift and (e) Wadi El Kuu Rift. All these rifts contained two or more basins. These rift basins have been the subject for exploration and extensive geophysical research (Binks and Fairhead, 1992).

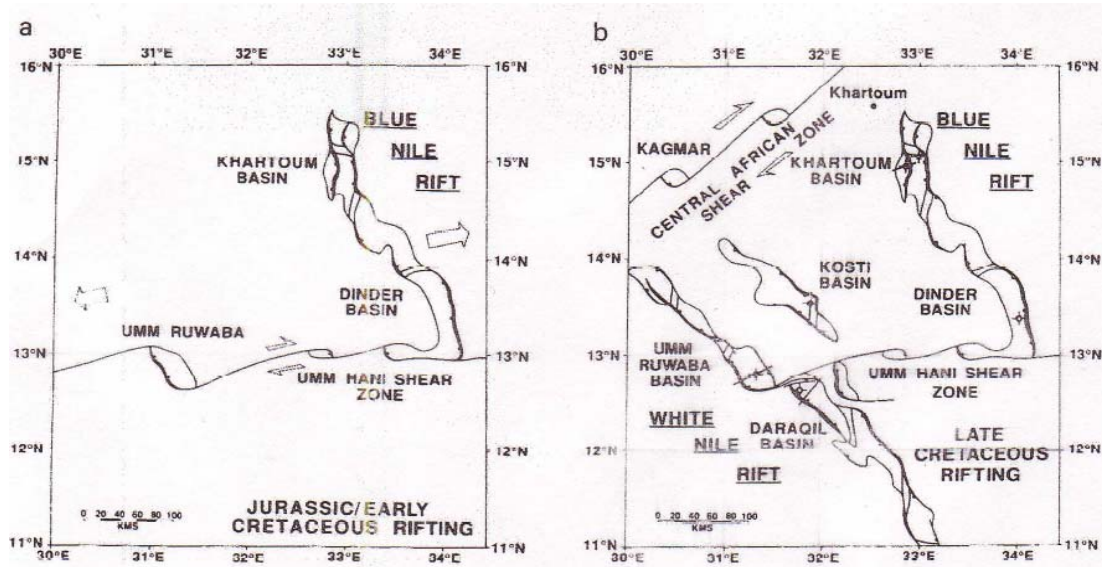


Figure 1.5: Geometry of rifting recorded in the northern Nile basins of central African rift system, (a) Late Jurassic /Early Cretaceous rifting, confined to basins north of the Umm Hani shear zone, (b) Later Cretaceous Early Tertiary rifting (Bosworth, 1992)

The central Sudan contains two major Cenozoic rifts, the White Nile Rift (WNRS) and the Blue Nile Rift (BNRS). These rift zone began to develop in the late Jurassic-Early Cretaceous during the separation of South America from Africa (Bosworth, 1992). Intra-cratonic extensional forces resulted from the opening of the Atlantic acted upon and along the African continent facilitated the formation of these basins. Movement along different major fault trends continued and resulted in the formation of several deep fault- bounded troughs.

Seismic studies estimated the thickness of sediments in the deepest basins to be 5 km (Geology Research Authority of Sudan (GRAS) 1990); (Abdalla, 2006). The deposition of thick sediments in central Sudan rift are associated with three main rifting phases (Schull, 1988), each rift phase was contemporaneous with uplift in the source area. Uplift apparently taken place in north eastern part of the studied area, which contains two basins [Bara and Khartoum] and extend from White Nile rift (WNRS) to the

Blue Nile rift (BNRS) with a general northwest-southeast trend. Oil explorations conducted in the region have enabled the subdivision of the rift system into smaller sedimentary basin and sub-basins. The WNRS contains basins, such as the Bara basin complex, which is composed of the three major sub-basins named El Beshiri, Umm Ruwaba and Dar Agil. The BNRS contain basins such as the Khartoum basin and the Kosit basin complex (Abdalla, 2006; Bosworth, 1992) (Figures 1.9 and 1.5). The studied region south of Central African Shear Zone (CASZ) and forms the northern extension of WNRS. The CASZ extends from the Cameroon through the Chad to Sudan (Fairhead, 1988) (Figure 1.5). The end of the Umm Rawaba basin in southern part of study area is associated with Umm Hani Shear Zone (UHSZ) trending NE- SW. It is interpreted by gravity to be active during Late Cretaceous rifting (Bosworth, 1992) and indicates that the compression stress in the area is oriented N-S. The UHSZ extends from the end of the Umm Rawaba basin in the west, to the Dinder basin in the east within the southern basins of BNRS. Some crustal extension may have occurred north of CASZ in the vicinity of Blue Nile rift (Browne and Fairhead, 1983). The CASZ is parallel to UHSZ which means that central Sudan is under extensional forces. All these basins were believed to be formed by the shear zones associated with the pull - a part basin in central Sudan. The extensional regime is supported by focal mechanism of the August 1993 earthquake CMT solution (Larson, 2006) (Figure 1.3). The limit of the extensional system is poorly known. The continental extension of these fracture zones are associated with historical seismicity (Ambrasey and Adams, 1986), indicating that these fracture zones are weak and still able to dissipate stress into the adjacent continental arc (Binks and Fairhead, 1992).

The tectonic stresses presented by World Stress Map(Dong and Shah, 2005), suggest a E-W compression in response to the ridge push force from the Red Sea, the Atlantic Ocean and East African Rift System (Figure 1.6). The ridge -push forces play a leading role, while extensional forces from the rift act as modifiers. This is seen in central Sudan, where present day state of stress is an N-S extension with an average orientation of 10°N. The expected stress field based on NW-SE trending Mesozoic- Early Tertiary faults is a NE-SW extension (Bosworth, 1992) (Figure 1.5). Inversion of focal mechanism data shows a stress tensor which has near vertical  $\sigma_1$  and sub horizontal  $\sigma_3$



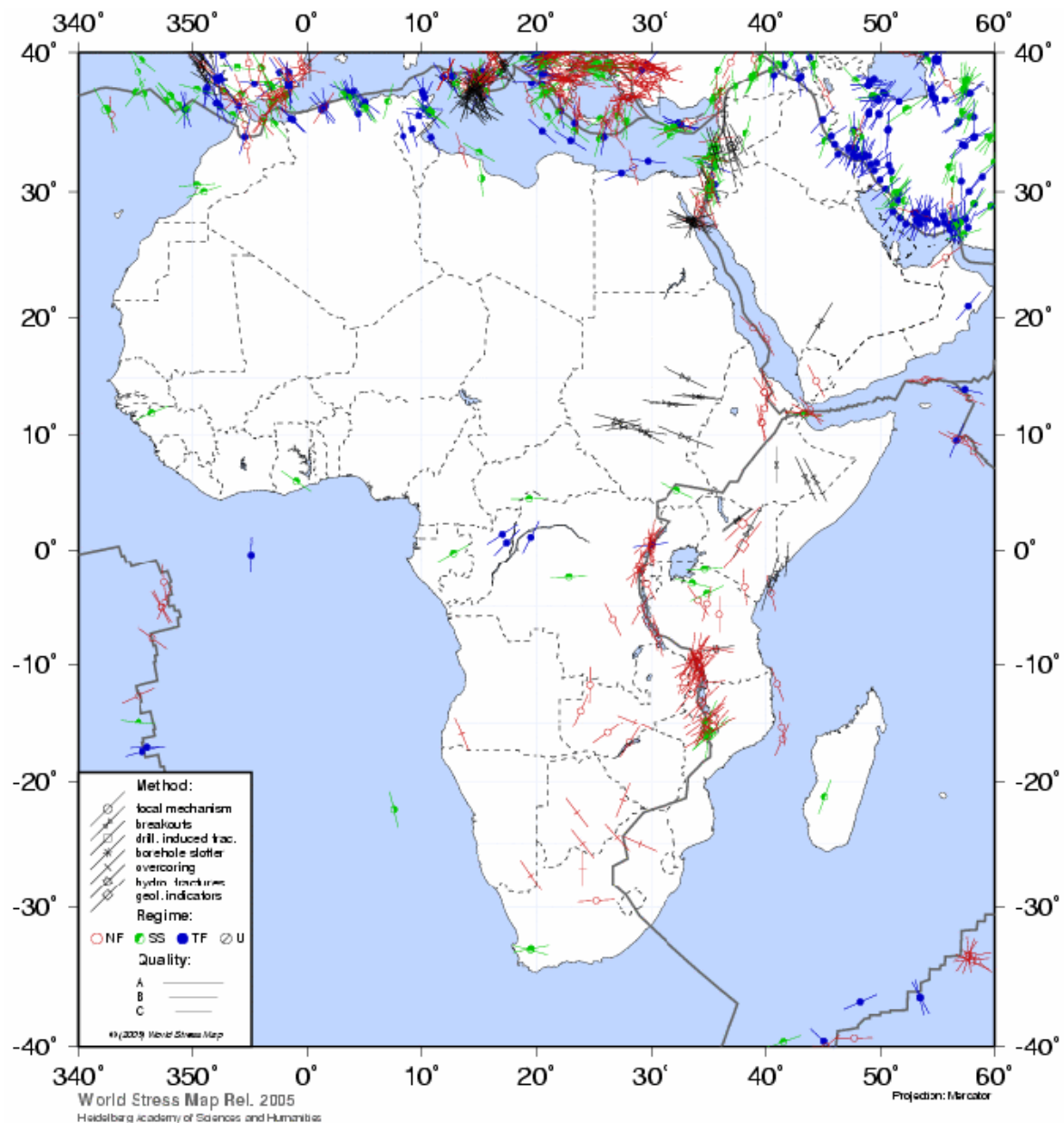


Figure 1.6: Africa stress map shows the direction of stress, the down left rectangle shows different methods. In Sudan region we can see the stress made by breakout method in central mostly trend E-W and SE-NW compression. Focal mechanism in southern Sudan have stress compression trend SE-NW (Dong and Shah, 2005).

suggesting normal faulting regime (Chapol, 1997) (Figure 1.7). The geophysical studies such as the gravity indicated many rifts which were formed by extensional forces during the Jurassic- Early Cretaceous (Bosworth, 1992; Fairhead, 1988). At that time the extension was E- W oriented, which formed the rifts. The relationship between plate motions and intra-plate stress regimes are determined from focal mechanisms, in situ

stress measurement and borehole breakout studies (Dong and Shah, 2005). They show that the maximum horizontal stress is sub-parallel to the direction of plate motion. An alternative way of viewing this relationship is to consider that the poles of rotation, which were describing the progressive opening of an ocean basin, provide the data to map the relative regional stress directions existing at that time (Binks and Fairhead, 1992). The ductile nature of central Sudan rift could indicate that the stress field observed is due to influence of forces from outside the region which also affected the active southern Sudan or East African Rifting System (EARS).

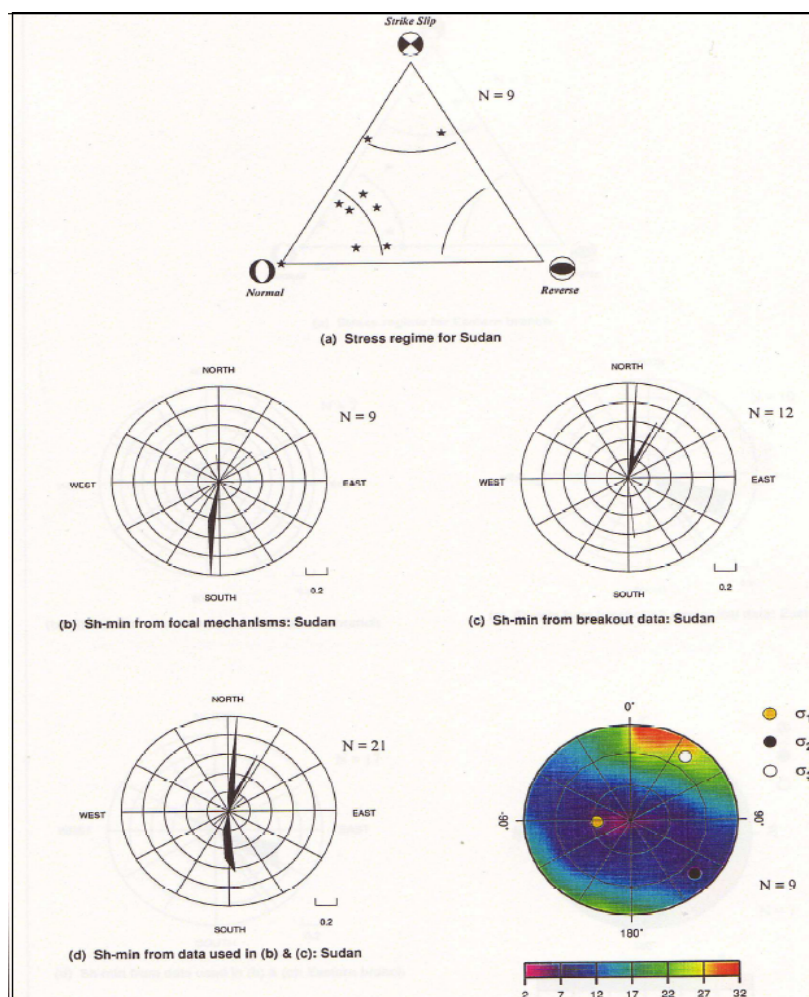


Figure 1.7: Triangular diagram of stress regime (a). The rose diagrams showing the minimum horizontal stress (Sh-min) direction with different methods. The rose b and c showing stress regime from focal mechanism and breakout data respectively. The rose d shows both methods together. The equal area lower hemisphere projection for Sigma-1 stress axis from inversion of focal mechanism (e) for Sudan region. N is number of events (Chapol, 1997).

## 1.5 Geology of Central Sudan

### 1.5.1 Regional geology of the Central Sudan

The study area includes many different geology settings. The basement complex is shallow seated basement rocks of Precambrian age (Vail, 1978) and occurred in boundaries of each sedimentary sub-basin. The basement rocks outcrops around El Obeid and south of El Rahad and are mainly composed by granites gneiss, which are migmatized in Jebel Dumbier, Ed Dair, Hagiart and in the Nubian mountains. The Nubian mountains have master joints that follow two major trends NE-SW and NW-SE while in Jebel Dumbier the trend is north-south. Marble and syenite are recorded in Jebel Ed Daeir and south east of El Rahad (see the modified geology map of Sudan (GRAS, 1988-2006), fig. 3.1 and 3.2).

Sedimentary rocks can be found in three formations in the studied area. The first one is called Nawa formation. Andrew and Karkanis (1945) found it in water wells around the Nawa village north of El Rahad (GRAS, 1988-2006; Whiteman, 1971). Nawa formation consists of sandstone overlying the basement complex, the thickness of this formation is estimated to be 300 m from water wells (Vail, 1978). The second sediment formation deposit during the Jurassic age occurred in thin basalt lava flow layer and includes alluvial fan deposit indicating the first stage of rifting (Abdalla, 2006) (Figure 1.9). The third sedimentary formation called Cretaceous unit was deposited during rifting phase that initiated in the beginning of Mesozoic (GRAS, 1988-2006; Wycisk et al., 1990). Cretaceous sediment comprises intercalation of sandstone, mudstone and conglomerates. The top of cretaceous sediment is covered by Umm Ruwaba and Khaseeb formation with a thickness around 2.5 km. The last formation is sand dunes and superficial deposit which cover most of the area except the southern part of the study area. Two normal faults trend NW- SW trendy associated with sub- basin (Figure 1.8).

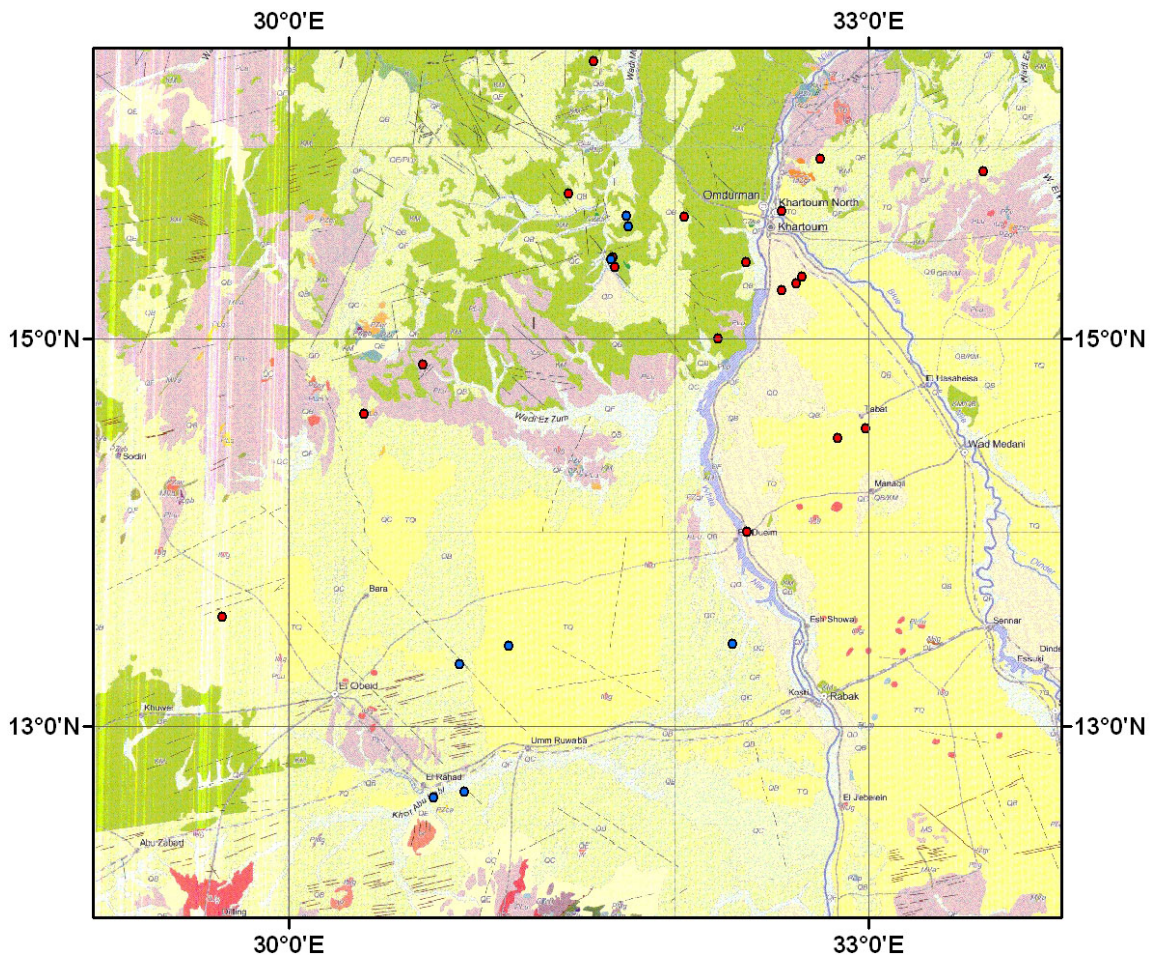


Figure 1.8: Geological map of the study area. Different geological formations are visible as blue and red circles, showing the location of the older and recent earthquake respectively. For each formation on the map we see its corresponding geological complex and the rock type that compose it. The rock type, structure and rivers on the map should be read as follows;

- Recent alluvium and Wadi deposit.
- Older alluvium, raised terraces, younger gravel and sand plains.
- Quaternary, lacustrine deposit, alluvial fans, and dune fields.
- Tertiary -Quaternary, Ruwaba formation; Gravel, sand, silt and clay.
- Cretaceous, fluviatile sandstone, lacustrine and mudstone and siltstone.
- Jurassic sediment, fluviatile sandstone.
- Upper Proterozoic, Basement complex, mate sediments, granite and marble.
- Late upper Proterozoic Older intrusions including older granite, gabbro, anorthosite and quartz porphyry.
- Younger intrusions of granite, syenite and gabbro.
- Blue color is Nile, River.
- Black line is Normal fault.
- Grey color is fracture.
- Black line is strike slip fault.

Modified from the geological Map of the Sudan (GRAS, 2006):

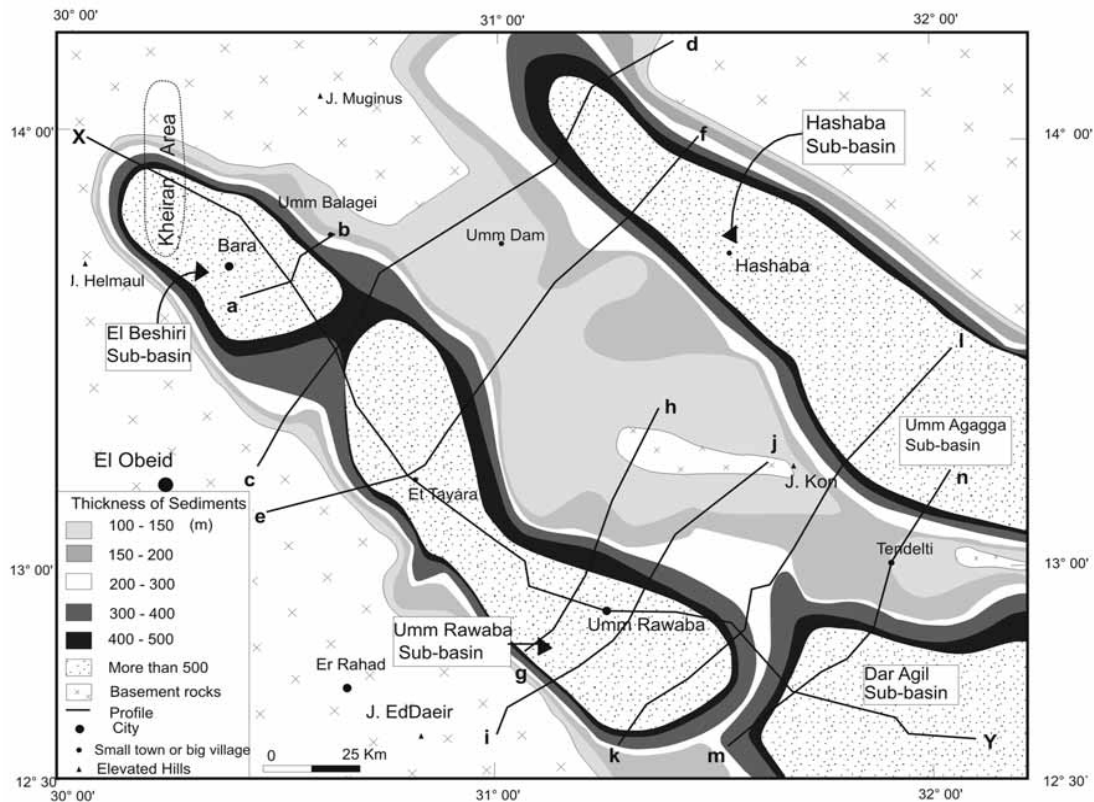


Figure 1.9: The sedimentary sub-basin in the area study and the thickness of the sediments. It shows the basement rocks are surrounding the sub-basin (Abdalla, 2006).

### 1.5.2 Local geology of the area around Khartoum

General treatment of geology and illustration of the geological formation based on the geological map of Sudan (GRAS, 1988 and 2006) was presented by Andrew (1948), Whiteman, (1971) and Vail, (1978). Review of published data and additional observation of the author were carried out during the reconnaissance study.

The principal geology units (Figure 1.10 and 3.4), encountered in the study area and the surrounding are summarized as follows:

- 5-Superficial deposit (Quaternary)
- 4-Gerzira Formation (Tertiary)
- 3-Volcanics mainly (late Tertiary)
- 2-Nubian Sandstone Formation (Mesozoic)
- 1-Basement complex Rock (Pre- Cambrian – lower Paleozoic)

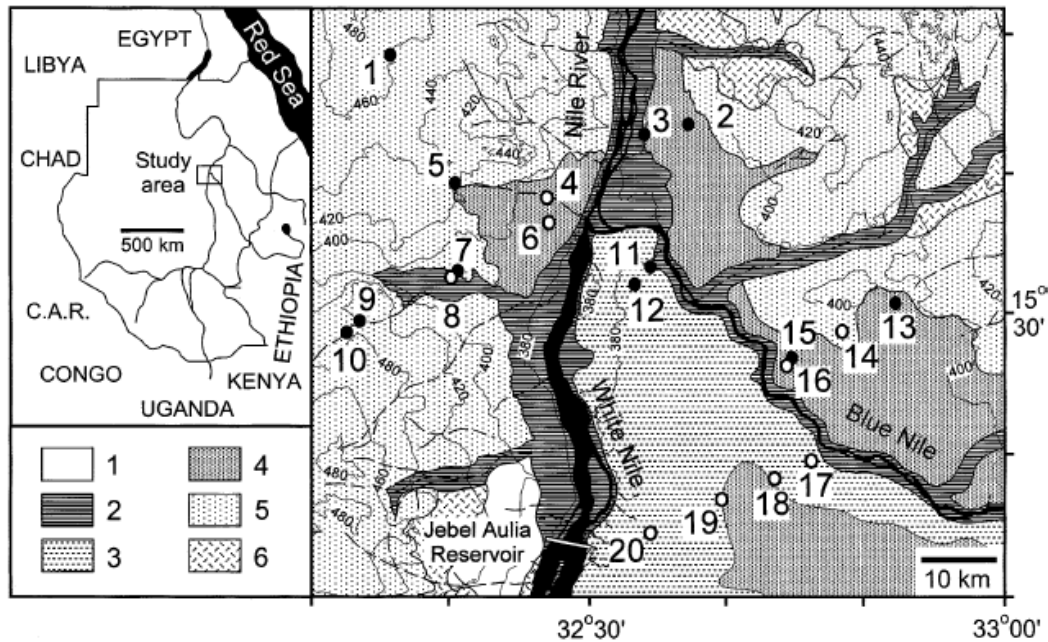


Figure 1.10: Geological map of the study area. Shown all formation unit as number in below the map; Basement complex (6), Older alluvium (5), Gezira formation (4), Omdurman formation (3), Recent alluvial (2) and Dense (1). (Modified from GRAS 1988 and 2006). Note, Gezira formation at north western area are adopted to lower Omdurman formation from another research (Bireir, 1993; Farah et al., 1997).

### Basement complex

The term Basement Complex Pre- Cambrian to early Paleozoic used to embrace all formation older than the Nubian sandstone (Andrew, 1948; Whiteman, 1971). The basement complex occurs in different places in central Sudan. The oldest rocks include igneous, metamorphic and metasedimentary rocks. The basement complex is overlain by horizontal and sub-horizontal Paleozoic and / or Mesozoic sedimentary or igneous rocks.

In the study area the basement rises above the surrounding plain. It is exposed at two sites, one in southern, another in northeastern part of the area. In south the Basement complex is overlain by sedimentary sequences. Both outcrops are small inliers and occurring close to Jebel Mandera in the southern part of the area (Figure 1.11). It is composed by micaceous schist brecciate with felsites dykes. Basement rocks are also known in the area in borehole at variable depth, where they are tapped at shallow levels in borehole to the west of Jebel Aulia (Ibrahim, 1993).

The Basement complex in northern part of Khartoum area is occurring within a large area, called Sabalok Basement complex. It is described by (Almond et al., 1969; Dawoud

and Abdelati, 1988) as a large group of anorogenic igneous complex in Sudan. It is characterized by predominance of acidic rocks (younger granite), shallow level of emplacement, and the common present of structure as; rings of volcanic intrusion, normal and strike -slip faults that cross the area.

### Nubian Sandstone Formation (Mesozoic)

Nubian sandstone formation is used to describe the late cretaceous sandstone in the Nubian Desert in the northern African. Most of the area discussed in this work is covered by sandstone. Whiteman (1971) was the first who proposed the term Nubian Sandstone Formation in Sudan. These are unmetamorphosed bedded and usually flat-lying sedimentary rocks which are made up of conglomerates, grits, sandstone sandy-mudstone and mudstone, which are considered to be of post Paleozoic and pre Tertiary age. A geologist gives different interpretations of the term Nubian sandstone. Kheiralla (1966) used the term Nubian sandstone formation for the sedimentary strata of variegated colors around the Khartoum state and divided the Nubian sandstone into five lithological units from Khartoum to the Shendi area. There are areas in Merkhayat Sandstone with high silicified bed, located north of Omdurman is a part of the Nubian sandstone formations. It is made of clastic sedimentary rocks sandy and conglomerate poorly cemented. The beds are generally horizontal or gently dipping. The following lithological unite were established by Kheiralla (1966):

- 1-Pebble conglomerate
- 2-Intra – formational conglomerate
- 3-Merkhiat sandstone
- 4-Quarzone sandstone
- 5-Mudstone

Hussein (1992) suggested sandstone environment as a tropical fluvialite. Omer (1983) describes it as a semi-dry to tropical paleoclimate and upper cretaceous age. (Schrank and Awad, 1990) adopted the term of Omdurman formation depending to palynological study from subsurface strata. They suggested that near Khartoum, the predominantly sandy Omdurman formation is of Albian to Cenomanian age.

Bireir (1993) based on his study on observations on lithology, grain size, heavy minerals content, geochemistry, clay minerals content, paleogeography and depositional environments, subdivided Omdurman formation into two formations;

- Upper Omdurman formation (outcropping sediments)
- Lower Omdurman formation (subsurface strata)

Upper Omdurman formation is a clastic sedimentary sequence of the Khartoum State. It comprises a flat-lying or gently dipping sedimentary rocks lying unconformable on an originally uneven basement surface, and characterized by an irregular outcrop pattern (Hussein M, 1992). This formation is exposed at the Abu Weledat and Ummarahik hills. The area northwest of Omdurman and the Aulia hills in southern of Omdurman contain sandstone with various grain sizes (coarse, medium or fine) cemented by siliceous, kaolinitic and ferruginous materials.

Lower Omdurman formation is composed by the surface and sub-surface strata. (Barazi and Berl, 1985) proposed that the depositional environment of the exposed strata is fluvial, while the sub-surface units display a lacustrine environment. Lower Omdurman formation is composed of fine and less coarse grained, poorly to moderately sorted, siliclastic sediments (Bireir, 1993). The sediments of this formation were almost transported as subsided particles with rolling and a considerable amount was deposited under fluvio-lacustrine conditions. The sandstone is the dominant rock type it is almost friable, except too the mudstone horizons which are frequently compacted and hard (Farah et al., 1997). The mudstone can reach more than 90 m thickness, especially in the southern part of the Omdurman area. Mudstone clasts and lenses are characteristic of this formation, especially in Omdurman. This formation shows fining upwards, and stacked-channel sequences, ranging in thickness from 25 m to 35 m, rapid lateral and vertical changes of facies (Bireir, 1993; Farah et al., 1997).

### Tertiary volcanics

Volcanic rocks have been reported in many locations e.g. Jebel Marra at (Whiteman, 1971) and Bayuda desert in western and northern of Sudan respectively (Almond et al., 1969). (Andrew, 1948) correlated that with Tertiary volcanoes East Africa and Ethiopia. In the area between the Khartoum and Shendi regions, it is observed that basic volcanic igneous rocks are interbedded in the Nubian Sandstone Formation (Khiralla, 1966) which



are contain mainly basalt and dolerite dykes. The Basalt is found at Jebel Toriya which forms a low hill about 11 km western of Khartoum (Figure 3.5). Extensive geophysical and geological investigations have been carried out (Qureshi et al., 1966). On the evidence of centripetally dipping flow bending inclined at moderate to steep angles, it is suggested that the basalt is an intrusion rather than a flow. Dolerite dyke and basalt are reported in north eastern of Khartoum city, known as Sabaloka Igneous complex (Dawoud and Abdelati, 1988). The dolerite dykes of N- S orientation was observed in the western parts of the study area. This is found by drill holes in Nubian Sandstone formation, when were penetrated at variation of depth between Jebel Aulia and Khartoum (Farah et al., 1997).

### The Gezira Formation

The formation deposited in a triangular area formed by conjunction between the White Nile and the Blue Nile is called Gezira formation (Figure 1.11). It is characterized by flat and featureless clay. Anderw (1948) was the first use this term for the unconsolidated clay, silts, sand and gravels in Gezira area. (Bireir, 1993; Vail, 1978; Whiteman, 1971) believed that the Gezira formation uncomfortably on the Nubian Sandstone formation and is overlain by brown clay and another superficial deposits. Farah et al. (1997) classified the Gezira formation, into two major formations, the upper and lower Gezira formations (Figure 1.11). The upper Gezira formation is composed of unconsolidated sands, clays and silts. It is characterized by high percentage of smectite, low percentage of kaolinite and unstable heavy minerals (Bireir, 1993). The uppermost layer is known as the black cotton soil which is cracking on a surface of clay. It is represented by the weathering condition. The thickness of upper Gezira formation is approximately 10 m to 90 m. The thickness of most of the northern area near to Khartoum is about 10 m to 50 m, while it increases thickness in the south of Khartoum. The lower Gezira formation consists of interbedded sands and clays. The sands consist predominately of loose, medium and fine grained. The depth of this formation is identified in the borehole data section at depth of 205 m to 240 m (Bireir, 1993).

The thickness of the upper Gezira formation near the White Nile is around 15 m to 25 m. The Geological Research Authority of Sudan (GRAS) produced maps in 1988 and 2006 showing that the Gezira formation has taken place in part of the Omdurman

area (Figure 1.10). While this part, described by Farah et al (1997), as lower Omdurman sandstone formation with a dominated mudstone interbedded layer into sandstone. The Geriza formation between the White and the Blue Nile is unconsolidated clays, silts, sandstone and gravels (Figure 1.10).

However, the Gezira formation is used in the present work in order to know the sediment strata and distribution of the clay surface layer. We will focus on the eastern part of the study area located in the eastern bank of the White Nile strata. It is employed to designate the interbedded sand and clays which has given response of the site effect in uppermost layers. The considerable thickness of sedimentary layer may help to correlate that with the microzonation seismic study.

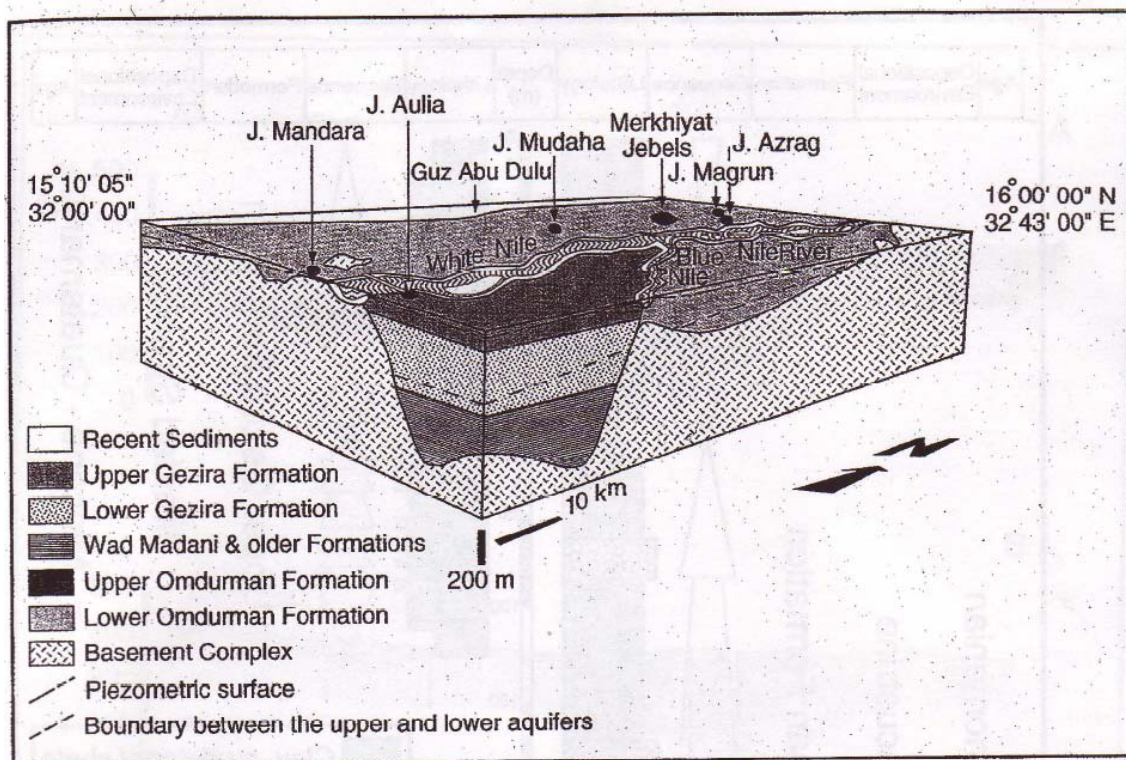


Figure 1.11: Sketch black diagram of the northern part of the Khartoum basin. It shows the geological and stratigraphical unite study area (Farah et al., 1997).

### Superficial deposits (Quaternary)

The recent deposits encountered in the study area include sands, the White Nile alluvium and Wadi-deposits (streamer channel) (Whiteman, 1971). It is occurring in many places with different characteristics. The eolian sands cover most parts of the compresses between the White Nile and the Kordofan State (Whiteman, 1971). There are

deposits of unconsolidated sand, silt, sand, gravel and loosely compacted with silt can be found along the bank of the White Nile between the dunes and Wadi-deposit (Figure 1.10). The recent deposits at the western bank of the White Nile and in the south of the study area are more compact and larger than the one found in eastern bank of the White Nile.

## 1.6 Geological structures

Khartoum basin is one of the Blue Nile Rift systems, and it was formed in early Mesozoic, in response to sinistral movement of a major NS oriented strike-slip fault. The thickness of the sedimentary sequence generally increases from NE and E (Sablouka basement) to more than 900 m in the W and SW. From the southwestern part of the study area and the north of the Aulia dam, the basement rock outcrops towards into northwest near Khartoum, this basement rock reaches 900 m depth in Khartoum (Figure 1.11). The predominantly sand formations in upper and lower Omdurman in the western part of the study area are common in the northern part of this basin. (Awad and Schrank, 1994) interpreted as beginning deposited in a NW- SE trending zone of subsidence along the trend of the Blue Nile Rift. Salam (1985) showed that the Blue Nile Rift is bounded by a series of strike NW- SE, NE -SW and E-W. (Hussein M, 1992) mentions that the structures of the strikes may possible as the defaulting basement complex rejuvenated later during Tertiary. These orientations created a series of basins. Khartoum basin has repeatedly been active in the Umm Udam borehole in the northern Gezira Paleozoic deposits that occupy a NE channel. The Central African Zone is crossing the Bagbag basin at the western Khartoum basin which is suggested to be a border zone of deformation (Ebinger and Ibrahim, 1994).

The Nubian Sandstone Formation, which is mainly horizontal or gently dipping, rests unconformably on a dissected Basement Complex surface and was later affected by faulting (Farwa, 1978).

In the southern part of the study area at Aulia hill, a major NW trending fault is observed cutting the Nubian sandstone near to Aulia dam with NE direction thrown down more than 1000 m. (Mula, 1971) reported the normal faults trend N-S to NNW with

down throws normally to E and NE with a displacement of more than 1200 m (Figure 1.8).

## 1.7 Other environmental conditions

Most of the study area is lying on soft sediments; subsurface layers in some parts are mudstone horizons which are frequently compacted and hard occurring in southern parts of Omdurman area. In the northern part there are mainly mudstones with clasts and lenses of Cretaceous sandstone layer, with its hard silicified. These different strata may give a different acoustics of ambience wave that come from below.

The drainage water system in the study area with high population does not always drain into the river Nile. This remaining water is recharged into subsurface layer. This may affect the underlying saturated layer of loose to medium dense sand in Khartoum area and mudstone lenses in Omdurman, and thus as a result, the discharged water may give a different acoustic wave. This might have a very serious impact on buildings and infrastructure. Therefore the awareness of this geotechnical situation is very important in earthquake hazard analysis.

# 2 Relocation of earlier events and focal mechanisms in Central Sudan

## 2.1 Analysis methods and results

### 2.1.1 Relocation of earlier events.

To locate the source of earthquake is an important task for a seismologist. The locating process involves determining both hypocenter coordinates and the source origin time. Location determination requires identification of seismic phase and measuring their arrival times, as well as knowing the velocity structure between the hypocenter and the seismic station. The location of seismic sources can be given by calculating the travel time for any particular phase to a seismic station anywhere in an arbitrarily complex velocity model (Stein and Wysession, 2003). The problem of finding the earthquake location can be usually tackled by three methods depending on the available data, the single station location, the multi phase location, and inverse problem.

#### Signal station method

Single station method is used when we have one station with three recording components. It is used to obtain a crude estimate of the epicentre. It requires three components recordings of ground motion. Since P-wave are vertical and radial polarized, the P-wave motion vector can be used to infer the azimuth to the epicentre. Figure (2.1) displays the nature of P-wave polarization and procedure of location. The vertical motion of the P-wave is upward with positive value. The radial component of the P-wave is directed away from the epicentre. If the vertical component is directed back toward the epicentre, the event is at back azimuth, this occurs specifically when the earthquake has a

single station both horizontal seismometers will record the radial component of the P-wave. The ratio of amplitudes of the two horizontal components ( $A_E$  and  $A_N$ ) can then be used to find the vector projection of the P- wave along azimuth ( $AZI$ ) to the seismic source.

$$AZI = \arctan \frac{A_E}{A_N} \quad (2.1)$$

The apparent angle of incidence can be calculated by using the amplitude of vertical components:

$$A_R = \sqrt{(A_E^2) + (A_N^2)} \quad (2.3)$$

$$I_{app} = \arctan \left( \frac{A_R}{A_Z} \right) \quad (2.4)$$

Where  $I_{app}$  is the apparent angle of incidence and  $A_Z$  is the amplitude of component. (Wiechert, 1907) obtained the true incidence angle ( $I_{True}$ ) of P-wave as;

$$I_{True} = \arcsin \left( \frac{V_p}{V_s} \right) * \sin 0.5 I_{app} \quad (2.5)$$

The true velocity is important to calculate the local seismic velocity below the observing station by

$$V_{app} = \left( \frac{V_c}{\sin I} \right) \quad (2.6)$$

The distance to the seismic source is obtained from the difference between the arrival time of two phases (S and P). The earthquake epicentre distance can be approximated by:

$$D = (t_s - t_p) * 8.0 \quad (2.7)$$

where  $t_s$  and  $t_p$  is arrival time for S and P wave respectively in seconds, D is distance in km. Eq. (2.7) for “normal medium age” crustal conditions with  $V_p = 5.9$  km/s. For distance  $20^\circ < \Delta < 100^\circ$  the relationship  $\Delta^0 = [(t_s - t_p) - 2] * 10$  still yields reasonably good results with errors  $< 3^\circ$ . The use of the available global travel-time table such as IASP91 (Kennett and Engdahl, 1991) are recommended for calculating distances more than 20 degree.

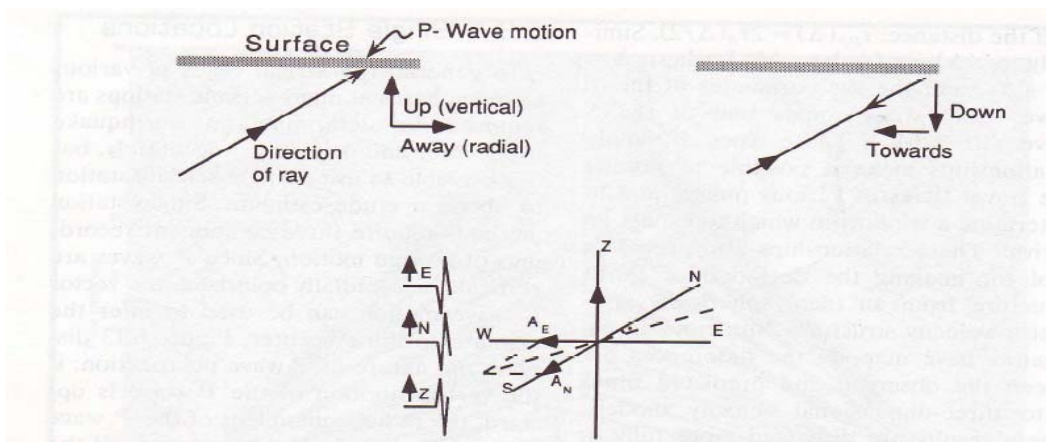


Figure 2.1: Procedure for determining the azimuth to the source of a recorded P-wave by using the three –component vector ground motion and the fact that P-wave motions are polarized in the vertical and radial plane (Bath, 1979).

Since the amplitude ratio between the components should remain constant not only for the first swing of the P-phase but also for the following oscillation of the same phase, we can with digital data, use the predicted coherence method to calculate automatically back azimuth as well as the angle of incidence. This method is faster and more reliable than using manually readings.

### Multiple station location

When at least three stations are available, a simple manual location can be made from drawing circles with the centre at the station locations and the radii equal to the epicentral distances calculated from the S- P time. This distance can be calculated by using the same method as before. The circles drawn around the stations with radius epicentre distance will rarely cross in one site, which indicates errors in the observations and/or that we

have wrongly assumed a surface focus. If they are not crossing at one site, then we will calculate the epicentre area with boundary at the crossing of the three circles. Or by using chord method, which is to draw a straight line passing through the crossing sites among three neighbouring circles.

The last two manual methods provide insight into location problem, called inverse problem. This is to locate an earthquake and finding its origin time using the arrival time of seismic wave at various stations. The velocity structure is then known and after wards it is possible to estimate from the travel times (Stein and Wysession, 2003). The calculated arrival time  $t_i^c$  at station 'i' can be written as:

$$t_i^c = t(X_i, Y_i, Z_i, X_0, Y_0, Z_0) + t_o \quad (2.8)$$

where  $t$  is the travel time function of the location from station  $(X_i, Y_i, Z_i)$ . in order to calculate the hypocenter from Equation 2.8 must to find four unknowns. So in principle, four arrival time observations are needed from at least three stations in order to determine the hypocenter and the origin time. If we have ' $n > 4$ ' observations and ' $n$ ' equations, the above system of equations is over-determined and has to be solved in such a way that the misfit or residual  $r$  at each station is minimized;  $t_i$  is defined as the difference between the observations  $(t_i^o)$  and the calculated travel time  $(t_i^c)$ :

$$t_i = (t_i^o - t_i^c) \quad (2.9)$$

Since the travel time function is a nonlinear function of the model parameter, it is not possible to solve the equation with any analytical method. However, the travel time of all seismic phases to any point to calculate the epicentral by using a model. The method is to perform a grid search over all possible locations and origin time, and compute the arrival time at each station (Sambridge and Kennett, 1986). The hypocenter is the point that gives the best agreement between the observed and calculated time. This means that some measure of best agreement is needed; particularly many observations are used to



find the minimum misfit by using least squares. This is to find the minimum of the sum of the squared residual ( $e$ ) from the  $n$  observation;

$$e = \sum_{i=1}^n (r_i)^2 \quad (2.10)$$

where  $r_i$  is residual of station. The root means squared residual RMS is defined as  $\sqrt{\frac{e}{n}}$ .

The RMS gives an indication of the fit of the data.

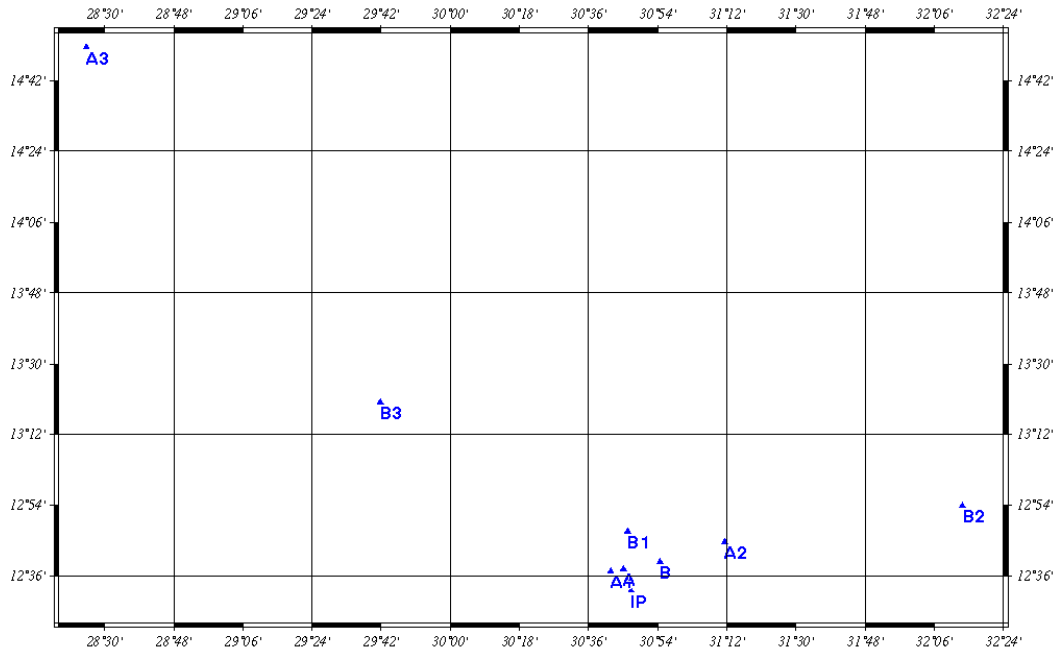


Figure 2.2: Plotting of the relocation of Mainshock (A) and aftershock (B) events of 1966 earthquake with different relocations. ISC locations named A and B. (A,B)1, (A,B)2, and (A,B)3 are show the possibly relocation using the P, P/S and all phase respectively of both event A and B. IP is location of mainshock event in 1966 from macroseismic map.

In this study the events were relocated considering different methods depending on the data availability and developed programs. For the available data eight instrumental events are collected from ISC. There are only four events data are available with arrival times. About twenty- two waveforms of the local events are compiled from SSN, seven events are recorded by one station and four event recorded by two stations and the rest recorded by three stations. These events were checked and re-analyzed. Among those events we used relocation of single station as available data. The analysis shows that the SSN

locations are considered a best location and there are no variations either in RMS or locations. For the developed programs hypocentre location program (HYP) is applied, which is part of SEISAN software (Havskov and Ottemöller, 2005).

*Table 2.1: Old and new relocations of the southern central Sudan event, period between October 9, 1966 to June 23, 2006. The depth is fixed in the last column depending on surface rupture and other factors. The rest of open columns with mark (-), they are data available, from 2004 to 2006, and are not relocated because they are more accurately than the original data.*

Time	Magnitude	Co. location and depth (Km)	Co.Relocation use All phase	Co.Relocation use P-Wave only	Co.Relocation used both P and S-wave	Depth fix (Km)
9/October 1966 6:48	5.1 Mb	12.630N 30.750E Depth 22km (ISC)	14.841N 28.421E ±2.2km	12.620N 30.696E ±22.59km	12.745N 31.190E ±56.5km	5
9/October 1966 10:28	4.1 Mb	12.660N 30.910E Depth 50km (ISC)	13.339N 29.696E ±3.4km	12.790N 30.769E ±4.9km	13.640N 32.222E ±28.3km	5
17/March 1974 07:31	4.6 Mb	13.318N 30.884E Depth 33 km (ISC)	13.603N 30.932E ±1.9km	13.385N 30.802E ±3.3km	13.663N 30.838E ± 4.3km	5
28/Jul 1987 19:52	4.6 Mb	13.413N 31.139E(ISC) Depth 30 Km (ISC)	13.563N 30.471E ±1.4km	13.769N 30.739E ±1.9km	13.990N 30.937E ±5.7km	5
01/August 1993 00:20	5.1Mb	15.412N 31.666E Depth 12.5km (ISC)	-	-	-	-
17/December 2004 17:54	3.2MI	14.866n 30.692E Depth 10 km (SSN)	-	-	-	-
6/May 2006 18:53	3.0MI	14.01N 32.373E Depth 0.1km (SSN)	-	-	-	-
23/June 2006 09:11	4.0MI	13.563N 29.652E Depth 15.0 km (SSN)	-	-	-	-

The reason of the relocation of events by using HYP is to be able to use all phases, because ISC uses only P- waves. Moreover, ISC use bulletin travel time tables which are old, whereas HYP uses IASP91 tables which are new. Since there is no station nearby and no depth phase reported before, the depth must be fixed. The depth was fixed to five kilometers for four events (Table 2.1), since one of the events had surface rupture.

Figure 2.2, shows the distribution of three relocations of the two events of earthquake in 1966. We will discuss the first one in 1966 (main shock) event, since we know the correct location from felt area and the location accuracy can be evaluated. It seems that the location is close to the true location when only P-phases are used. Using all phases gives incorrect locations indicated by many misidentified phases. The main shock with only P-phase now lies in 12.620N, 30.696E, just about 12 kilometres west from the end of the observed fault rupture and more centrally within the isoseismic map. The ISC and Hypocenter solution with only P-phase are close to each other. However the ISC solution is a bit closer to the true epicentre than our hypocenter solution.

Three events are recorded at Addis Ababa station after 06:48, October 1966 (USGS). There, only the second event was recorded with worldwide stations five hours after the mainshock considered as aftershock of the 1966 earthquake (Clark and Browne, 1987; Qureshi and Sadig, 1967). It is relocated following the same procedure as the mainshock. This event is recorded with fewer stations than for the mainshock. The use of Hypocenter gives also better solution when only P-phase is employed. While all phases used in relocations have high RMS value compared to P-phase, therefore are considering as unreliable location. The relocation with P-phase location shifted about 22 kilometres northwest of ISC location. The ISC location lies about 10 kilometres east from the surface rupture. Both the hypocenter with P- phase only and the ISC location are close to the 1966 (mainshock) event location given by the macroseismic results of Qureshi and Sadig (1967). The ISC location is closer to the epicentre than the P-phase relocation. For this reason we preferred an ISC location.

Figure 2.3 shows the two relocated events of 1974 and 1987 with different phases used. The figure also includes the ISC location. About 39 and 30 stations from 1974 and 1987 earthquake records respectively are used. The solutions with only P-phases give the smallest shift from ISC location compare to all phase. The relocation of the 1987 event

using all phases, gives north and south location relative to ISC location. The relocation with only P-phases is closer to the ISC location than other relocations (S and PP, PKP...) in both events. The relocations of the event in 1974 with other phases (S, PP, PKP...) are toward the north of ISC location. We have no absolute solution to compare with, so we assume that the location with smallest shifts represent the most reliable solution as well as the RMS values is small.

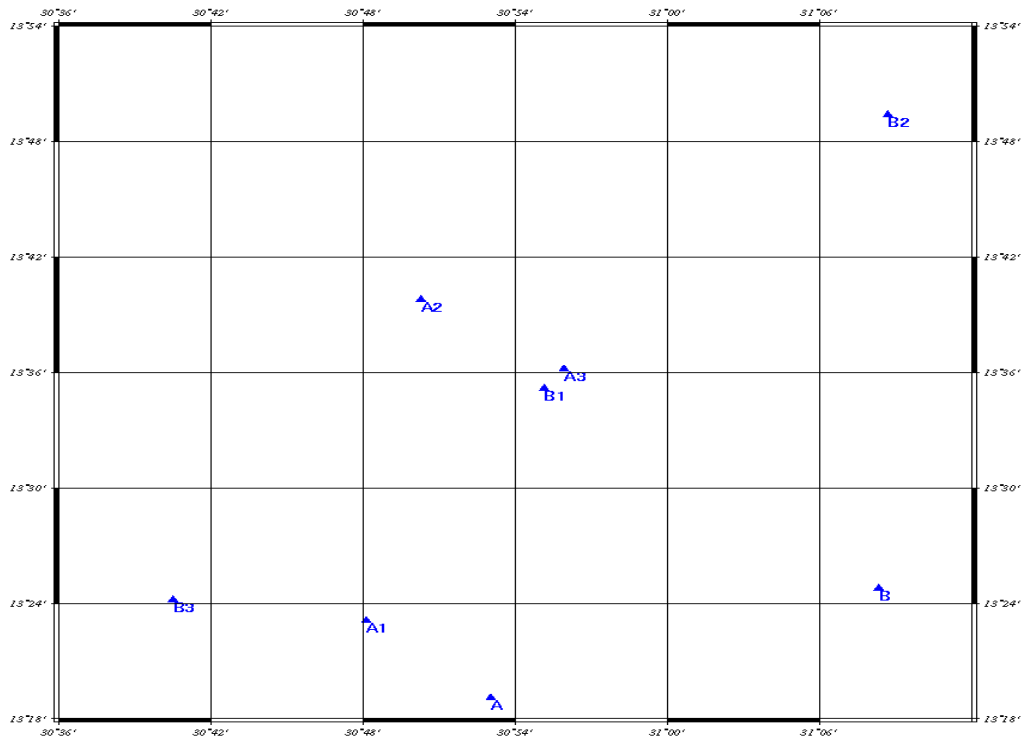


Figure 2.3: Three possible relocations of event in 1974 and 1986 marked A and B respectively. (A,B)1, (A,B)2, (A,B)3 show the possibly relocation using the P, P/S and all phase respectively of two events. The ISC locations of these two events named A and B respectively.

### 2.1.2 Relocation using master event

The study area has many recorded aftershocks of the 1966 earthquake. We tried to locate two of these events relative to each other. This method is called master event (Stein and Wyssession, 2003). The methodology of master event method is to consider particular (often the largest) earthquake in a group as the best located (master event). Then locate a group of nearby earthquake using travel time correction used at each stations derived from residual at each station for master event.

*Table 2.2: locations of aftershock relative to main event (master event method, different stations and RMS value.*

Event	Lat	Long	Type of wave used with number of stations	Residual (RMS) <i>sec</i>
The main	12.630	30.750	P-wave only with 29 stations	0
Aftershock	12.795	30.768	P-wave only with 24stations	Less than 1.5
Aftershock	12.799	30.773	P- wave with 20 stations	Less than 1
Aftershock	12.750	30.726	P-wave with 17 stations	Less than 0.6

In this study we used the hypocentre location program. It is part of SEISAN software (Havskov and Ottemöller, 2005). Figure (2.4) and Table (2.2) show the result and distributions for locations. Twenty nine stations recording only P-phases in both events and only stations with residual less than 2.5 second were used. These residuals were then used to correct the reading for the aftershock. It turned out that several stations of the aftershocks have residuals larger than 2.0 second. These stations were not used and a new location was made. RMS was now 0.6 second and the aftershock were then located 0.120 deg N and 0.115 deg east of the main shock. This distance is almost the same as the distance obtained from the ISC location; however ISC relative location was almost E-W while this one is NE-SW, more in accordance with the observed fault.

The master event is appropriate when the error in the result is small. The error is smaller when the distance is 10 km, used by inaccurate reading. The main shock and aftershock are on the same fault at a distance less than 25 km. In addition the RMS values for all results given by the master event (using different types of wave recorded) are high. Considering that the ground observation made (Qureshi and Sadig, 1967) gives a distance of 5 km. and that the RMS is high and the master event method seems too inaccurate to be used.

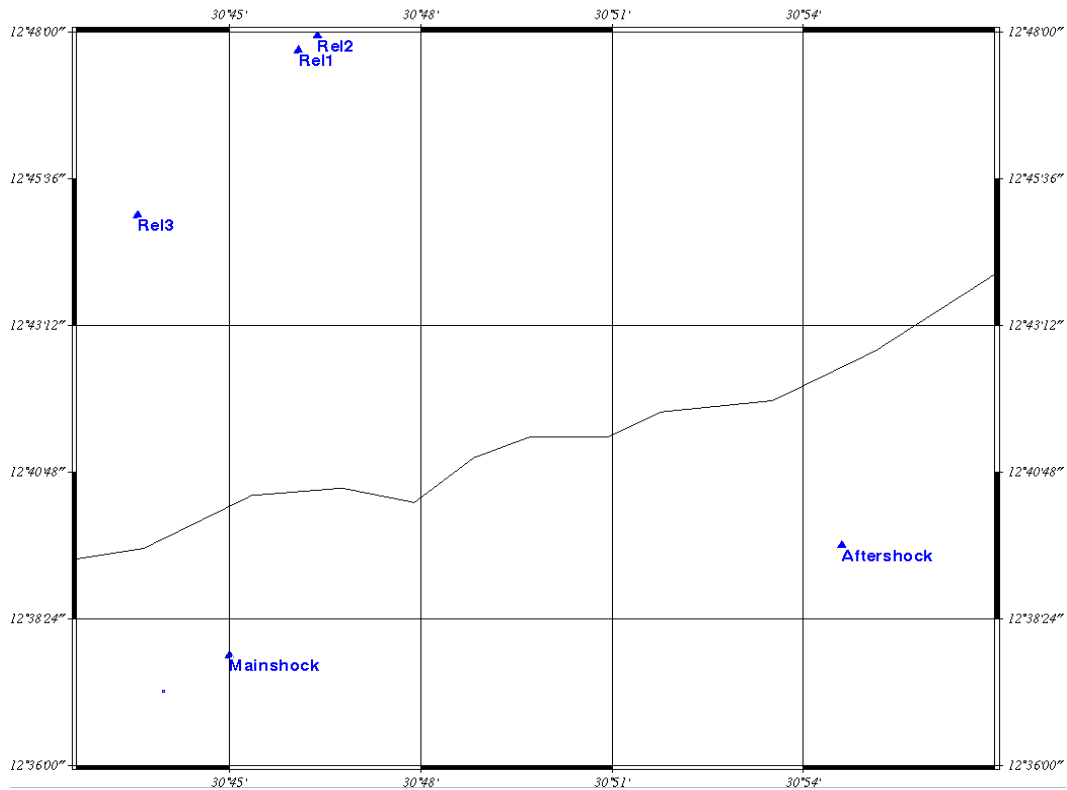
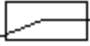


Figure 2.4: Mainshock and aftershock of the 1966 earthquake location with three possible solutions of relocation using master event methods. The aftershock event located relative to mainshock event named as Rel1, Rel2 and Rel3 according to the RMS order in Table 2.2.  Small stream is trend to eastern area.

### 2.1.3 Intensity

The 1966 earthquake was felt in a large area, with varying intensity from the epicentre to Khartoum city about 380 km away. The highest intensity was close to Jebel Dumbeir area. Two isoseismic maps were published for this event (Figure 2.5 (A and B)). Both studies show high intensity along Semeih, Jebel Dumbeir and Sidra villages (intensity VIII). The shapes of the isoseismic curves are elliptical with long axis parallel to fault rupture trending about  $20^{\circ}$ N. It seems that intensity was affected by the local geology. The El Obeid area had experienced higher intensity (V) than the Umm Ruwaba area (IV) about 60 km from epicentre. Thickness of sedimentary rocks over the Basement in Umm Rawaba is about 500 meters while El Obeid area, about 90 km from the epicentre, has no sedimentary rocks and has just fractured rocks (Figure 2.5A). This difference in intensity is not shown on the map but it was explained in the text (Qureshi

and Sadig, 1967). Due to this reason, all original observations were taken from Qureshi and Sadig (1967) text. In addition, more observations from the text added more information. This gives a more complete data set as in Table 2.3 and therefore a better intensity; a new macroseismic map was made (Figure 2.6). The highest intensity is on basement rock and the lowest one is on sedimentary rock. This is opposite to what we expect. This could be due to some local structures or bad observations. Ambrasey and Adams, (1986) made reviews of historical seismicity in Sudan area by considering the low intensity observations, which included the 1966 earthquake but without mentioning the original data (Figure 2.5B).

The macroseismic data with different scales were obtained in order to observe variation within the area. The lowest and highest intensity ellipses are elongated northeast to southwest, which is the same as fault rupture trend. The medium levels intensity such as V and IV has shapes of circles. This could be due to geological and topographical effects.

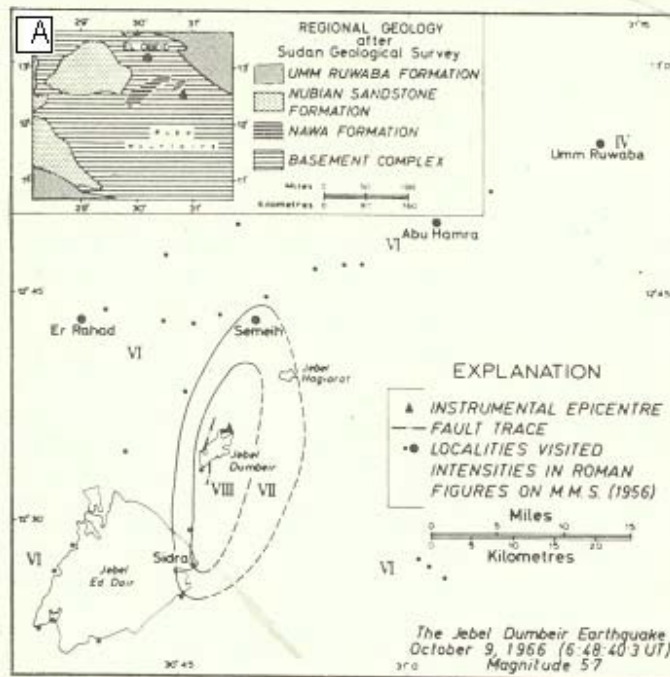


Figure 2.5: Two intensities and isoseismic maps. **A** map shows the intensity and fault trace associated with the Jebel Dumbeir Earthquake of October 9, 1966, the inset shows regional geology in central Sudan and epicentre of earthquake (Qureshi et al., 1966). **B** map shows review of intensity observations for the Sudan region made by (Ambrasey and Adams, 1986). The intensity in the square is for the Jebel Dumbeir earthquake. Both of them are made by using a modified Mercalli scale.



Table 2.3: The sites location with intensity observation of earthquake in 1966. These data are compiled from (Ambrasey and Adams, 1986; Qureshi et al., 1966; Qureshi and Sadig, 1967) using Mercalli intensity scale.

Late	long	intensity	site name
14.625	30.000	3.0 EMS	
10.250	29.000	3.0 EMS	
12.875	28.375	3.0 EMS	
13.000	33.000	3.0 EMS	
11.125	30.000	4.0 EMS	
12.000	31.375	4.0 EMS	
12.000	29.125	4.0 EMS	
13.500	30.500	4.0 EMS	
12.904	31.206	4.0 EMS	Umm Ruwabah- under sediment
12.725	30.635	6.0 EMS	Ar Rahad-
12.718	30.836	7.0 EMS	Seimeih- under sediment
12.464	30.743	7.0 EMS	Sidra- granit
13.191	30.215	5.0 EMS	Al obeid-under the basement
12.567	30.783	8.0 EMS	Jebel Dumbeir- synite
12.469	30.765	8.0 EMS	
12.467	30.686	6.0 EMS	Jebel Ed Dair-granit
12.479	30.637	6.0 EMS	
12.449	30.620	6.0 EMS	
12.660	30.867	7.0 EMS	Jebel Hagiarat
12.500	30.823	7.0 EMS	
12.565	30.768	8.0 EMS	
12.823	31.028	6.0 EMS	Abu Hamra
12.583	30.786	8.0 EMS	
12.667	30.824	8.0 EMS	
12.467	31.010	6.0 EMS	
12.633	30.733	6.0 EMS	
12.427	30.740	6.0 EMS	
12.742	30.842	6.0 EMS	
12.823	30.800	6.0 EMS	
12.606	30.793	8.0 EMS	Trace fault( Dumbeir)
12.537	30.784	8.0 EMS	Trace fault
12.743	30.798	7.0 EMS	
11.625	30.375	5.0 EMS	
12.500	31.125	5.0 EMS	
12.250	30.125	5.0 EMS	
13.000	30.625	5.0 EMS	
15.250	32.375	3.0 EMS	

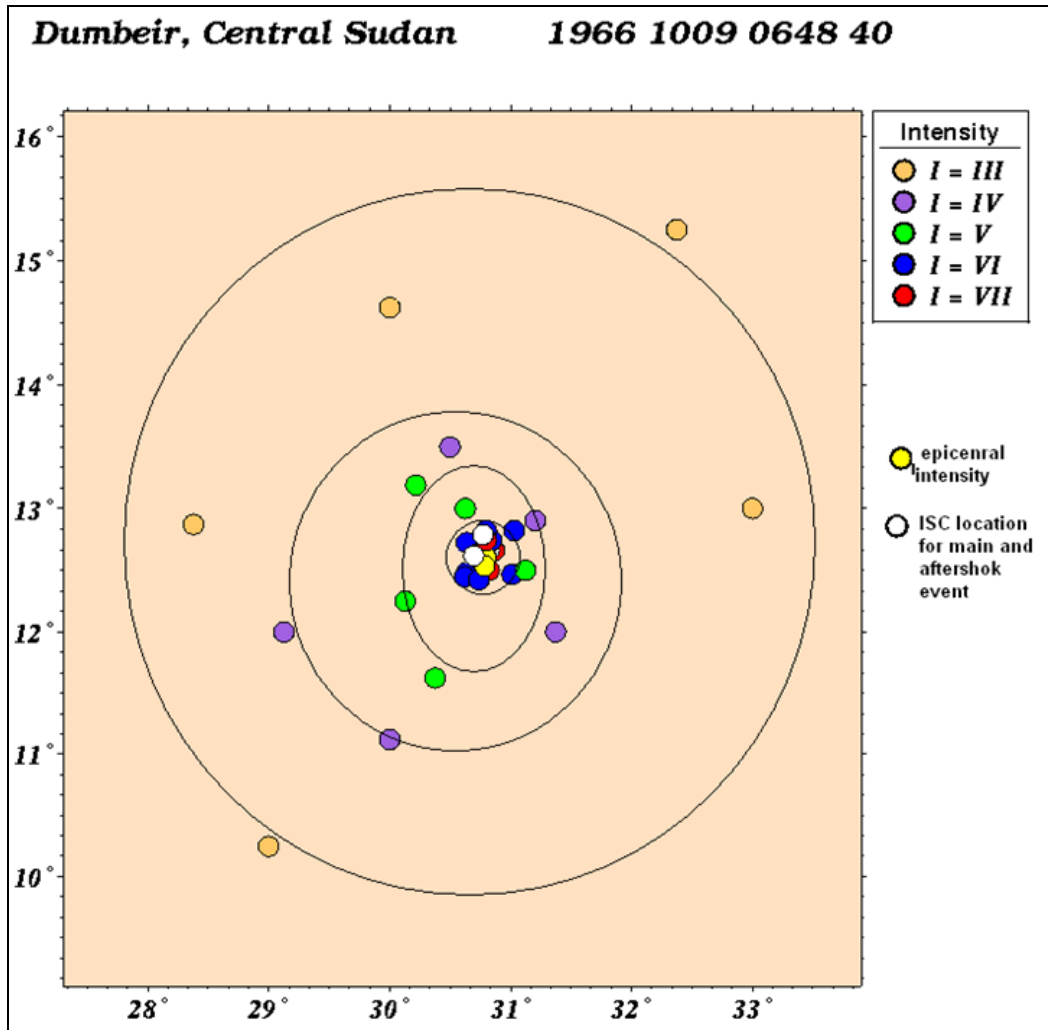


Figure 2.6: Isoseismic map and ISC location of the main and aftershock of 1966 earthquake. These data come from felt reports and include data from Qureshi and Sadig (1967). The yellow circle is the epicenter that is calculated as the centre of highest intensity circle. The white circle is ISC location for main and aftershock.

### 2.1.4 Magnitude

The surface magnitude of earthquake in 1966 was not published by ISC and an attempt will therefore be made to determine it from the felt area. Both Ambrasey and Adams (1986), and Qureshi and Sadig (1967) mentioned that the event in 1966 has  $M_s$  of 5.7 and 5.6 respectively, but do not give any source of the calculation.

Several seismologists have published the relationships between magnitude and felt area. Several expressions from different regions were used to determining the surface wave magnitude.

Singh et al (1980) made relationships for different regions in Mexico; we have chosen that relationship to estimate of MS for regression of intraplate earthquakes, which is the most similar to central Sudan. Singh et al (1980) also give the relationship with intensity VII–IV. We chose the relationship for intensity IV since the area for large intensities will be small and therefore uncertain. Also the high intensity area is highly affected by hypocentral depth. The relation is;

$$M_s = \log A_{IV} + 1.38 * A_{IV} \quad (2.11)$$

where  $A_{IV}$  is the area in square kilometres with intensity  $IV$ . From Figure 2.6, the area for intensity for  $IV$  is  $5 * 10^4 \text{ km}^2$ , which gives  $M_s = 5.7$ . This is similar to what is mentioned by Qureshi and Sadig, (1967).

Also we used two expressions made by Johnston (1993) with a data set from stable continental interiors. This is a similar tectonic environment as the central Sudan region. The first relation gives seismic moment from felt area with intensity III. And the second relation gives  $M_s$  from seismic moment. Using Equation 2.12 and data in Table 2.3, we get a seismic moment  $10^{24}$  dyn-cm. The relation between seismic moment and felt area is:

$$\log(M_0) = 47.34 - 10.81 * \log(A_{felt}) + 1.17 * \log^2(A_{felt}) \quad (2.12)$$

where  $M_0$  is seismic moment in (dyn- cm),  $A_{felt}$  is area in ( $\text{km}^2$ ) from the level III intensity.

The relation between,  $M_0$ , and surface magnitude,  $M_s$ , as determined by two steps for intraplate earthquake it (Johnston, 1993) is:

$$\log(M_0) = 22.47 - 0.4 * \log(M_s) + 1.17 * (M_s)^2 \quad (2.13)$$

where using equation 2.13, we get  $M_s = 5.5$ .

However, for lower magnitudes the moment magnitude  $M_w$  is close to surface wave magnitude (Stein and Wysession, 2003). The standard moment magnitude scale calculated by Kanamori, (1977) is:

$$M_w = \left(\frac{2}{3}\right) * \log M_0 - 10.73 \quad (2.14)$$

where  $M_w$  is the moment magnitude, gives 5.5 .

The values of the  $M_s$  from intensity relation have an uncertainty of  $\pm 0.3$  (Singh et al., 1980). This is due to unknown focal depths, regional attenuation, site response and type of building construction. We used two different relations for  $M_s$  against intensity for intraplate area, and got a value of  $M_s = 5.5$ . Considering the consistency of  $M_s$  and  $M_w$  values, we believe that  $M_s = 5.5$  is a good estimate.

### 2.1.5 Length of fault rupture

The seismic moment can be used to calculate the length of the fault. Wells and Coppersmith (1994) derived an empirical relation between the average slip, fault length and the moment. The relationship between surface rupture length (SRL) in km and moment magnitude ( $M_w$ ) is:

$$M_w = 5.08 + 1.16 * \log(SRL) \quad (2.15)$$

Using  $M_w = 5.5$  a surface rupture length of 2.3 km is obtained from the relation above. This is close to the same length observed as fault trace. The relation between average displacement (AD) (m) and surface rupture length (SRL) (km) obtained by Wells and Coppersmith (1994) is given below:

$$\log(AD) = -1.43 + 0.88 * \log(SRL) \quad (2.16)$$

The average displacement (AD) is 8.0 cm. Qureshi, and Sadig (1967) observed tension gashes about 4.0 cm. the average displacement obtain in Equation 2.16 is not observed. There are various reasons for this discrepancy. There was no obvious vertical displacement, because there was no linear feature crossing the belt. The magnitude of horizontal displacement along the fault could not be estimated well. Since the gash showed only a little distortion at superficial deposits (clay) which means the horizontal displacement was small.

These observations do not support any evidence of surface fault rupture; they are probably related to surface cracks associated with ground shaking.

### 2.1.6 Focal mechanisms

The first motion technique of focal mechanism solution is to project the polarity of the first arrival at stations on to the focal sphere (Stein and Wysession, 2003). The focal mechanism for the selected event was constrained using FOCMEC program (Snoke et al., 1984), which is part of SEISAN software package (Havskov and Ottemöller, 2005). The program uses polarities (Table 2.4) and finds possible solutions with a minimum number of wrong polarities for a given grid search. All possible solutions are then plotted on a stereo net with their P and T axes. And then one can choose the best solution by picking the most representative P or T from the possibility of P or T solutions. Two focal mechanisms were made with different dataset

#### Focal mechanisms using ISC Bulletin data

Polarities from twenty- nine stations collected for the October 9, 1966 event from the ISC Bulletin are given in Table 2.4. The majority of the stations are in Europe and Asia. The polarities were available from the ISC bulletin. The search was made with a three degrees grid and five polarities error and no solution was available. Figure 2.7 and Figure 2.8 show two possible solutions with 1 or 3 degrees grid search with 6 to 7 polarity errors respectively. The best consistent strike slip solution was found with three degree grid search with 6 polarities of error (Figure 2.9). The two nodal planes are; left lateral strike – slip motion with a trend of 28°N or right lateral strike slip motion trend of 315°N.

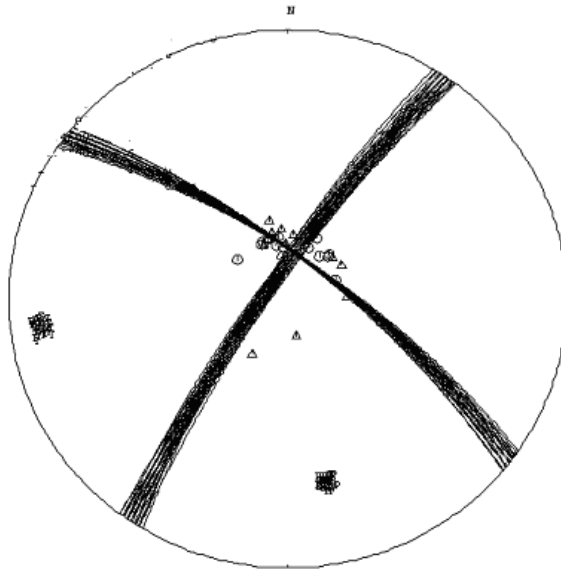


Figure 2.7: All possible solutions of the 0648/10/1966 event with 6 errors of polarity and the grid search is in 1 degree intervals.

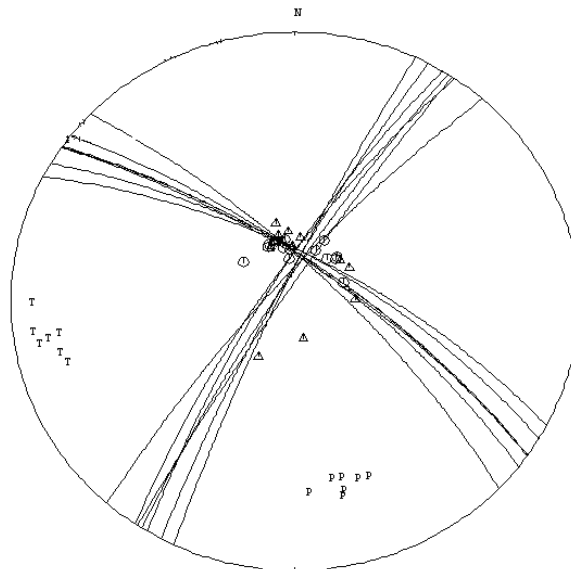


Figure 2.8: All possible solution of the 0648/10/1966 event with 7 errors of polarity and the grid search is in 3 degree intervals. Note, there are small different between high and low Strike/Dip/Rake solutions is (205 to 221)/(77.8 to 85.4)/(-15 to -20) respectively.

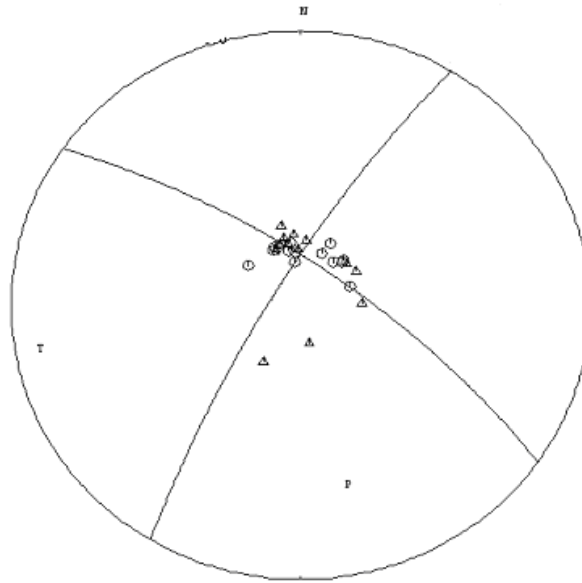


Figure 2.9: Focal mechanism solution determined in present study with only ISC polarity data; it shows the possible solution for the event 0648/10/1966 given by FOCMEC program. The open circles are the compression readings, the triangles are dilatation readings. P and T are pressure and extension axis respectively, projection is on lower hemisphere equal area stereo net. The solution is made by using 6 polarity errors and the three degrees interval of grid search, strike/dip/rake = 208.5/80.2/-17.5.

Table 2.4: Data used in focal mechanism determination for 04:8 GMT October 9, 1966 mainshock are compiled from ISC bulletin. The stations have compression onsets or dilatational onsets and mark as C or D respectively.

Station- Code	Polarity	Arrival time of P-wave (hh mm sec)	Distance (km)	Take of angle (degree)
VAM	D	06 53 52.80	2609	346
RHO	D	06 53 54.40	2650	355
ATH	D	06 54 16.20	2894	347
GRS	C	06 54 53.00	3351	24
SDB	D	06 55 12.80	3587	212
SIM	D	06 55 17.00	3599	4
UZH	C	06 55 49.00	4071	351
VIE	C	06 55 56.50	4172	344
NIE	D	06 55 58.20	4194	349
QUE	D	06 56 00.00	4201	57
IFR	C	06 56 08.00	4310	308
KHC	D	06 56 08.80	4348	342
KRL	C	06 56 23.00	4531	337
DSH	D	06 56 39.00	4726	46
DOU	C	06 56 44.10	4794	335
TAS	C	06 56 50.00	4910	42

KOD	D	06 57 05.00	5099	88
SVE	C	06 57 33.00	5532	21
LHN	C	06 57 40.20	5618	348
TRO	C	06 58 30.30	6395	355
SHL	C	06 58 39.30	6538	68
NOR	C	07 00 01.90	7994	353
BNS	D	06 56 40.20	4761	338
DUR	D	06 57 37.00	5463	336
LHN	C	06 57 40.20	6518	348
KJN	D	06 57 46.60	5724	358
SEM	C	06 58 16.60	6129	36
FRU	C	06 57 25.00	5358	351
MAW	D	07 01 11.90	9275	168

### Focal mechanisms using ISC Bulletin data and data from Clark and Browne (1987)

Clark and Browne (1987) published two alternative fault plane solutions for the 1966 earthquake using both amplitude and polarity data. In order to improve our solution above, we included Clark and Browne data with ISC data into one dataset. About 19 polarities data are added which are based on original readings by Clark and Browne. The total number of polarities which is used now is 44. All those 19 stations are different from our stations except four stations. Among these four stations, one station has the same polarity while three are different. An example of this is the KOD station where the polarity of ISC data is dilatation and the polarity of the Clark and Browne data is compression. The other three polarities from Clark and Browne were not used. From the original seismogram it looks like dilatation, so we use dilatation. The procedure of the focal mechanism is the same as the focal mechanism solution using only ISC data. The result of solution is also a strike slip solution. The search was made with a three degrees grid and 11 polarities of error (Figure 2.12). The two possible solutions of fault plane are a left lateral motion trending  $54^{\circ}\text{N}$  and right lateral motion trending  $330^{\circ}\text{N}$ . Comparing the ISC data and ISC + Clark and Browne data solutions, it is seen that they both represent similar strike slip faults with a difference of up to 26 degrees. These two solutions are compared to Clark and Browne alternative solution given in figure 2.13. They seem to all represent similar strike slip faults. But the different is that the ISC solution a pure strike slip fault while Clark and Browne solution is strike slip fault with



normal fault.

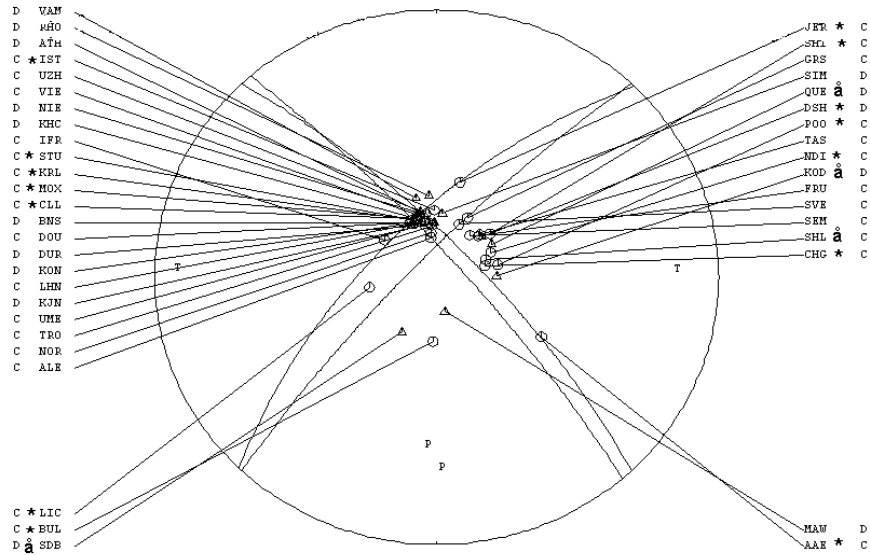


Figure 2.10: Two solutions with 11 polarity errors and 2 degrees grid are strike/dip/slip = 224.5/66.0/-10.4 and 223.7/80.58/-15.4. The star symbol indicates the data from Clark and Browne (1987), the stations without label showing ISC data, and (ã) is the stations that are the in both sources.

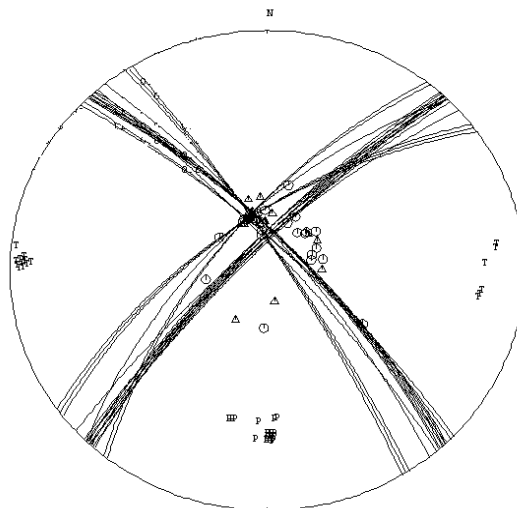


Figure 2.11: Focal mechanism solution of 1966 earthquake; show the many possible solutions with 12 polarity and 3 degrees grid search. These solutions have different strike of about 5 degrees. The two polarities in south and west quadrants near the nodal plan are given some idea about the uncertainty.

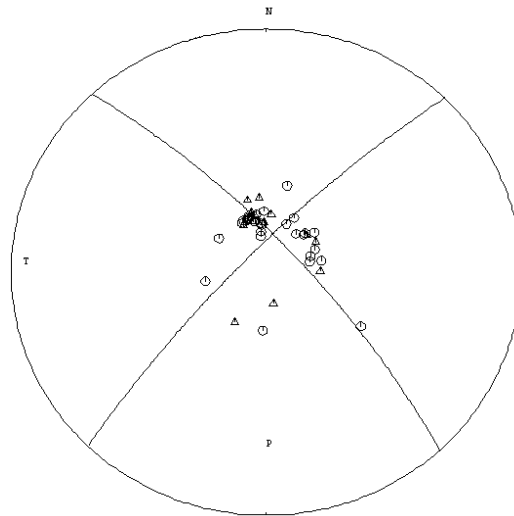


Figure 2.12: Focal mechanism solution determined in present study includes all ISC Bulletin 1966 data and Clark and Browne (1987) data. It shows the possible solution for the event 0648/10/1966. The open circle are compression, triangles are dilatation readings.  $P$  and  $T$  are pressure and extension axis respectively. Projection is on lower hemisphere equal area stereo net. The solution was made with 11 polarities of errors and grid search is in 3 degree interval. Strike/Dip/Rake is 234.97/65.4/-14.7.

### Uncertainty of solutions

Two main sources of uncertainty of those two focal mechanism solutions (figure 2.12 and 2.9) were observed during the study. The first observation is that the data available is densely concentrated in two clusters in the centre of the stereonet meaning it is uncertain to constrain the solution, with several possible fault plane solutions passing through the centre of the stereo net. This is due to poor station coverage of African local stations (e.g. AAB, Talgar Kazakhstan station) and bad azimuthally coverage with worldwide station. The second observation is that several critical points have incorrect polarity as shown by abundance of mixed polarity readings in two northern quadrants. Incorrect polarity readings could result from human error since ISC data contain routine readings from both short and long period records. Some of these errors could also be due to emergent P - wave arrivals that is common on short period records.

Figure 2.7 and figure 2.8 show the solution using only ISC data. In both solutions it seems that the stations LIC and JER have wrong polarity, which will give uncertainty in the solutions. These two stations will have an influence on the accuracy of the solution. This case is also represented in the second solution (ISC+ Clark and Browne data). It is

clear to see the uncertainty when applying the different grid search intervals (five and three degree) with different polarity errors as show in figure 2.10 and figure 2.11.

The ISC and ISC + Clark and Browne illustrated in figures (2.9 and 2.12), give similar fault plane solution with a small difference of strike; both of them are pure strike slip faults. In the ISC solution, one plane trending 28°N (lateral strike slip motion) is comparable to the field observations trending 20°N (ground surface rupture) (Qureshi and Sadig, 1967) the same is the case for the ISC +Clark and Browne (1987) solution (Figure 2.12).

Our two solutions are different from the Clark and Browne solutions (1987) (Figure 2.13). The Clark and Browne polarity solution is based on a few points, and gives a large deviation from surface rupture direction about 60 degrees to the east (see text of Clark and Browne 1987). They also made a solution with relative amplitudes, which represents NNE- SSW normal fault with minor strike slip component.

Our solution is based on four times more polarities. Therefore it is considered the most reliable. Since the area had no observation for vertical displacement, the strike- slip solution is also the most reliable (see text Qureshi and Sadig 1967). Other reason for strike- slip is that in the region, close to the study area, the August 1993 earthquake (Figure 1.1) occurred and it had a similar stress condition represented by our two focal mechanism solutions as in the present study.

The geological structure of the area close to the 1966 earthquake may support our focal mechanism solution. The master joints in Jebel Dumbeir itself and Jebel El Dira are following a NNE-SSW direction. The normal fault solution interpreted by Clark and Browne (1987) shows that there are no geological features to interpret the normal fault since the epicentre of the Jebel Dumbeir earthquake is at about 50 km to the north (Figure 1.8).

From geology, the extension is in the northeast direction. This is similar to the extension obtained from the fault plane solution. Both the Hydrogeology studies (Abdalla, 2006) (Figure 1.9), and gravity studies of Umm Hain shear zone which boundary between Umm Ruwaba and Dar Agil sub basin (Bosworth, 1992) (Figure 1.5) indicate a structure parallel with the surface rupture. This also gives support to our solution.

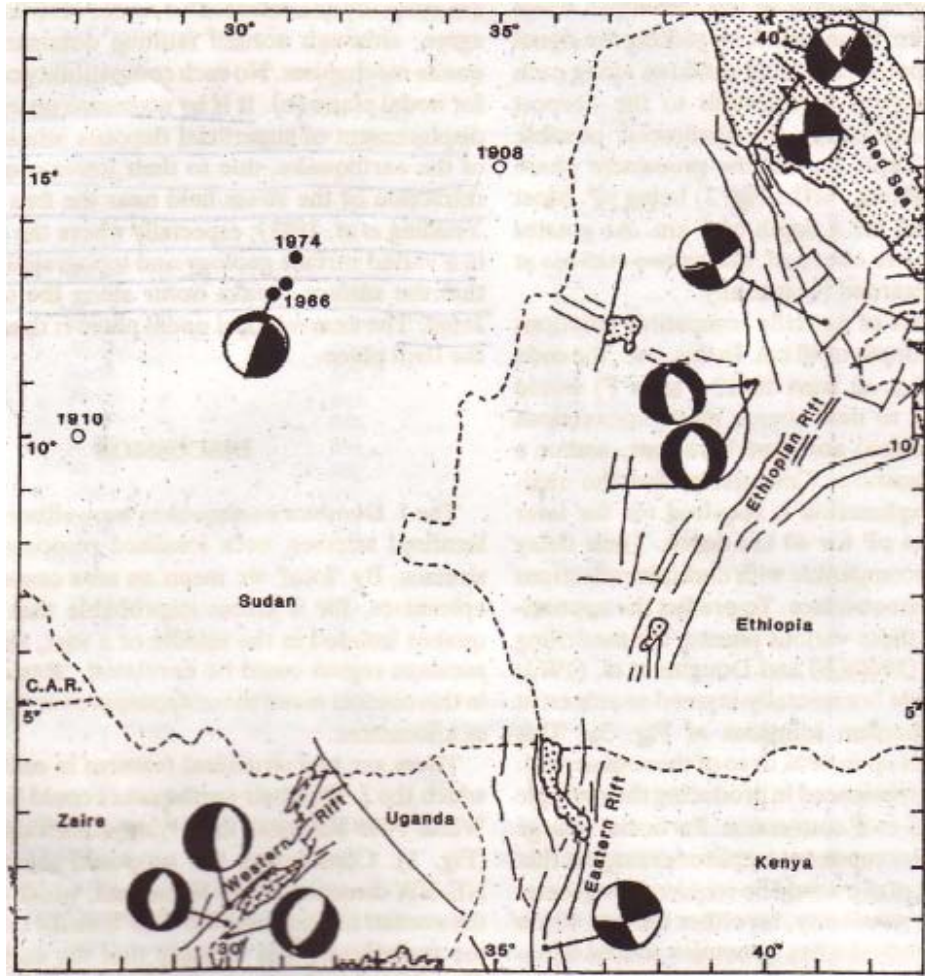


Figure 2.13: Focal mechanism of the earthquake in 1966 made by Clark and Browne (1987) in central Sudan (Clark and Browne, 1987).

## 2.2 Discussion of the seismotectonics

In this section the results based on the analyses in section 2.1.1 to 2.1.6 are discussed. Here we would like to discuss these results in the light of understanding the seismotectonics of the central Sudan- particularly the area around Jebel Dumbeir in the southern part of central Sudan. Two focal mechanisms for the 1966 earthquake show pure strike slip faulting (Figures 1.9 and 1.12). These two solutions are estimated better than the one given in Clark and Browne (1987). There are three reasons supporting our results, firstly the new solutions are based on more polarity data and therefore considered more reliable, secondly since the area has no outcrops with vertical displacement, the strike slip solution is more reliable than the mechanism represented by Clark and Browne (1987)

which is a strike slip faulting with significant vertical component (normal fault). Thirdly the distribution of the aftershocks and the isoseismic map of intensities are also conformable with the strike of one of the nodal planes in our solution. In addition to these, the observed crack on the surface has also the same orientation (Qureshi and Sadig, 1967). We therefore believe that our solution is reliable with the fault plane oriented NE-SW.

The location of the aftershocks using a master event technique shows a trend similar to the orientation of the nodal planes (NE-SW). This supports further our fault plane solution.

In addition, the geology of area around this event shows joints oriented NE- SW (Figure 1.8) which is also similar to the trend of our solution. Moreover the geometry of the sub-basins and the boundary between the Umm Ruwaba and Dar Agil sub-basin shows us NE-SW trend (Figure 1.9).

Another indication as mentioned in chapter 1 (section 1.5.1) is the linear gravity anomaly associated with the Umm Hani shear zone which trend NE- SW. This shear zone is part of the White Nile rift which was active during Mesozoic- Early Tertiary (Bosworth, 1992) (Figure 1.9). Considering these factors we argue that the fault plane from our solution is the nodal plane trending NE-SW.

The main regional stress field in Sudan is controlled by the opening along the Red Sea in the east and influence of the Ethiopian rift in the south. As a result larger parts of central Sudan are under E-W compression (Bosworth, 1992; Dong and Shah, 2005). On the other hand, the borehole breakouts data show different orientation than those determined from seismological data such as focal mechanism.

Now, there are two focal mechanisms available in central Sudan; one is the focal mechanism solution of the 1966 earthquake in the present study and the other is the focal mechanism as earthquake in 1993 (Figure 1.1). These earthquakes occurred in the same region and had almost similar mechanism, which further supports the solution presented in section 2.1.6. We believe that the stress condition represented by those events is stronger evidence than the stress given by bore-hole breakout data.

However, these solutions are difficult to explain when we consider the regional stress field based on the bore-hole breakout data. It is likely that the preview zone of

weakness associated with the White Nile Rift and the Blue Nile Rift system plays a role here.

# 3 Local site effects in Western Khartoum

In many earthquakes the local geology and soil conditions have a profound influence on the site response. This influence may result in high damage and death-toll, e.g. such as the 1906 San Francisco earthquake, the 1985 Mexico City earthquake, the Loma Prieta earthquake in 1989 and the 1999 Izmit earthquakes in Turkey (Özel et al., 2002). The factors influencing the local modification to the underlying motion are topography, nature of bedrock and geometry of unconsolidated sediment deposits. Khartoum city is an urban setting located on sedimentary deposits. Local site effects occur due to the amplification of incoming seismic waves as a result of the impedance contrast between the unconsolidated sediment (soil) and the bedrock. Amplification occurs at frequencies where the damping in the soil layer is overcome. In addition, the surface effect (reflected seismic wave on the surface) also contributes to the amplification.

The effect of site response on the built environment is dependent upon the type of building structures. In case where the fundamental frequency of the building corresponds to the fundamental soil layers, resonance phenomena occurs, giving rise to significant structural damage or collapse. Local site effects therefore should be seen relative to the soil-structure interaction. However, in this section the site effects related to the local unconsolidated sediments and hard rock are addressed.

As we mentioned in chapter two (section 1.3.2), the western Khartoum area has moderate earthquakes and most of them are located in the western part of the Khartoum city. Furthermore these events i.e. those shown by the focal mechanism of August 1993 in figure 1.3 and the focal mechanism of October 1996 earthquake in section 2.1.6, are located along the same azimuth orientation with respect to the Khartoum city about 180 km and 373 km respectively. These events were felt in Khartoum area (ISC, 1993; Qureshi and Sadig, 1967). In addition to that, most of the local events are located close to those two earthquakes. Hence, the Khartoum earthquake in 1993,  $M_s = 5.5$ , has caused

widespread damage in Khartoum city resulting in few building collapses and two deaths. The local site effects in western Khartoum and Omdurman town are of importance especially for the planned infrastructure in these areas. In addition to that the population density is high causing increased vulnerability.

### 3.1 Methods and data for empirical estimation of the site effects

The methods for local site effects estimation can be classified into two major groups. The first group the analytical-numerical modeling methods based on the available geotechnical information pertaining to physical parameters of surface structure (Mohamedzein et al., 2006; Schnabel et al., 1972). The second group includes analysis of observations or measurements (empirical) of seismic wave records. In the empirical group there are two methods used to obtain the site response; the Standard Spectral Ratio (SSR) method and the Single Station Spectral Ratio (SSSR) methods. The different methods used in the site response evaluation have been discussed in several papers (Aki, 1988; Atakan et al., 2004; Bard, 2004). In this study we will focus on the second group that uses natural sources. Based on the type of records these can be divided into three subgroups;

1-H/V spectral ratio of ambient noise recordings

2-H/V spectral ratio of weak motion

3-Standard Spectral Ratio of weak motion

In following sections we will discuss methods based on SSSR an SSR methods. Since a particular empirical method to estimate the local site effects in western Khartoum capital are conducted, we will highlight the empirical currently used.

#### 3.1.1 Methods

##### H/V spectral ratio of ambient noise recording

The H/V spectral ratio method of the horizontal to the vertical spectra of microtremor was first introduced by Nakamura (1989). It is called (QTS, Quasi – Transfer Spectra). The technique uses the ambient seismic noise that is always present in the earth. It is based on the following assumptions for the fundamental characteristics of microtremors.



The microtremors are essentially composed by Rayleigh waves, LR, propagating in soft surface layers. This source is one of the main advantages of this method. The method is also cheap and easy to use for the site response spectra estimation. Its uses fit very well to describe the dynamic characteristics of the ground and structure.

Nakamura (1989) gives the theoretical base of the H/V method. There are four Fourier spectral amplitudes involved: horizontal and vertical components of the motion at the surface (S) and at the bottom (B) of the layer ( $V_S$ ,  $H_S$ ,  $V_B$ , and  $H_B$ ). The microtremors are originated by local near surface sources such as River tide and they have no contribution from deep sources. The amplification of the vertical component of motion is exclusively related to the depth dependence of surface (Rayleigh) wave motion.

Usually it is assumed that the transfer functions of surface layers can be given by the ratio:

$$S_T = \frac{H_S}{H_B} \quad (3.1)$$

where  $H_S$  is the horizontal spectrum of the ground recorded motions on sediment site and  $H_B$  is the horizontal spectrum of recorded on interface between the bedrock and the sedimentary layer. However, considering the great contribution of Rayleigh wave propagation for the ambient noise, it will be necessary to correct the ratio (Equation 3.1), in order to estimate a transfer function from microtremor measurements. Assuming that the vertical tremor is not amplified by the surface layers, the ratio  $E_R$  defined below should represent the effect of the Rayleigh wave on the vertical motion:

$$E_R = \frac{V_S}{V_B} \quad (3.2)$$

Assuming that the effect of the Rayleigh wave is equal for both vertical and horizontal components  $E_R = 1$ . Therefore the interface of the bedrock/sediment is one. It is possible to define a corrected modified spectral ratio  $S_T$  (Equation 3.1), by obtain another transfer function (3.3) below:

$$S_{TT} = \left( \frac{S_T}{E_R} \right) \quad (3.3)$$

$$S_{TT} = \left( \frac{H_S}{H_B} \right) / \left( \frac{V_S}{V_B} \right) \quad (3.4)$$

As a final condition it is assumed that for all frequencies of interest, and according to the observations conducted by Nakamura, the ratio horizontal to vertical is around one (Nakamura, 1989):

$$\frac{H_B}{V_B} = 1 \quad (3.5)$$

Thus, an estimate of the transfer function is given by the spectral ratio between the horizontal and the vertical components of the motion at the surface:

$$S_{TT} = \left( \frac{H_S}{V_S} \right) \quad (3.6)$$

(Nogoshi and Igarashi, 1971) compared H/V of Rayleigh waves with microtremors H/V of and concluded that microtremor motion was mostly composed of Rayleigh wave. The theoretical studies such as Lachet and Bard (1994), Konno and Ohmachi, (1998), suggested that peak on H/V ratio can be explained with the fundamental mode of the Rayleigh wave. Many researchers agree on the following arguments; First, H/V is basically related to the ellipticity of the Rayleigh waves, which are predominant in the vertical component. Second, that ellipticity of the Rayleigh wave is frequency dependent and exhibits a sharp peak around the fundamental frequency for sites, with a high enough impedance contrast between the surface layer and the bedrock layer. (Nakamura, 2000) reports that the peak in the H/V ratio from microtremor of earthquakes cannot be explained with Rayleigh waves, because the Rayleigh wave energy is very small for the peak frequency but high on the trough of the H/V ratio. As it is

explained by Nakamura (1989), H/V of microtremor at peak frequency range can be explained with vertical incident SH wave.

The H/V method is attractive because the data can be easily collected and it can be applied in areas of low or even no seismicity. Other researchers have pointed out the correlation between the H/V peak and the fundamental resonance frequency of the site is used to mapping the layers underground. Recently H/V method has been used to estimate the site effect in large urban area (SESAME European project, Site Effect Assessment using Ambient Excitations) (Atakan et al., 2004).

### H/V spectral ratio of weak motion

This method consists in taking the spectral ratio of the horizontal and the vertical components of the shear wave part of weak motion recordings. This method is in fact a combination of Langston's (1979) "receiver- function" method for determining the vertical structure of the crust from the horizontal to vertical spectral ratio of teleseismic P-waves and Nakamura's proposal (1989) to use this ratio with recordings of ambient vibrations (Equation 3.6). The only thing is different from H/V ratio method obtained by using ambient noise is the wave source comes from below and with S, P and coda waves are considered. This method is obviously interesting, because of its simplicity and economy. It was first applied to the S-wave portion of the earthquake recordings obtained at three different sites in Mexico by Lermo and Chavez-Garcia (1993). These recordings exhibit very encouraging similarities between the standard spectral ratios (see next section) and the H/V ratio method, with a good fit in both, the frequencies and amplitudes of the resonant peaks. The same technique has been also checked on various sets of weak and strong motion data (Bonnilla et al., 1997; Chavez-Garcia et al., 1996; Lachet et al., 1996) from which several conclusions appear well established.

Theodulidis et al. (1996) showed that H/V spectral ratio can be applied to earthquake data records to study site response. Site response estimations analyzed by the H/V spectral ratio and other methods were compared and evaluated by Field and Jacob (1995). (Wen et al., 2006) observed the shape of the horizontal to vertical spectral ratio exhibits a good experimental stability. It is also well correlated with surface geology, and much less sensitive to source and path effects "a warning should be issued for near field recordings

of large events, because of the strong directionality of the near-source "fling" or "killer pulse" (Wen et al., 2006).

### Standard Spectral Ratio of weak motion

One of the most common methods for estimating the site response is called Standard Spectral Ratio (SSR), introduced first by Borchardt in 1970. It is still widely used for estimate the site effect in regions of moderate seismicity. The method involves recording microtremor data from the sites which will be investigated. It requires a reference station on hard rock, and another stations recording on sediments (soft-soil). It is assumed that signals from the hard rock site are equally amplified well at all frequencies. On the other hand, a soft-soil site amplifies the signal at its resonance frequency, which depends on many factors such as the soil type and the basement configuration. Hence, if the source and the path effects are negligible, then we should get a flat spectrum at a hard-rock site and spectra showing peaks at resonance frequencies at soft-soil sites. It is assumed that the source of microtremor and the path through which the surface wave's travels to both the sites are identical. This assumption holds true when both sites are very close to each other.

In estimating the site amplification, the large amplitude S- wave part of the seismogram is extracted using a pointed window and the extracted data is used to calculate the spectral ratio with respect to the reference station. This method is designed to minimize the source and the path effect. Several researchers have presented the theoretical backgrounds of this method. Borchardt (1970) gave a simple description of it. The effect on the seismogram can be visualized as follows:

Assume that  $e_{ij}(t)$  is the source effect of the  $j$ th event (input) and the output seismogram  $s_i(t)$ . The ray paths are affects for the  $i$ th station and  $j$ th event by three elements- earth's crust ( $h_{ej}(t)$ ), geology of the site ( $h_{gj}(t)$ ) and the recording instrument ( $h_{rj}(t)$ ). In first approximation each effect on the seismogram can be considered as linear. Hence, the final seismogram may be given as;

$$s_i(t) = e_{ij}(t) * h_{ej}(t) * h_{gj}(t) * h_{rj}(t) \quad (3.7)$$

where “\*” denotes the convolution operator. In the frequency domain, we operate a Fourier transformation by changing small letters to capital letters. And by changing the convolution operator into multiplication “.”, it is become the expression takes the form;

$$S_i(f) = E_{ij}(f) \cdot H_{ej}(f) \cdot H_{gj}(f) \cdot H_{rj}(f) \quad (3.8)$$

The ratio of the absolute value of the Fourier transform of a seismogram recorded on the sedimentary layer ( $S_s(f)$ ) to that recorded at a nearby bedrock station ( $S_b(f)$ ) is called SSR. It providing that has been made was that the two sites are close to each other and the source and path terms are considered to be same. If we use the same type of instruments at the both sites then the influence of the instruments can also be considered the same for the two sites under investigation. The ratio for the two sites can be reduced to:

$$\left( \frac{|S_s(f)|}{|S_b(f)|} \right) = \left( \frac{|H_{gs}(f)|}{|H_{gb}(f)|} \right) \quad (3.9)$$

Bedrock doesn't change the frequency characteristics of the signal as much as a thick sedimentary layer; hence the ratio  $|S_s(f)| / |S_b(f)|$  will, to a first approximation, be the seismic amplitude response of the sedimentary layer. The ray path contribution between the source and the local site must be small in order for the method to hold (Borcherdt, 1970).

The motions from the 1957 and 1906 earthquakes in San Francisco caused great damage, and the geological conditions may have been the amplification factor (Borcherdt, 1970). The amplification effect of the local geology could was estimated analyzing the nuclear- explosion recordings. The amplifications for the sedimentary site are better estimated from ground motions generated by nuclear explosion, than from those generated by moderate earthquakes. Therefore, due to the non- linearity, as the magnitude increased, the amplification at a certain frequency decreased. However the site effect estimated by SSR techniques may be considered an overestimation or upper limit

of the actual site effects at high frequencies, and a slight underestimation at frequencies below to fundamental frequency (Borcherdt, 1970).

When using the SSR technique two factors must be considered; first, the reference site should be located near enough to the site of test to ensure, that differences between each site are only due to site condition. The difference in source radiation pattern or travel path must be larger, which is generally valid when the hypocenter distance is larger than about 10 times the distance between the sites. Second, the reference site should be unaffected by any kind of site effect, which is the case when the reference site is located on an unweathered bedrock.

(Theodulidis et al., 1996) obtained good correlation between (SSR) and H/V ratio in southern part of California. According to him, this motions give more information about the site effects than the commonly used average shear- wave velocity in the upper 30 m. Suzuki et al (1995) both microtremor and strong- motion data in Hokkaido, Japan, showed that the frequency from the H/V spectrum seems to correspond well to frequency estimated theoretically from the thickness of the alluvial layer.

There are some disadvantages of the SSR technique as mentioned by several studies (Atakan et al., 1996; Bard, 2004) that we discussed below.

1. The trigger recording of the network. If we operate a network that use triggered recording, then often due to difference in the noise level at different site not all station from our network will trigger. Then if the reference station does not trigger it will be impossible to compute standard spectral ratios.
2. A proper reference site is sometime impossible to find. The best choice for reference site is at the situated on flat crystalline outcrop. If we have two different reference sites (crystalline rock outcropping) at more than one place in the study area we will get different response, and the site reference sites will have site response that will influence our estimations.
3. The influence of the surface topography. The buildings are suite on hill tops have suffered much more damage than the site located at the low sites, because of topographic effects (Hasancebi and Ulusay, 2006). There is also very strong instrumental evidence that surface topography considerably affect the amplitude and frequency content of the ground motion. Theoretical and numerical models

- made by Pedersen et al (1994) predict complex amplification and de-amplification patterns on hill slopes, resulting in significant motion. Very often, measurement show larger effect than what is predicted by the simulation. A possible explanation is that in many cases weathered rock is found at the top of hills which further reinforces the topographic effect (Pedersen et al., 1994).
4. Earthquake parameters such as distance, azimuth, magnitude and thickness of the sediment basin are important factors of the site response estimation. We will take for example the study in Mexico City which explained the effect of the spectrum effect in site response. According to Castro et al (1988) the frequency at which maximum relative amplification occurs varies from site to site in near Mexico City. He suggest that  $f_0 = \beta/4H$  where  $f_0$  = frequency at which maximum relative amplitude occurs,  $\beta$  and  $H$  are the shear wave velocity and thickness of the soft layer respectively. For a given lake bed site the maximum relative amplification and  $f_0$  are roughly constant, independent of magnitude, depth, and azimuth on the source if site at located more than 200 km away.
  5. The SSR method is expensive and time consuming. If we want to measure many places to investigate the site response, we will need more instruments and employees. In addition we need to wait for an earthquake with a significant magnitude. If the area studied has a low seismicity, it takes a longer time to have any relevant result. This may give high cost and it might take time to get information.
  6. Quality of data set. The nonlinear site effects in strong- motions are very common. Reviews from such nonlinear site effect studies may be found in (Wen et al., 2006). The soil tends to damp more the energy from large amplitude ground motion. The nonlinear amplification means that the site response must also be calibrated as function of the amplitude. Nonlinear amplification at sedimentary sites was inferred by Chin and Aki (1991) who report that for sedimentary stations within 52 km of the epicenter of the Loma Prieta earthquake. According Inazki (2004) to the evaluation of the nonlinear properties of near-surface soil under strong motion may be estimated by using shear wave vibrator as a dynamics loading source.

### 3.1.2 Description of the two sets of data

#### Ambient noise record used

The method used to estimate the site response spectra in Omdurman and the eastern area of Khartoum city is based on the H/V spectral ratio technique using ambient noise record. The method has already been explained in section 3.1.1. The method was evaluated thoroughly and a dedicated software (J-SESAME) has been developed during the European project “Site Effects Assessment using AMbient Excitations (SESAME)” (Atakan et al., 2004; Bard, 2004). More information about the SESAME project can be found in the web page <http://sesame-fp5.obs.ujf-grenoble.fr/>

In following sections, a short description of the instrument, software used and the data collected during the survey is given. The focus is in particular the sequence of steps that have to be performed and to obtain the site response spectrum at different sites.

#### Measurement Sequence

The source of ground motion of the ambient seismic noise is present in the ground. In our survey, the ambient noise recording in different sites was recorded and the J-SESAME package software (<http://www.geo.uib.no/seismo/software/jsesame/jsesame.html>) was used to compute the spectra ratios (Atakan et al., 2004). Four instruments are used:

- 1-Three components seismograph portable seismic station (model GeoSIG GBV-316) from the Department of Earth Science (GEO) at the University of Bergen (UiB) is used. It is used to record the ground motion of the ambient noise. The seismometers are three-component 4.5Hz geophones, perpendicular to each other. The GeoSIG GBV 316 is a very compact and complete 16-bit seismograph with built in sensor and battery. The recording capacity is up to 64 Mb, which at 100 Hz sample rate gives 5 days of continuous recording, although it is more typically used with smaller memory and in triggered mode recording. It contains a GPS, which consumes typically 3 W and through the serial line one can communicate with the acquisition software SEISLOG (Utheim et al., 2001).

- 2-Computer with software installed to transfer the digital data from sensor into database folder.



3- Global Positioning System receiver (GPS) to determine the exact location, direction, and elevation of the site measurement.

4- Magnetic compass to determine the orientation of the instrument.

### Instrument testing

The acquisition system (SEISLOG software) is used with parameters in order to record and transfer data from sensor. The specifications parameters are given in Table 3.1. Before the survey started, several tests are made in order to ensure that the instrument is working properly. The tests are made both inside and outside the seismological laboratory of the GEO-UiB and also in the study area. Figure (3.1) and (3.2) show the noise power spectra of the vertical-channel tests of the GeoSIG GBV-316 seismic sensor. These two tests were made on two different sites in our study area (hard rock and soft soil site). The noise power spectra at the sedimentary site have higher amplitude. In sedimentary sites the ambient noise is due to sources generated by traffic on upper layers.

*Table (3.1) the main specification of the GBV-316 and the seismic data acquisition system are used in our survey. Modified from (Havskov and Alguacil, 2006).*

<i>Sensor</i>	3 geophone( BGV-316)
Frequency response	4.5 Hz
Sensor generator constant	28 V/(m/s)
Amplifier gain	$131 \cdot 10^6$ counts/V
<i>Digitize</i>	
A/D converter	16 bit
Noise	$\pm$ bit at gain 1000
Sampling rate	100 sps per channel
Bandwidth	20 Hz
Input rang	$\pm 2.5$ V DC
Anti aliasing filter	6- poles antis filter at 18.5 Hz
Rs-232	1 sec data buffer or sample per sample
<i>Data recording</i>	
Pre event memory	1 to 30 s

Post event memory	1 to 100 s
Compression factor	2.0
<i>Triggering</i>	
Level triggering	no
Lower band limit	0.1 Hz
Upper band limit	3 Hz
Trigger threshold	0.1 to 100 % full scale
STA/LTA triggering	
STA- base	0.1
LTA base	1
STA/LTA	No
Solid state memory	2 to 64 Mb
<i>Power supply</i>	
Type	External power supply 17 to 30 VDC
Internal battery	12 V rechargeable lead acid battery
Battery regulator	Internal
Autonomy	48 hours
Power consumption	1 W at 12 v Dc
<i>Time base</i>	
Clock accuracy	10 ppm(10 min/year)at – 10 <sup>0</sup> C to +50 <sup>0</sup> C
External time interface	GST optional
<i>Communication</i>	
Serial ports	2
Baud rates	2800
Communication protocol	Binary
Protocol securities	Checksum and software handshaking
Communication	PC/RS-232 port or modem
<i>Environment/Housing</i>	
Operational temperature	-20 <sup>0</sup> C to + 70 <sup>0</sup> C
Humidity	0% to 100%(non condensing)

Site	18*18*10 cm
Weight	5.2 kg with the battery
Protection	IP54
Connectors	
RS-232	Communication, parameter setup, data download, time tagged data buffer output
GPS	Continuous or cycled operation
External sensor	Connection of external sensor
Power	External power supply, external battery

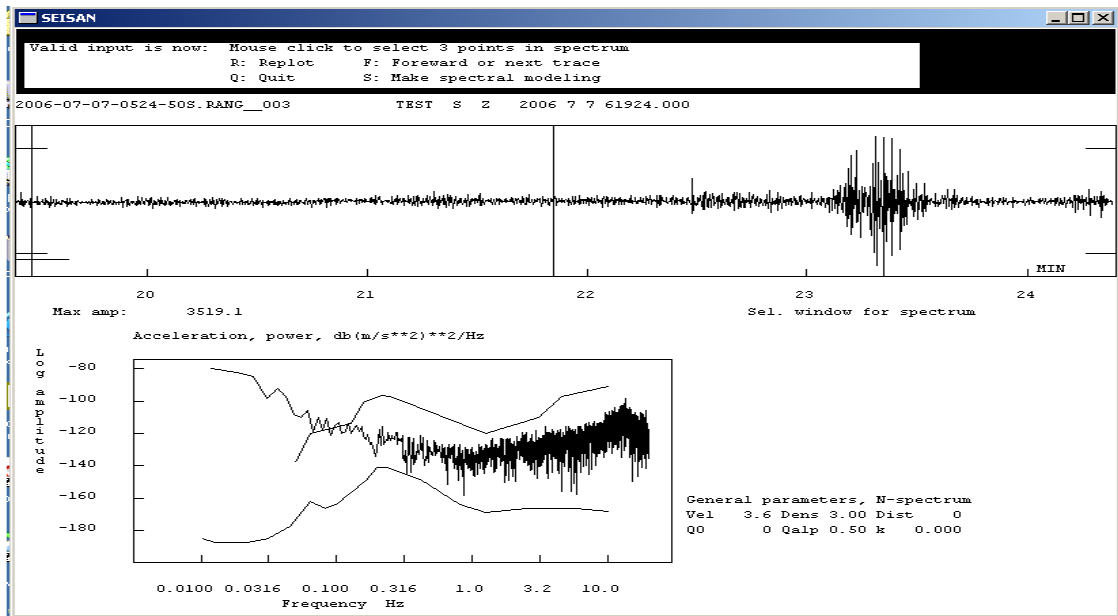


Figure 3.1: Recording and Power noise spectrum from basement complex rock site in the north eastern Khartoum area. The upper figure shows the seismic noise recording of the Z- component. The lower figure shows the equivalent ground acceleration noise power spectrum for a short period seismometer using GBV-316. The smooth curves on top and bottom are the Peterson Lower- Noise and high- Noise models, given as reference.

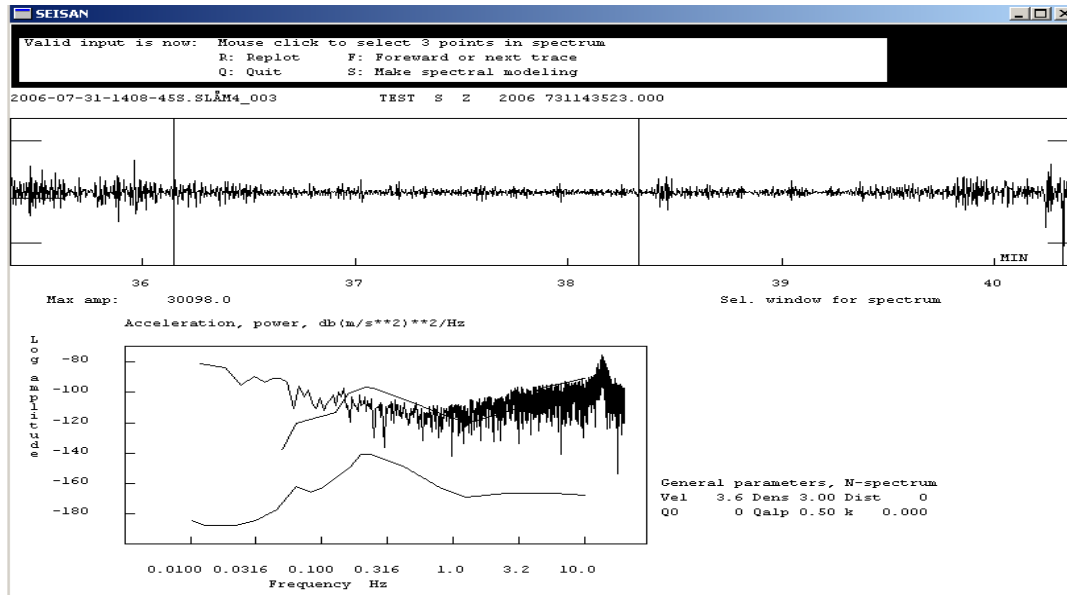


Figure 3.2: Recording and Noise spectrum of seismic noise in sediment rock site on the Khartoum basin. The upper figure shows the seismic noise recordings of the Z-component. The lower figure shows, the equivalent ground acceleration noise spectrum for a short-period seismometer, using GBV-316. The smooth curves on top and bottom are the Peterson Lower- Noise and high- Noise models, given as reference.

The capital city of Sudan, Khartoum is divided in to a grid of points on the map to conduct the site measurements. Considering the time for the survey, two plans are made in order to cover the whole study area. The first step was to create a grid which is able to cover most of the homogeneous geological units in the study area. The second step is to conduct further analysis which is focused on collecting more measurements in each unit. In order to have the best measurements, the quiet places are chosen away from possible noise sources (e.g. streets with heavy traffic). Also the buildings under construction, factories, and other industrial sources that may introduce man made noise in our data were avoided. To keep away from direct sun light on sensor and pocket computer was also necessary to make the instruments work. The variation of temperature in the period from 29<sup>th</sup> June to 14<sup>th</sup> August affected the response of the instruments. The average temperature was around 30<sup>0</sup> C.

Once the site was selected, the flat places where the instrument could be placed horizontally were found. The magnetic compass was used in order to orient the instrument to the north. The instrument was connected to the pocket computer and with

GPS by a serial line. The pocket computer had a SEISLOG program which is used for seismic data acquisition (Utheim et al., 2001).

DATE		HOUR		PLACE	
OPERATOR			GPS TYPE and #		
LATITUDE		LONGITUDE		ALTITUDE	
STATION TYPE		SENSOR TYPE			
STATION #		SENSOR #		DISK #	
FILE NAME				POINT #	
GAIN		SAMPL. FREQ		REC. DURATION	
		Hz		minutes seconds	
WEATHER		WIND <input type="checkbox"/> none <input type="checkbox"/> weak (5m/s) <input type="checkbox"/> medium <input type="checkbox"/> strong		Measurement (if any): _____	
CONDITIONS		RAIN <input type="checkbox"/> none <input type="checkbox"/> weak <input type="checkbox"/> medium <input type="checkbox"/> strong		Measurement (if any): _____	
		Temperature (approx): _____		Remarks _____	
GROUND		<input type="checkbox"/> earth ( <input type="checkbox"/> hard <input type="checkbox"/> soft)		<input type="checkbox"/> gravel <input type="checkbox"/> sand <input type="checkbox"/> rock <input type="checkbox"/> grass = ( <input type="checkbox"/> short <input type="checkbox"/> tall)	
TYPE		<input type="checkbox"/> asphalt <input type="checkbox"/> cement <input type="checkbox"/> concrete <input type="checkbox"/> paved <input type="checkbox"/> other _____			
		<input type="checkbox"/> dry soil <input type="checkbox"/> wet soil		Remarks _____	
ARTIFICIAL GROUND-SENSOR COUPLING <input type="checkbox"/> no <input type="checkbox"/> yes, type _____					
BUILDING DENSITY <input type="checkbox"/> none <input type="checkbox"/> scattered <input type="checkbox"/> dense <input type="checkbox"/> other, type _____					
TRANSIENTS		MONOCHROMATIC NOISE SOURCES (factories, works, pumps, rivers...)			
		<input type="checkbox"/> no <input type="checkbox"/> yes, type _____			
		NEARBY STRUCTURES (trees, poles, buildings, bridges, underground structures, ...)			
		(description, height, distance)			
		cars			
		trucks			
		pedestrians			
		other			
OBSERVATIONS		FREQUENCY:		Hz	
		(if computed in the field)			

Figure 3.3: The field measurement sheet and the boxes where we write the local name, location, local time and GMT, instrument, environment, weather conditions, geology (either outcrop or borehole) From (Atakan et al., 2004).

The first step is to configure the device and the channels correctly in the SEISLOG program, which must have three components installed, one vertical component and two horizontal components E-W and N-S. To check that the system is running well, it is necessary to monitor all channels for some time, to perform a test by pushing the instrument and checking that it works in the display of the screen. The name of the site of the measurement was written in a way to identify the data later on during the analysis. In order to get clean records, it was necessary to have a delay time before the start of the recording, in order to avoid that the noise associated with human activity which influence our measurement. The recording time duration at each site was approximately 30 minute length on about 80% of total sites. In other sites recordings were made with 10 minute duration. A stopwatch was used to determine the time of recording. During the recording time, the notes on a special field measurement sheet given in figure 3.3 were collected. The field measurement sheet was taken from the SESAME project (Atakan et al., 2004). In this form, the most important observations mentioned are the date, GMT time, local time, geographical coordinates as given by the GPS, name of the site. Also the presence of all nearby sources that may generated transient noise are noted. There are other things taken into account, such as the temperature and the noise, as well as the weather conditions caused by wind or rain.

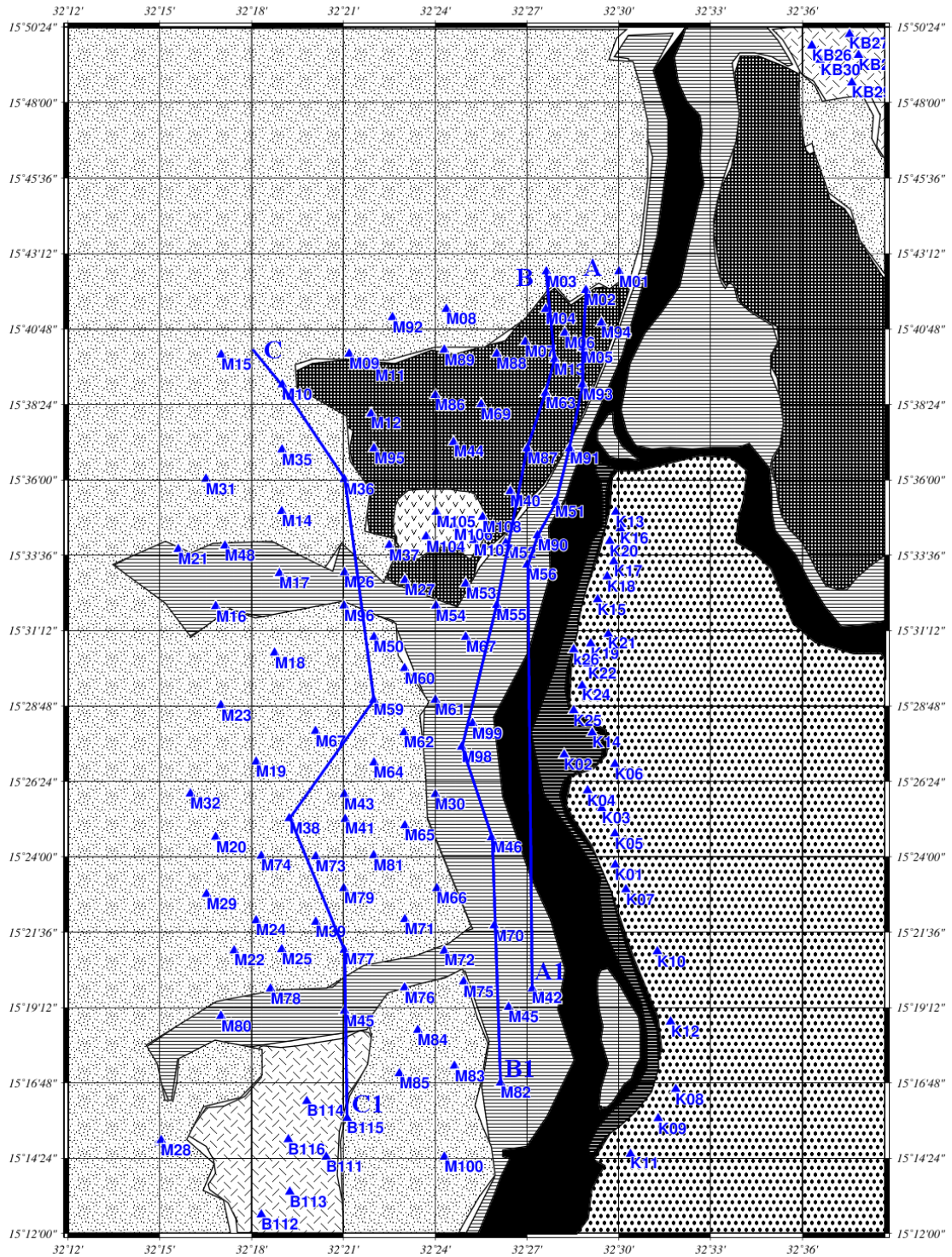
After the measurements at the end of the day, the data is transferred from the instruments to a computer, where all waveform data are collected in a folder called WOR.

### Distribution of measurement sites








The collected data set during the survey in western Khartoum consists of 147 sites. Figure 3.4 shows the location of these sites and the different geological units. All measurements were collected during the summer holiday.

The measurements were taken during the day and sometimes during the night. The distance between the sites is about 500 m. Transportation of the equipment was conducted by a car. Each day about 10 to 20 sites were covered. In order to determine most accurately of the site location, two GPS receivers were used one inside the system and another extra outside (Garmin TM serial number V 93120003).

*West of Khartoum city– Geology and site location*

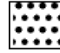


*Figure 3.4: Map of the study area (Western Khartoum) and locations of the sites - Blue triangle shows where the measurements were made. **M** is Omdurman site, **B** is basement complex rock in Omdurman site, **K** is Khartoum sites M104 to M108 are basaltic sites, **KB** is basement complex in Khartoum site). Three cross-sections are also shown which cross*

some of our measurement sites (A, B and C). The regions of interest with the geological formations are as follows;  Recent alluvial deposits with consolidated soil.  Recent alluvial with unconsolidated soil.  Older alluvium.  Gezira formation.  Cretaceous Sandstone.  Basaltic rock.  Basement Complex.  Nile River, Modified from (GRAS 1988 and 2006).

### Weak motion data used

As mentioned in chapter one section 1.3.2, there are about 22 local earthquakes in the area around Khartoum city. Among these, 12 events are located by the SSN during the period from November 2003 to March 2007. The remaining 10 events are located by global stations. Three stations of the SSN network are placed around the Khartoum city. Two of them are located on sediment layers (MRKH and JAWL) and one station was located on hard-rock basement complex (SLAT). More information about these local events is given in Table 3.2. The distribution of the stations and the location of events are shown in figure 1.3. Among those there are 7 earthquakes recorded by all stations, while the rest of the events are recorded and located either by one or two stations. In this study, only six events are selected and divided into two groups depending on the location and the distance from the recording stations; the first group contains two earthquakes shown as number *EQ10* and *EQ6* and the second group contains events that are numbered *EQ2*, *EQ3*, *EQ4* and *EQ8*. Other events are considered to be inappropriate, because either they are located close to the stations such as event *EQ7*, *EQ9* and *EQ5* or they were located far from the station but located only by one station such as *EQ1*, *EQ12*, and *EQ11*. Both these data sets violate the main assumption of the SSR method (i.e. far-field approximation). The method is only valid in cases where events are located far from both the sedimentary and bedrock stations.

Table 3.2 Local events were recorded by SSN. Each event number is given in the right column of this table the number is the same as the number in the figure 1.3.

Event number	time	lat	long	Depth (km)	Magnitude
1	20031105	15.864	33.598	10	2.9CSSN
2	20031114	15.374	31.688	22	2.8CSSN 3.0LSSN 2.9WSSN
3	20040112	15.424	31.677	15	2.5CSSN 2.5LSSN 2.7WSSN



4	20040214	15.750	31.448	10	2.5CSSN2.5LSSN 2.6WSSN
5	20040702	15.659	32.553	0	1.7LSSN 2.4WSSN
6	20040917	14.613	30.390	15	3.7C SSN3.2LSSN
7	20040321	15.396	32.370	4	2.0CSSN 1.9LSSN 1.8WSSN
8	20040516	15.004	32.225	5	2.4C SSN2.4LSSN 3.0WSSN
9	20060505	15.631	32.048	4	2.2C SSN2.2L SSN3.3WSSN
10	20060623	13.563	29.652	15	3.9CSSN 4.0LSSN 3.7WSSN
11	20060904	16.437	31.580	15	2.6CSSN 2.4LSSN
12	20070311	14.539	32.989	15	2.4C SSN2.5LSSN

## 3.2 Analysis and results

### 3.2.1 Analysis of H/V ratio of ambient noise data

#### Processing of the recorded data (with SEISAN and J-SESAME)

In order to determine the H/V ratio and fundamental site frequency from the noise recordings three software are used SEISLOG, SEISAN and JSESAME.

The first software SEISLOG was used for data acquisition and transfer of data from the instrument into the database folder. In this software it is possible to make adjustments to the site name, to triggering parameters (STA and LTA, lower and upper band), and the time duration of the recording. The second software used was SEISAN earthquake analysis software (Havskov and Ottemöller, 2005). The SEISAN package consists of a number of programs to analyze and process earthquake. Two programs are applied in SEISAN, called DIRF and WAVETOOL. The DIRF program is used in order to make a file with a numbered list of events called *filenr.lis*. WAVETOOL is a program used to convert files into different data format. Here, it is used to convert our data from SEISAN format in to GSE format. The GSE format is then used in the J-SESAME software.

The third software used is the J-SESAME (Atakan et al., 2004), which is designed to process and calculate the spectral ratio of the horizontal to that of the vertical components from the records of ambient seismic noise (the so-called H/V method). More information for the software can be found in the *Guidelines for the implementation of the H/V spectral ratio technique on ambient vibrations: SESAME European research project*

WP12- Deliverable D23.12 (Atakan et al., 2004). These guidelines are available through the following web-site: <http://www.geo.uib.no/seismo/software/jesame/jesame.html> .

The J-SESAME software consists of four basic modules that are; the browsing module, the window selection, the processing module and the display module.

The individual sites are inserted from the screen menu to create the site name and the measurements are then registered in a virtual database which is displayed in a subfolder. In these subfolders data files are inserted which consists of the waveform files of the seismic noise recorded at each site. All these waveform files are stored in GSE format. Calculating the H/V spectral ratios and different operations on the waveform files such as filtering, windows selection and processing are discussed below.

In the window selection module, specified time windows can be selected from the recorded trace with different lengths either manually or automatically. In the case of the automatic window selection a simple STA/LTA triggering and de-triggering algorithm is used to isolate the quiet parts of the signal. Manual selections are made only when the automatic selection algorithm does not function optimally on a given trace. The recordings could contain transient's pulses from various sources such as traffic or heavy machineries. The best way to avoid these transients is by manual selection. But this option takes time and it is not appropriate for processing large amounts of data.

Optionally, long term transients are excluded, which will not affect the (STA/LTA) ratio but will not represent the true seismic noise. Once a window is selected the algorithm looks for the next window until it covers all recording.

The processing module can perform several tasks, such as the filtering, the removal of the DC, smoothing, and computation of the H/V ratio. The parameters that are used to select windows in J-SESAME are given in Table 3.3.

*Table 3.3 parameter we used to select windows in J-SESAME software.*

Window	Time Period (sec)
Window length (sec)	10.0 or 20
Space between windows(negative for overlapping (sec)	1.0
<i>Windows selection parameter</i>	
Window length for the short term STA in (sec)	1.0

Window length for the long term LTA in (sec)	25.0
Minimum level for STA/LTA in (sec)	0.5
Maximum level for STA/LTA threshold	2.0
Window length for selected window in (sec)	10-20
Overlap percentage for selected windows	10.0
Level for bad points (sec)	0.0

An example of display of H/V spectrum with 10 seconds windows length is given in Figures 3.5 and 3.6 and 3.7. In the view output of the H/V ratio curve, the mean is shown in black curve. The mean multiplied and divided by  $10^{\sigma (\log H/V)}$  show in red and blue color respectively. The pink strip shows the frequency range where the data has no significance, due to the sampling rate and the window length. The grey strip represents the mean of the  $f_0$  plus and minus the standard deviation. It is calculated from the  $f_0$  of each individual window. The H/V ratio spectrum at each horizontal component as NS/SV ratio and EW/SV ratio are viewed individually. It can be discussed for evaluation which one between the two responses represented the most realistic result.

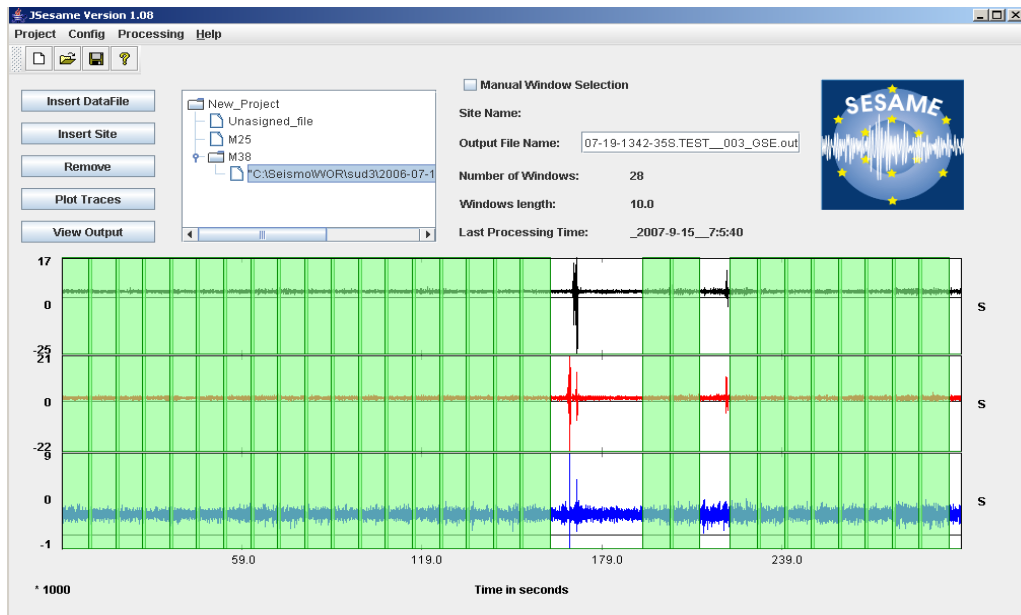


Figure 3.5: General view of graphical user interface of J-SESAME, taken from our data processing. We could see the graphical use where different operations can be performed. Selected windows are shown in green, tracing of three component of seismic ambient noise recording, number of windows that have been selected by automatic windows selection, algorithm with window length and structure of organization data.

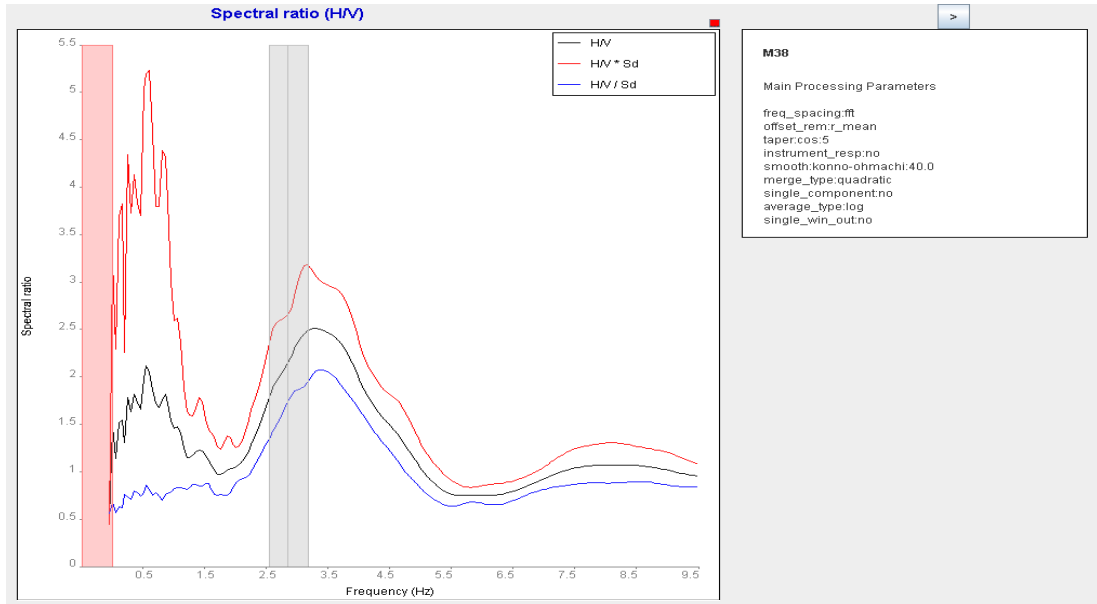


Figure 3.6: *H/V* ratio for the merged horizontal components (mean in black, mean multiplied and divided by  $10^{\sigma(\log H/V)}$  in red and blue). The pink strip shows the frequency range where the data has no significance, due to the sampling rate and the window length. The grey strip represents the mean  $f_0$ , plus and minus the standard deviation. It is calculated from the  $f_0$  of each individual window.

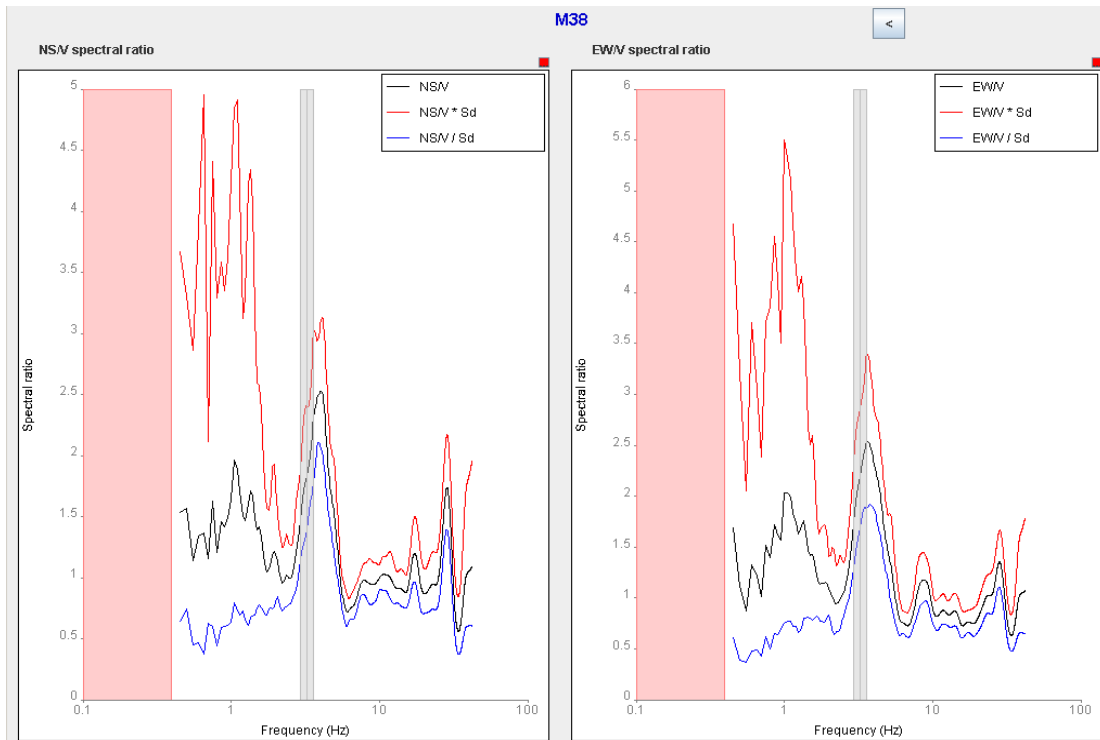


Figure 3.7: *NS/SV* and *EW/SV* are show in individual horizontal components with vertical.

## Description of the H/V ratios in terms of ambient noise and data quality

In order to achieve reliable results, the H/V spectral ratios ideally need to be correlated with analytical site response estimates. Such analytical analysis is highly dependent on the knowledge of the sedimentary layers and their parameters such as the thickness, shear-wave velocity and density. Since such data was not available to us, the present study is entirely based on observations on the H/V spectral ratios. In the future when geotechnical data available the results should be compared to analytical site response estimates. In this study we simply followed the guidelines that are available from SESAME project (Atakan et al., 2004). According to these guidelines, we discussed three major factors; the windows selection, the peak of the H/V ratio spectra and interpretation of H/V ratio in term of the site characteristics.

### Windows selection

Windows selection is an important factor to evaluate the data collected. The survey consisted in measuring the ambient seismic noise in an urban area and obtaining information about the local site condition observed there. It was observed during the survey that conditions such as traffic and building density might affect the data quality. In addition to that, we also observed that within different windows length we could find similar information in the same geological unit. On the other hand, in one of the sites choosing two different window lengths displayed different H/V spectral ratio. This is due to factors such as the duration for recording and the transients in the records. For these reasons, the windows selected for the entire database are categorized into two groups based on window lengths.

Figures 3.8 and 3.9 show two bar diagrams for the number of selected windows per site for the dataset collected in the study area with 20 and 10 second window lengths respectively. About 88% of all the dataset was made recording in 30 minute duration, while in a few sites in 10 minutes. Therefore, to estimate the average of windows selected in two diagrams, a 30 minute recording duration was selected. However, as shown from the two diagrams there is a significant difference in the number of windows selected. The number of windows with 10 seconds windows length is higher than the one with 20 seconds length. The average number of windows per point for the data collected with 10 seconds length is about 22. It was three times the average number of windows with 20

second length. This may be due to the fact that most of the site records were made in areas where transients contaminate the records.

The average number of selected windows per site in sedimentary formations is higher than in hard rock (basement rock and consolidated sandstone), and there the quality of data collected in general is good. According to the SESAME guidelines; in a record duration of 20 seconds, it is better to have 10 windows or above to obtain a reliable computation of the site response spectrum (Atakan et al., 2004). Since the 10 second length windows gives a wider range of recordings (30 to 2 minutes time duration), and as we have shown that in the average number of windows for the dataset is higher than what is needed, we believe that it was better to interpret the site response spectrum for dataset with windows length of 10 seconds.

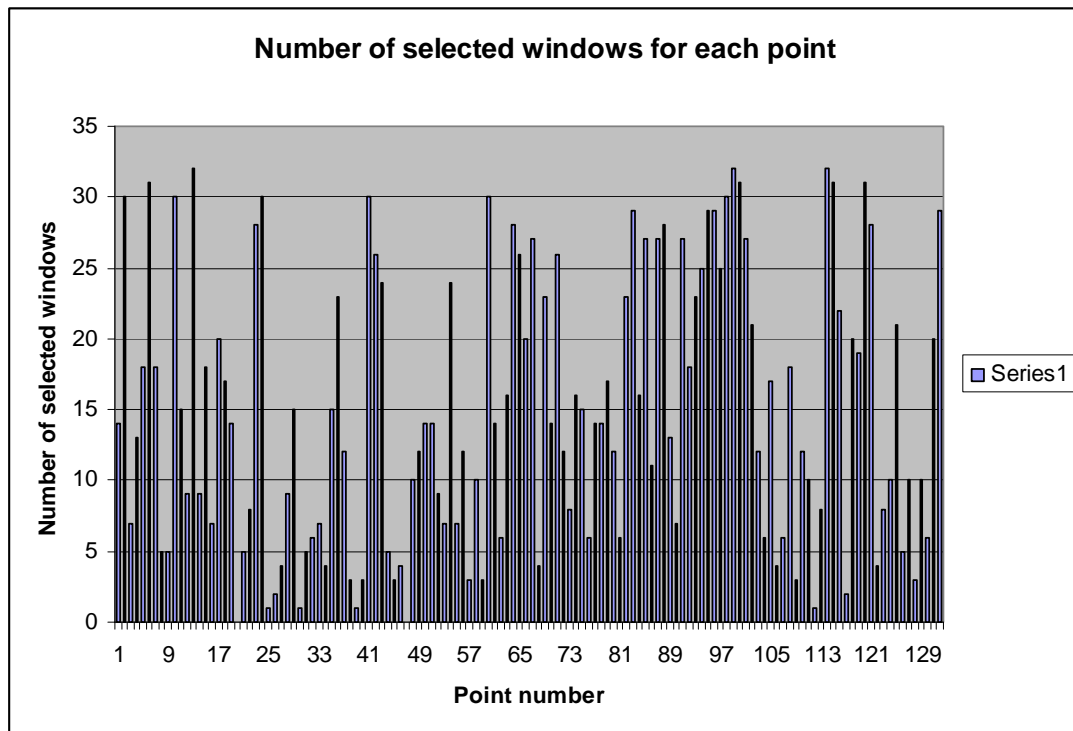


Figure 3.8: Bar diagram showing the number of selected windows for each site from the dataset with 10 second length windows.

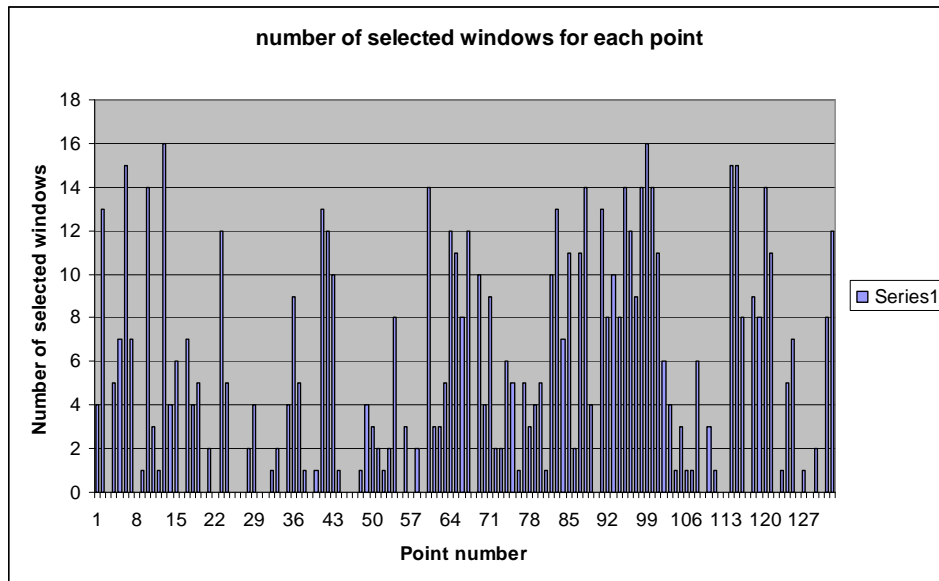


Figure 3.9: Bar diagram showing the number of selected windows for each site from the dataset with 20 second length windows.

### Classification of the H/V spectral ratio results

In order to make a reliable interpretation of the H/V spectral ratios the quality of each identified peak need to be considered. The variation of the shape of the peak in our data is observed and we classify the spectral ratios into three groups as follows;

- 1- H/V spectral ratios with a single clear peak.
- 2- H/V spectral ratios with more than one peak.
- 3- H/V spectral ratios having not a clear peak.

#### *1 H/V spectral ratios with a single clear peak*

The majority of H/V spectral ratios having one single clear peak are divided into two subcategories; the first one has peak amplification at low a frequency and the second one has a peak at high frequency. In the first case, the peak is represented at a frequency ranging 0.8 – 5.0 Hz, (e.g. sites M38 and M90 given in figure 3.10 and 3.11). The interpretations for these sites are relatively easy, because the spectral ratio which has only one high peak is interpreted to be the fundamental frequency. The resulting sharp peaks are usually due to a significant impedance contrast between the sediments and the underlying bedrock. The fact that the site has single peak in the low frequencies range is expected only for the sites where thick sediments exist. The second case where there is a clear peak at a high frequency may be caused by the thinning of the sedimentary layer

under the site, or may be influenced by the high noise generated nearby the site, such as a quarry. Another explanation about the site having high frequency may be due to fact that the site contains little or no sediments on top of the hard rock (e.g. Basement complex rock, given in figure 3.12 for site M114).

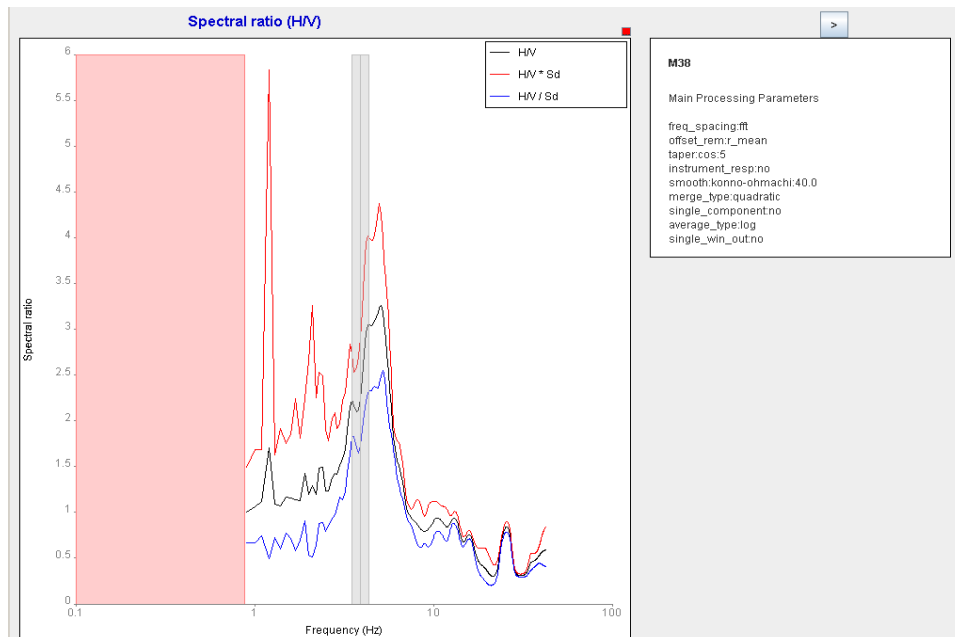


Figure3.10: Clear peak single spectrum computed at site M38, we consider the high peak to be around 3Hz.

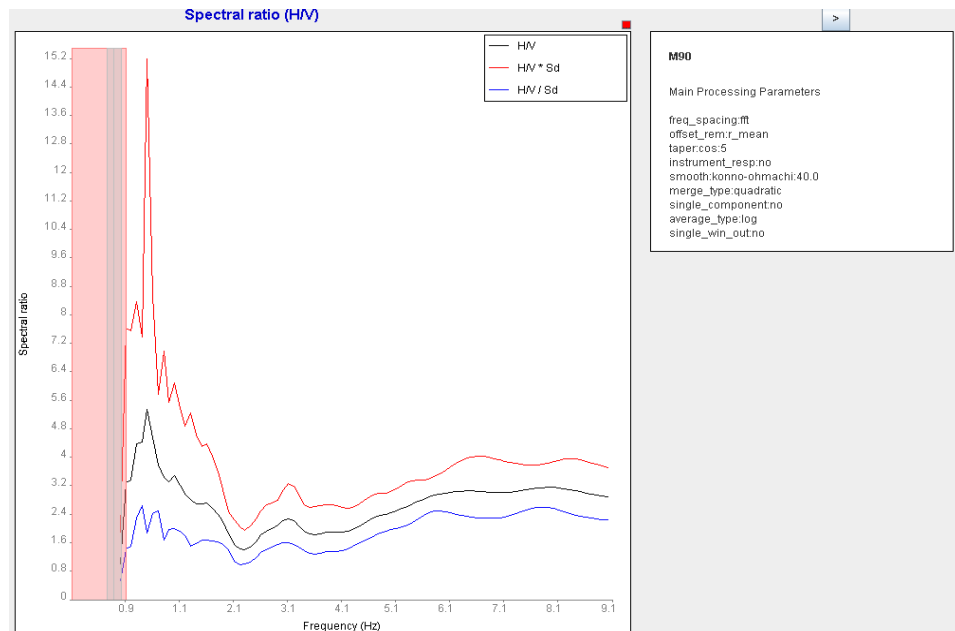


Figure3.11: Clear peak single spectrum computed at site M 90, we could see the clear peak around 1 Hz.



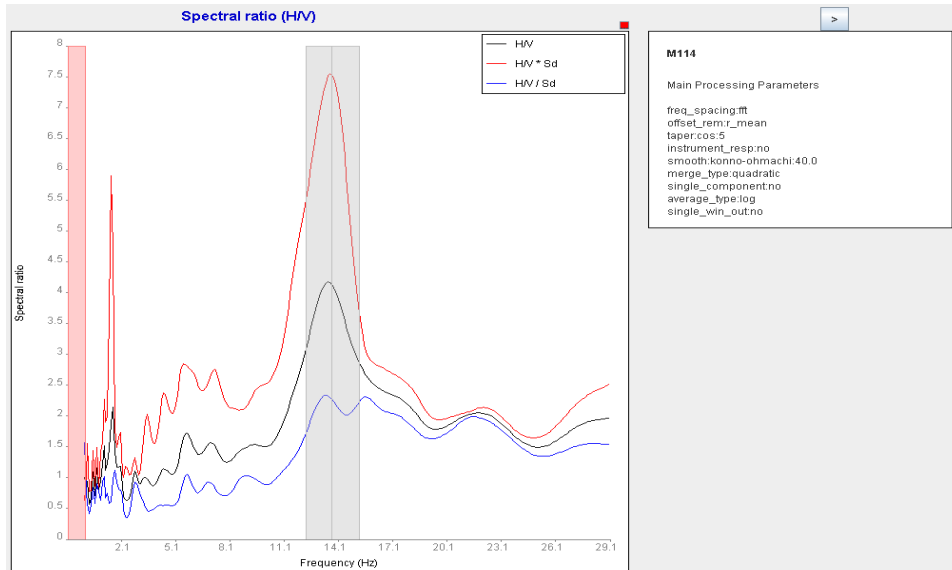


Figure 3.12: site response spectrum at site M114, it is located on Basement rock which clear peak at high frequency. This peak has specific seismic noise of industrial origin.

## 2- H/V spectral ratios with more than one peak.

Most of the site response spectrums in dataset have more than one peak. They are represented at frequencies range from 1 to 22 Hz. Figure 3.13 shows example of site response spectrum which has more than one peak, where we can see spectra computed from site K21. There are only two ways to interpret a site having many peaks; one way is from previous work that the peak at high frequencies does not have meaning if the points are occurring on sediment site. Another way to compute the real peak is to check the two horizontal components (EW and NS) and to establish by comparison which one is the closest to the average spectra, such as showing in figure 3.13. In figure 3.14 we could clearly see that the NS component of the site response spectrum at site K21 has two clear peaks, the higher one at around 3 Hz and smaller one at around 11 Hz, while the EW component has only one peak around 3 Hz. We believe that the reason for having such big difference between the two components may it's beneath site K21 there is an underground structure with a particular geometry such that its side NS direction much different than that in EW different. For instance we may have assumed that we have a simple parallelogram with its NS side much longer than its EW side. For such structure we would expect that the seismic wave will resonate in this direction, in which the distance between the walls of the underground structure is smaller. As the result the

resonant frequency will be visible on that component of the site response spectrum but not on the other one. The reason of the spectrum have double peaks might be by presence source of industrial noise. Or the seismic wave of that point has reflected from different boundaries layers under this point.

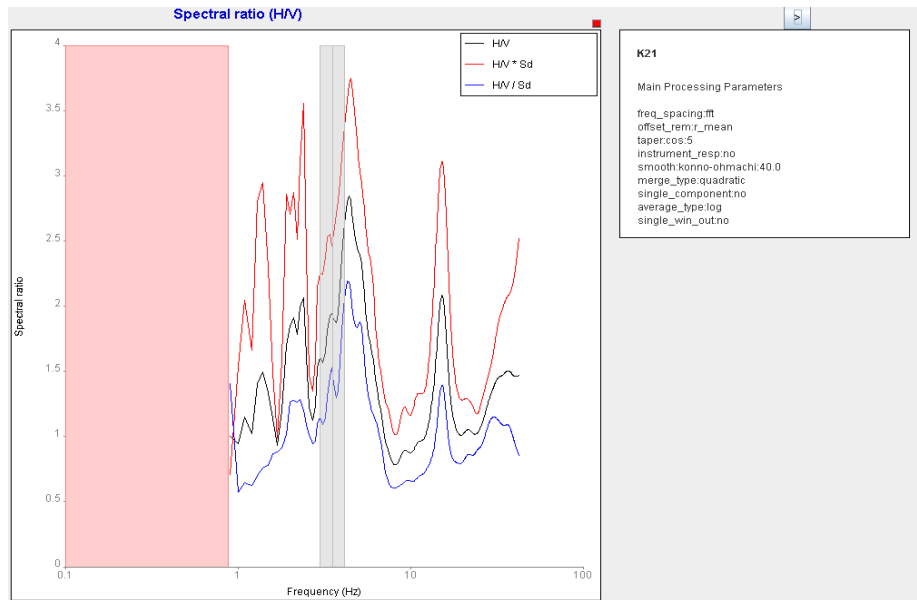


Figure3.13: Site response spectrum computed at site K21. It can see two distinct peaks.

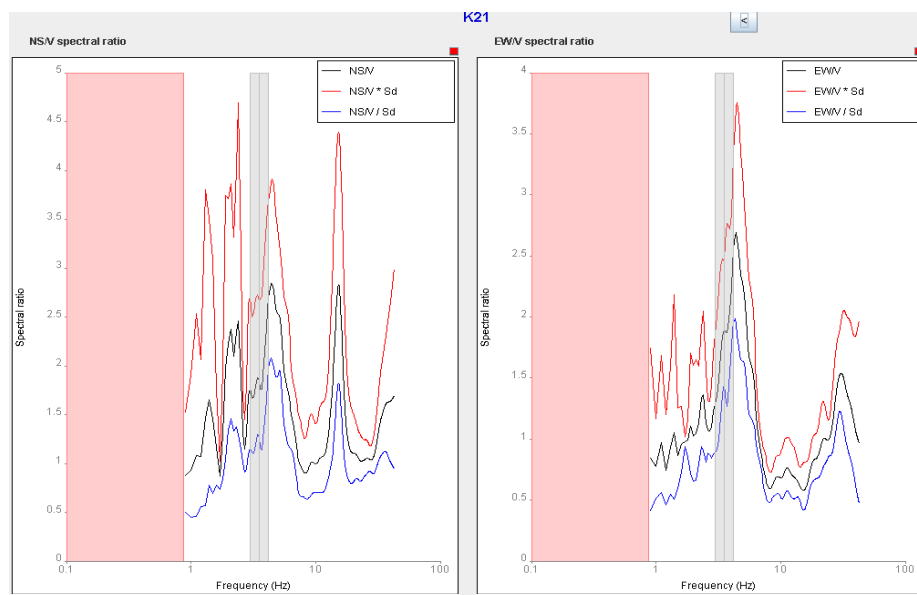


Figure3.14: NS/SV and EW/SV ratio of the site response spectrum computed from site K21. As we could see there is substantial difference between the two components. The peak around 3 Hz is visible on the both components while the one at around 12 Hz is seen less amplitude in EW component. Most likely the structure is elongated predominately in NS direction.

### 3- H/V spectral ratios having no clear peak or extensive shape.

A few of our dataset is composed by site response spectrum without any clear peak, or with peaks which are difficult to distinguish. It is difficult when we have the same shape in NS and EW components either in amplitude or in frequency. The reason for that is that the area underground that point is the structure more complex or some waves are produce as a result of human activity. We interpreted these sites with correlation to borehole data in the nearby measurement site. Figure 3.15 and 3.16 shows the example for this case computed from the site M66.

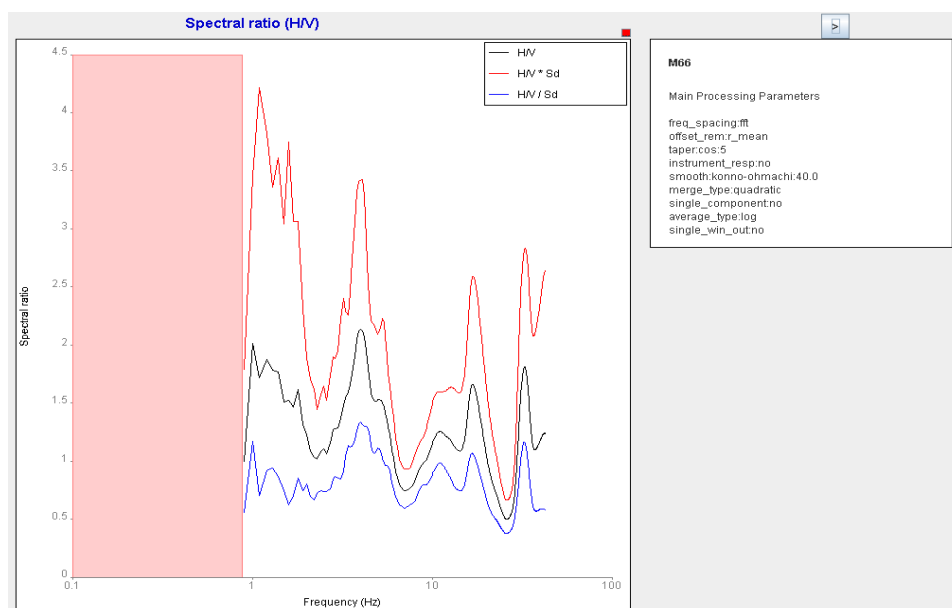


Figure 3.15: Site response spectrum at site M66. It can be seen its shape is very complex and no clear can be distinguished.

In all the case above, a different response is produced in the same formation. The concept of this method is to have a variation of the frequencies according to different sedimentary thickness. The clear high frequency peaks observed at the site M114, KB 29 and M106 are examples of anomalies with high frequency overlying hard rock (basalt and granite). The bedrock is expected to have amplitude around 1, but this value is not always represented in some sites. It is may be due to thin sedimentary layer between the sensor and the rocks that can account for the high frequency. Reiter (1990) observes the proportion between the thickness of the sediment ( $H$ ) and S- wave velocity ( $\beta$ ) in the layer. It is given the fundamental frequency ( $f$ ) in the following Equation 3.10;

$$f = \frac{\beta}{4H} \quad (3.10)$$

According to the equation above the very thick sediments have low fundamental frequency. In our study area, the thickness of the sediment is thinner in the northeastern-E sites and in the southwestern sites, in this area the frequency of the site must be very high, however in the some points the frequency does not fit with the equation above. The basalt areas like sites M105, M107 and sandstone area M40 into M51 correspond to the fundamental frequency obtained by H/V ratio. In these areas, the depth of the sediment gradually decrease, and the frequency increases according. There are two reasons that explain why the measurements do not fit in some areas; one is that sedimentary layers have different thickness. The second is that sediment layer has different consolidation degree, according to field work observation. In high frequency, in particular with the low amplification this method does seem to work well (Nakamura, 2000).

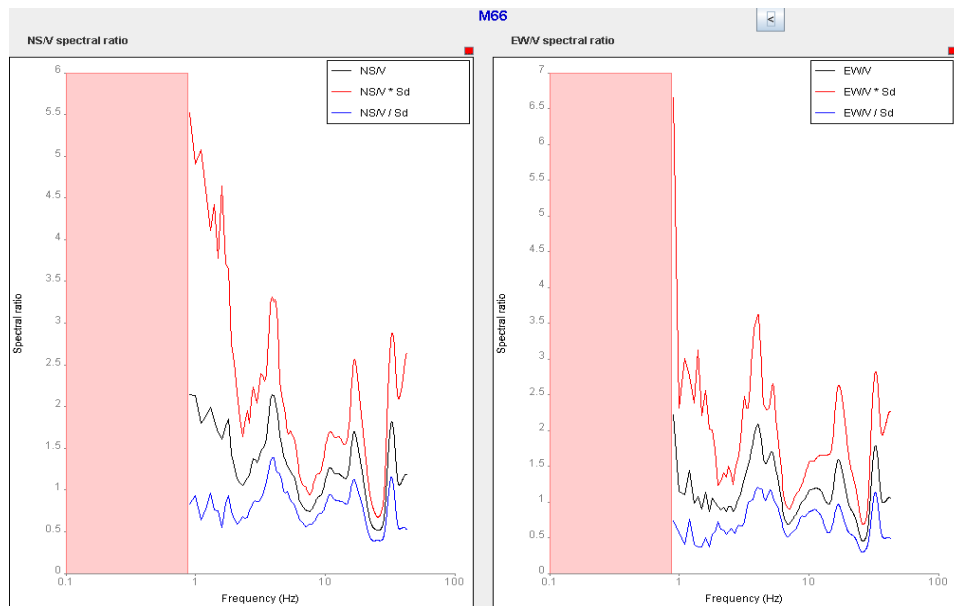


Figure 3.16: EW/SZ and NS/SZ ratio of the response spectrum computed at site M66. The two components are different and spectrum is difficult to interpret; the point may be occur above some very complex underground structure or close to a source of seismic noise of industrial origin.

## Classification of the spectra computed from the dataset collected in the study area based on the underlying geological formations

The site response spectra computed from the data collected could be classified in two major different groups. Each one has subgroups as follows;

- 1- Site response spectra at sites of overlying Basement Complex.
- 2- Site response spectra at sites of overlying sedimentary rock

We will describe these two groups with subgroup; we will follow the classical as depending of formation age;

### *Group 1, Site response at site of overlying Basement complex*

The measurements of sites of overlying hard rock have been done at three different locations

- 1- Site response at Omdurman Basement Complex site

The Cambrian granite rock outcrop can be found close to Awila dam, this is the place where the measurements were taken. The spectra calculated at these points were different from one site to another. The average of amplitude of these points was around 1.5. Some of them give flat spectra with H/V ratio of amplitude around 1.5 and another flat with a peak around 2.5 to 4, which are associated with high frequencies. Examples of site response with flat spectra are given in figure 3.17 and figure 3.18, computed at site M111 and M112 respectively. The example of a flat spectrum with high frequency peak is given (Figure 3.19) computed at site M116. The measurements recorded on Basement sites are expected to have amplification around 1. From our results this is not always the case. For example in sites such as M114 and M115 the average amplification is 1.5, while at site M111 it is around 1.2 or closer to what expected.

There are four factors that could be response to have high amplification in that area;

- Since some of these points are located close to Awila Dam which generated high noise.
- Topographic site effects, as described in section 3.1.1.
- During the measurements there were currents of air. It is probably can transmitted extra noise.

- The duration of the recording is short. Instead having place with extra noise, we need to have a long recording that can avoid that noise, where in those points it is not long.

In conclusion, it is difficult to estimate the local site effects by this method, because the method itself is based on the estimation of a transfer function through the bedrock overlain and layers with different acoustic waves. This method does not work, instead in one unit of rock. For that reason may, this method is not useful to estimate the amplification in basement rock.

## 2- Site response of site on Khartoum Basement area

The measurements done located in two different types of rocks in the northern study area, Proterozoic granite with Dolerite dyke close to Silate area and granite close to Sabaloka igneous complex. The site calculations show different spectra. The average amplification of all these sites is close to 1.3. The flat response computed at site KB30 with amplitude 3. This is closer to expected spectrum in hard rock, as seen in the given example (Figure 3.20) computed in site KB30. While there are other sites have high amplification in high frequency. It has a spectrum with peak amplitude around 2.5. This peak may represent by high noise close to measurement place.

Our results of site response spectra represented in basement Khartoum site show the same behavior as the Omdurman sites. They give again measurements that not coincide with what is the expected amplification in hard rock. One explanation, in addition to the reason mentioned earlier in the Omdurman case, is those sites are occur nearby the high noise could be generated by El Gili Oil refinery.

## 3- Site response spectra at site overlying volcanic basalt

Basalt rock sites are located in middle of the study area in the form of intrusion rock. In this case, the analyses of these sites consider them as hard rock. The aim of these measurements is to evaluate the impact of intrusion rock and to compare between Basement and sedimentary rock spectra. The average of the amplification from the site response spectra is computed around 1.3. Most of

these sites represent two different types of site response spectra, but all have peak amplitudes with higher frequencies. Examples for the type with flat spectra in low frequency range while it has more peaks amplitude at high frequency is given in figure 3.21, computed at site M106. More sites of this case are given in appendix (A). The mining activities are in progress in this area (Quarry). This may be the reason why we have this peak in the spectra. Instead the spectra shows low amplification in this hard rock may be considered as a good result.

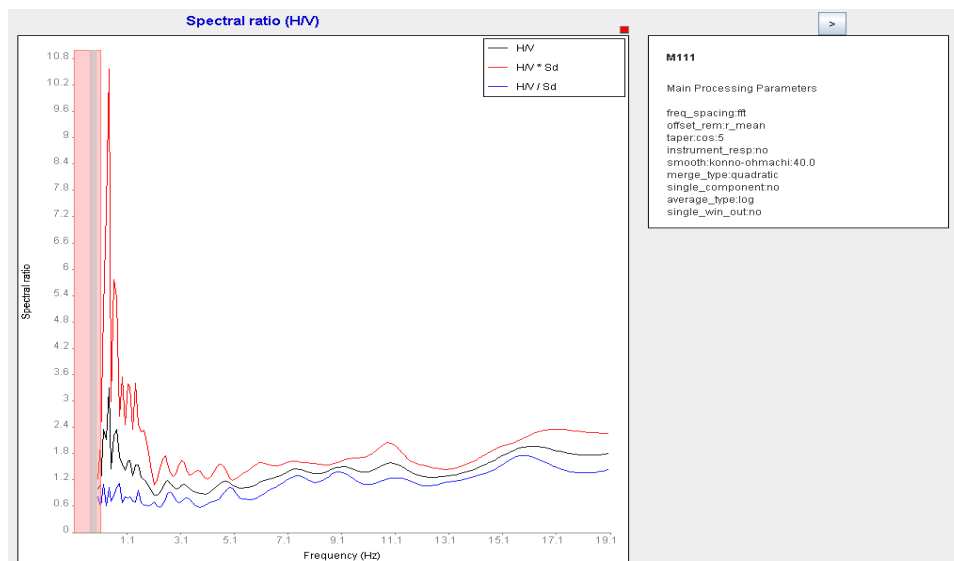


Figure 3.17: The spectrum calculated at site M111. It can be seen that flat site response from overlying rock, the average amplification is 1.5.

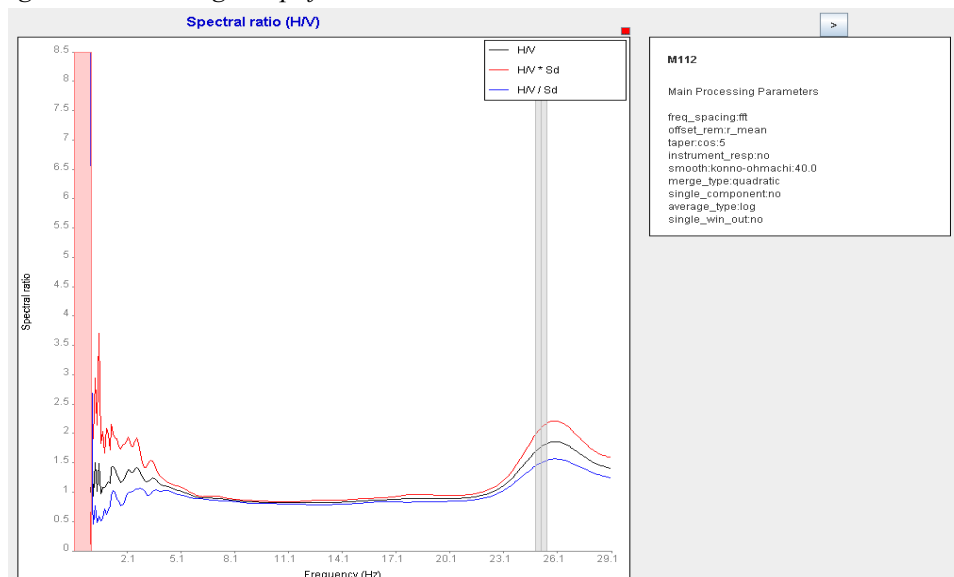


Figure 3.18: flat site spectrum computed at site M112 from Omdurman Basement Complex site. The average amplification is around 1.3 or as expected around 1.

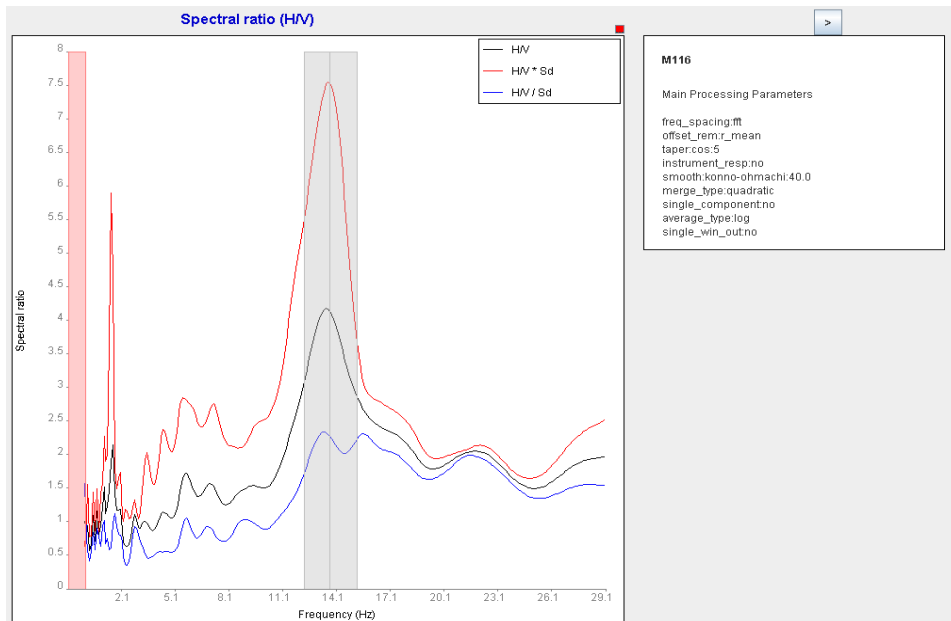


Figure 3.19: flat spectrum with peak calculated at site M116. It can be seen that the average of amplitude is 1.5. Here the peak may be cases by high seismic noise since the site is close to Aulia Dam.

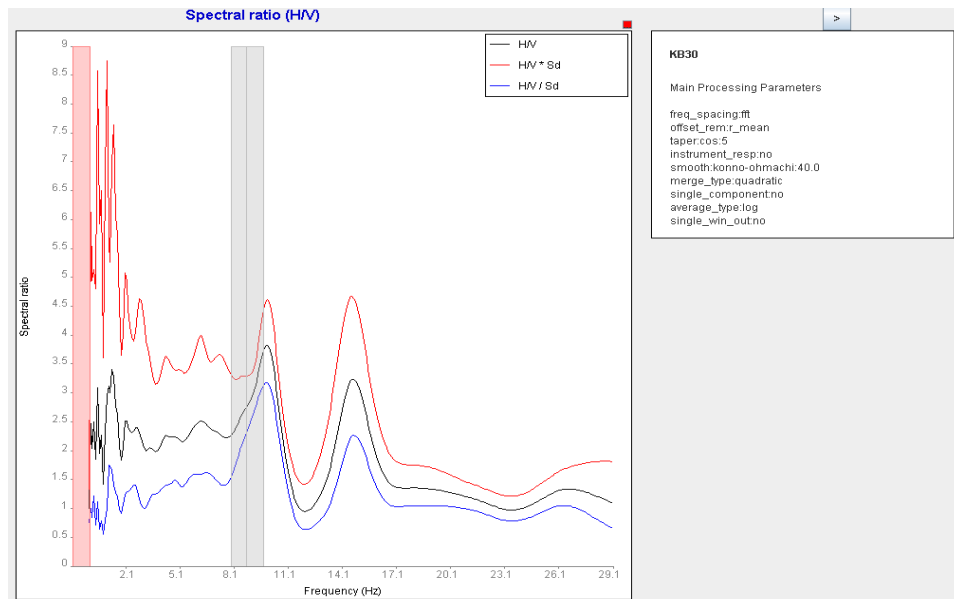


Figure 3.20: site response spectrum at site KB30. It seems the amplification around 3. The peak here may represent by high noise close the measurement area.



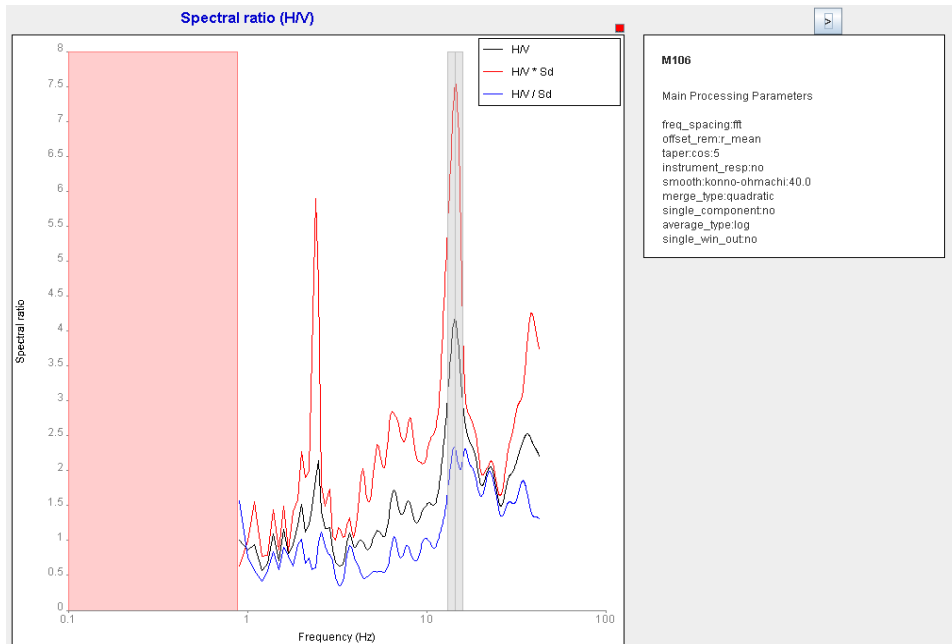


Figure 3.21: site response spectrum at site M106. Here it can be seen that the amplification is around 4 at high frequency around 11Hz.

#### Group 2, Site response spectra at sites overlying by sedimentary rock

Many part of our measurement have been taken at site located on different type of sedimentary rocks. Five subgroups are classified according to the age and characteristics of the rock. We will discuss each of these sites response separately;

##### 1- Site response spectra at site overlying by sandstone in Omdurman town.

The majority of site response spectra computed from data collection from the Omdurman area have a distinct clear peak in frequency range from 0.9 to 6 Hz with amplification around 3 to 5. Among these sites response there are two kinds of spectra either with peak amplitude around 1 Hz, or with two peaks at high frequencies. Examples of these variations of spectra are shown in figure 3.22, figure 3.23 and figure 3.24 computed at sites M11, M73 and M44 respectively. An explanation of this variation is the reflection of wave through the unconsolidated sedimentary rock underlying the surface. These site measurements have been done on consolidated sandstone, multilayered sandstone, with consolidate layers and unconsolidated ones in between. This can explain the variations of the peak amplitude. It is expected that the spectra calculated at the site located on hard rock should have less amplitude. This is the case recognized

in some sites such as site M44. Instead, the site responses with contraction with consolidated sandstone show higher amplification.

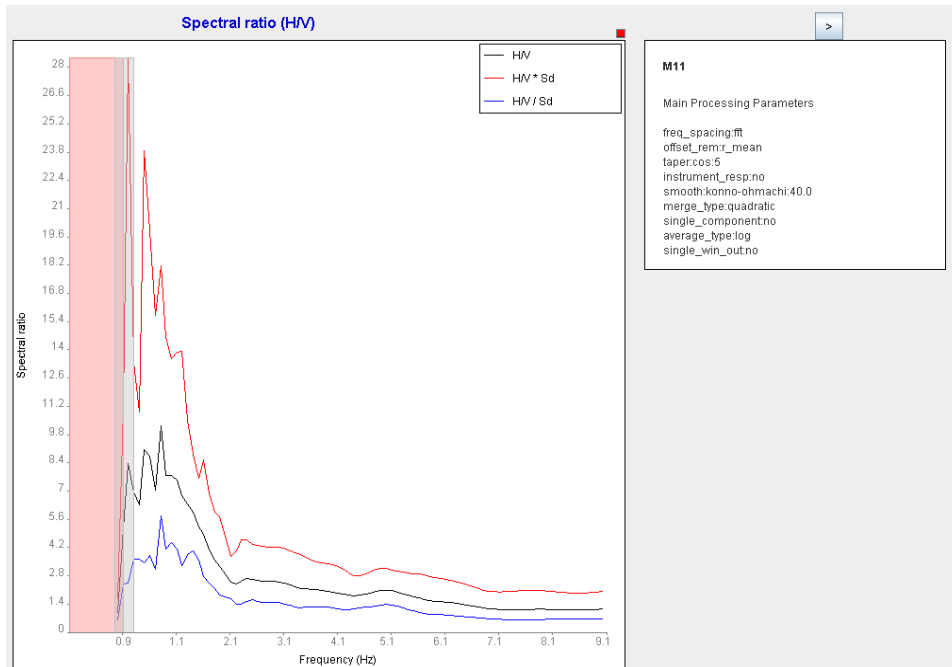


Figure 3.22: Site response spectrum computed at site M11 from the Omdurman dataset which has one peak of amplitude around 1 Hz.

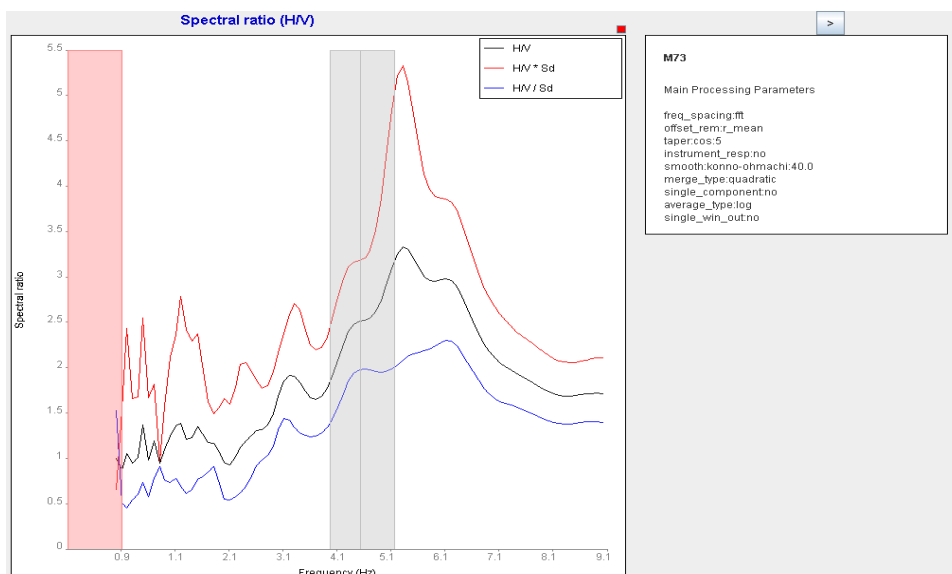


Figure 3.23: Site response spectrum computed at site M73. It has broad band of frequency. Here the amplification is high compared to another site, in which the thickness of consolidated sediment higher.

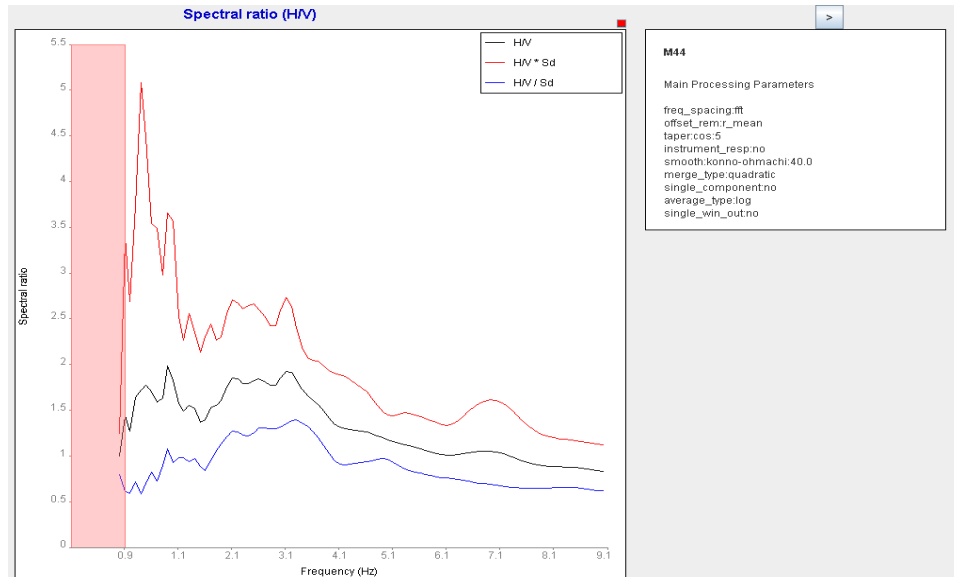


Figure 3.24: Broad band frequency of Site response spectrum computed at site M44. Here we can see that the lower amplification compared to another site may be caused by consolidated of sandstone.

## 2- Site response spectra at site overlying Gezira formation in Omdurman area

Most of our measurements have been taken north of basalt site and are located on a special geological area. That area has subsurface with lens of clay. The common sites response spectra computed from the data collection from these sites have more than one peak of amplitude with average amplification around 3. Examples of spectra are shown in figure 3.25 computed at site M13.

The majority of site repose spectra have the amplification factor is 3 with frequency 2.5 Hz and with more than one peak amplitude. The spectrum is more similar what expected in an area covered by thinning layers sandstone. Thus the variation of these peaks in spectrum can be reflected from different layer underground have different acoustic waves.

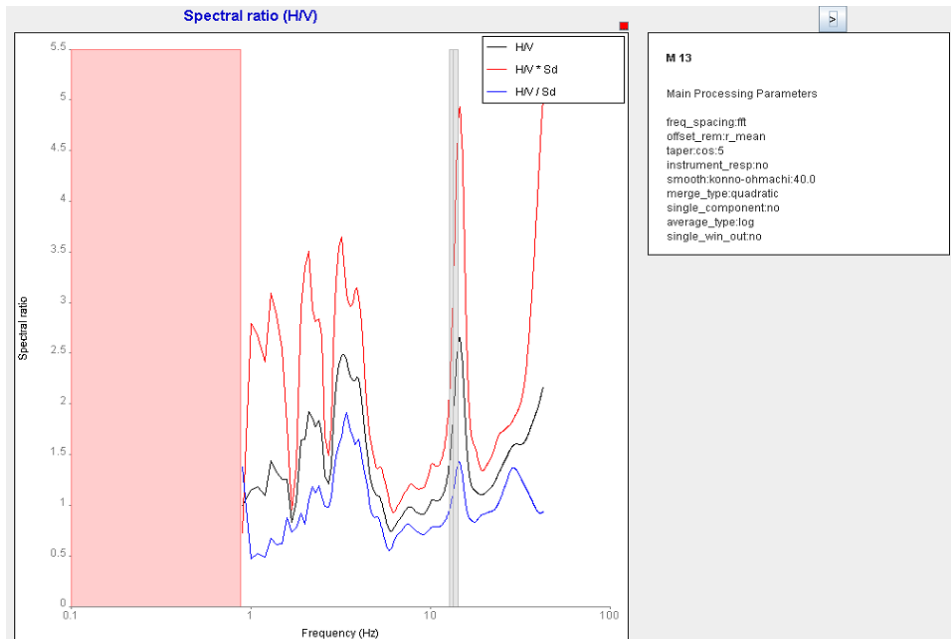


Figure 3.25: site response spectrum at site M13 from the dataset collected in the Gezira formation in Omdurman having more than one peak. Here the first peak may be representation of different stratigraphical layers.

### 3- Site response spectra at site overlying older alluvium deposit in Khartoum area.

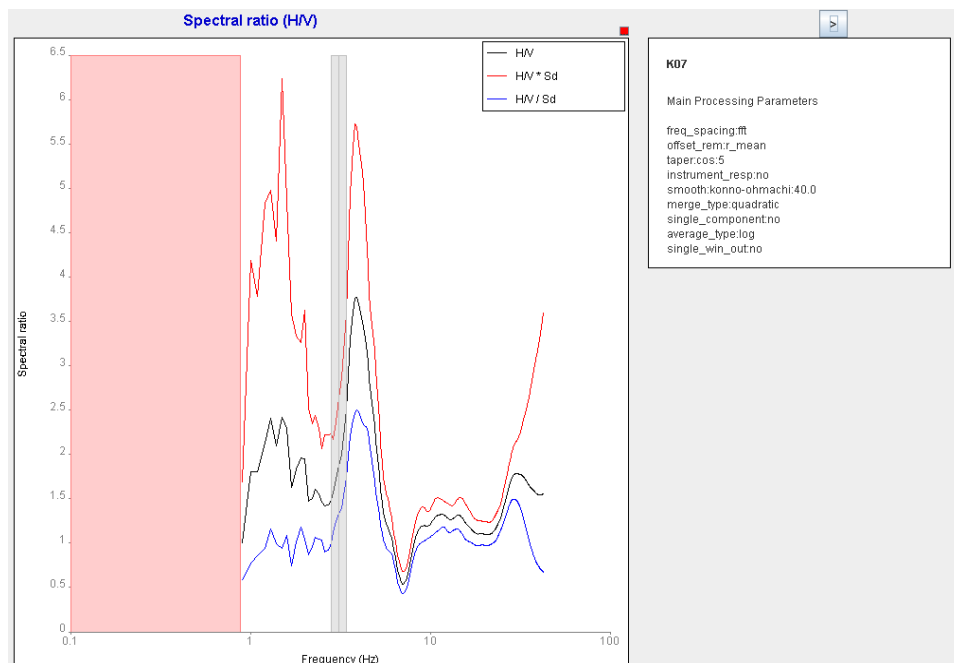


Figure 3.26: Site response spectrum computed at site K07 from dataset of older alluvium site in Khartoum area. Here we see clear peak amplification around 3.7 with frequency 3.5 Hz.

Sites response spectrum calculated from collection dataset from Khartoum area have clear peak with amplification factor around 4 at fundamental frequency of 3 Hz. Example of spectra is given in figure 3.26 computed at site K07. Almost sites have site response spectra with amplification factor around 2.2 but they have different peaks of amplification. The area has underlined unconsolidated of the cretaceous sandstone covered by clay, that could be the reason why they have several peaks of amplitude.

#### 4- Site response spectra at site overlying recent alluvial in Omdurman area.

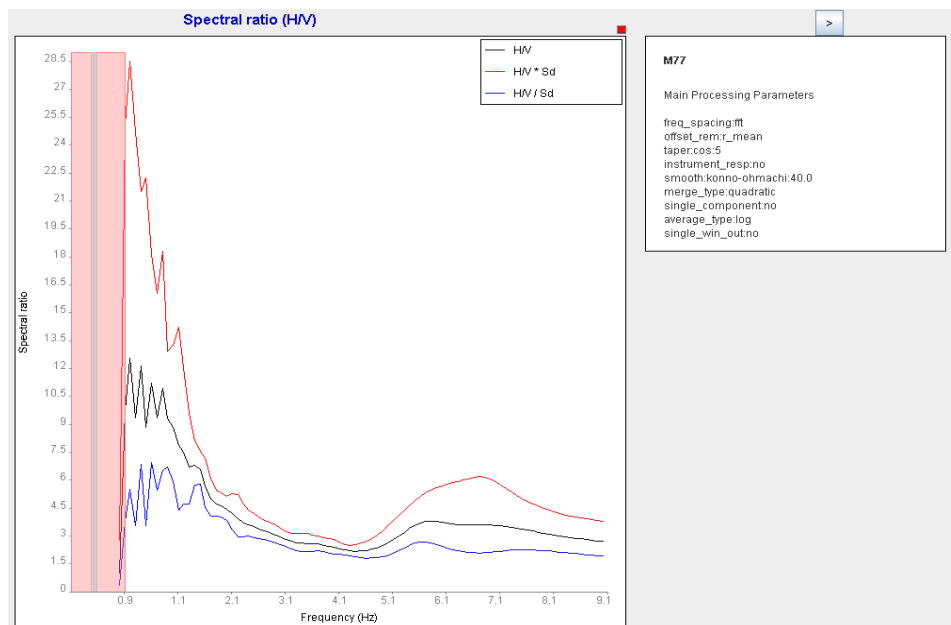


Figure 3.27: site response spectrum at site M77 from dataset from recent alluvial in Omdurman site. Here the amplification is about 12.2 high than what is expected in a site made of sandstone which is covering most of the study area. The fundamental frequency here is around 0.7 Hz

Most of our measurements have been done at recent alluvial sandstone – clay with consolidate rock. Most of these sites show different site response spectra either with high or low amplification but both of them have low frequency range from 0.5 to 0.8 Hz. The relation between amplification and frequency is inversely proportional observed through the points computed in this area. One example of site response is given high amplification with low frequency computed at site M77 (Figure 3.27). It is expected that a deep contrast between

unconsolidated and consolidated sandstone may give these spectra with high amplification at lower frequency. However, some site response were different from what we expected (high frequency with low amplification). That could be due to interaction between the hard rock and the sediment. Furthermore, it is significant that these spectra have a few small peaks which could be the behavior of alluvial deposit along the bank of the Nile. The sandstone layers with high consolidation found between the alluvial layers also can give these different of spectra.

#### 5- Site response spectrum at recent alluvial in Khartoum site

Close to the east bank of the White Nile, deposit of sedimentary has covered large area. The majority of site response spectrums have shown low frequency with high amplification computed at site K12 (Figure 3.28). South of Khartoum area close to the Nile shows the amplification increase relative to the thickness increasing of alluvial deposit.

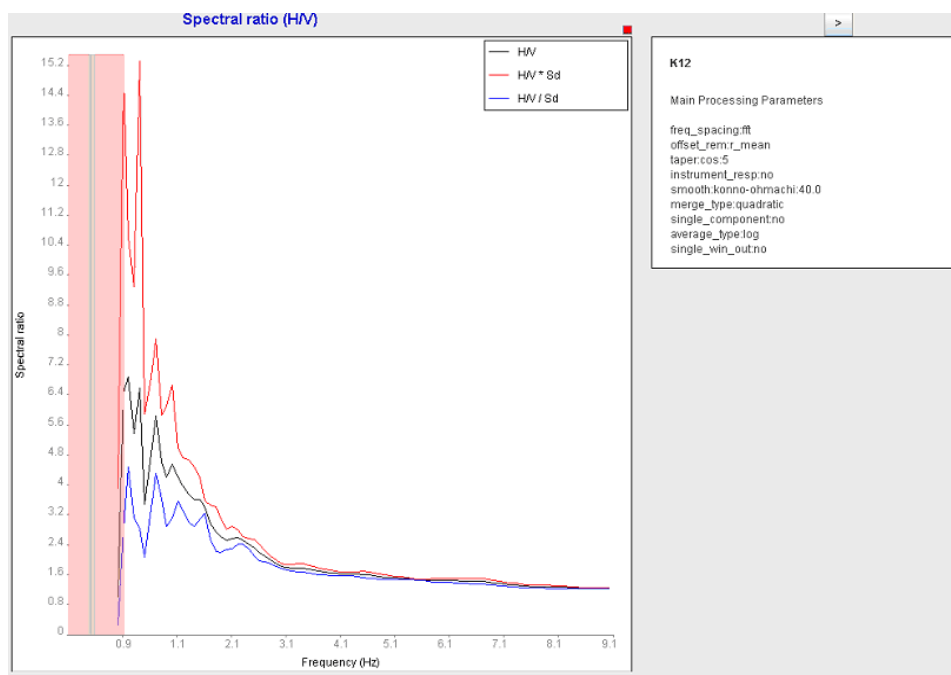


Figure 3.28: site response spectrum computed at site K12. It occurs on the recent alluvial deposit at Khartoum town. The amplification is 6.8 with frequency around 0.9 Hz.

### Spatial distribution of the fundamental site frequency and amplification factors for the western part of Khartoum city

Figure 3.29 and 3.30 show the spatial distribution of the fundamental frequency and distribution of the amplification factor respectively. It is observed that due to heterogeneous distribution of the measurement sites, these two maps that have two problems, which results in poor description. The first one is that, the area has high values of frequencies or amplification at some places and small values at others, and this factor will influence the interpretation. If we consider a small interval, less than 1 Hz between the lines, we obtain a dense line contour map, whereas if we consider an interval higher than 1Hz, we obtain a broad line. In this case we might lose details or information about some points. The second reason is that in some parts of the study area, the absence of data like in the western, eastern and northern part of the study area, gives interpolation lines that are not accurate. These lines do not show the real parameters of the site response (frequency and amplification). Here we considered the last contours line that passed through points at the boundaries of the study area are most represented the really value of fundamental frequency or amplification factor. However, in order to correlate these two maps with the one about geological formation, we made two operations; first, we marked each map with the same name of the site measurements. Second, the scale of each map -geological, the frequency and of the amplification is the same (Figure 3.5).

Our first idea was to look for agreement between the distribution of fundamental frequencies and amplification factors on the one hand, and distribution of rock unit on the other hand. For the first map, about the frequency response, three sets of anomalies can be observed. First set anomaly; three high anomalies are distinguished at three parts in the study area. As mentioned before in section 3.1.2 these sites were measured on hard rock (Basalt and Granite). It is assumed that there is thin a layer under the sensor that may have given these anomalies. Those anomalies have fundamental frequencies range from 10 Hz to 22 Hz. In two corners of the sites have fundamental frequency increasing inside and produce the shape as the geological boundaries of basement rock. The anomaly in the center of the area where the basalt rock occurs, that the contour line of the frequencies values takes the same shape than the boundaries of the basalt formation. According the geophysics study conducted by Qureshi et al., (1966), that the shape of basalt as intrusion rock. Since there are no gradual values of the frequency contours

between the sediments and basalt, which meaning is confirmed that basalt as intrusion. Second set anomaly; the areas have frequency range 3-6 Hz, located in three group, north of the basalt anomalies in the center, north of the south anomalies (Basement rock) and along the eastern bank of the White Nile (Khartoum area). Two group anomalies (North basalt and Khartoum areas) are similar with fundamental frequency around 3 Hz. They have the same geological condition but are occurring in different places. These two anomalies Khartoum and Omdurman have same frequency and the same geological unit, it confirms that this method can be useful for this area. In addition to that these sites have clear or more peaks in spectrum, this as mentioned earlier, may be because under these sites the boundary between the two uppermost layers is sharp. Also most of these sites have more than one peak which is reflected in the variation of layers. The third group anomalies, in the area between the south basalt anomalies and northern high anomalies in the southern study area, consist in sites M73, M74, M38, M19 and M68 have fundamental frequency range 5 to 6 Hz. These sites are located on sedimentary rock, and have relative high frequency compared to other as the same geological unite. This could be the result of three reasons; first reason is that the area has sediment of more high consolidated sandstone in the uppermost layer. The second reason is that our measurement site could be effected by its proximity the hills. The third reason could be the silification of the normal fault discussed by Mula (1971) which is made of high consolidated sandstone, thus might be the reason why we have high fundamental frequency.

Third set anomaly, is that the sites have fundamental frequency in the range from 2 to 0.5 Hz. Most of the sites in the study area are covered by this anomaly. Two groups are observed; one group has low frequency less than 1 Hz, mainly are located on the western Nile River Nile. It shows as irregularly white shape (Figure 3.29). It seen that those sites have low frequencies could be due to recent alluvial deposit area, Or due to the shallow basins scatter in area, specially the area between two high anomalies in the western Nile (Granite and Basalt) (Husseini M, 1992). Second group which have frequency around 2 Hz are located and cover most of the study area. As we known the sediment thickness increases from the basement rock in the south and north east to middle, close to the Nile river (Figure 1.11) (Farah et al., 1997), and the fundamental



frequency decreasing in the same way. But this systematic relation between thickness and fundamental frequency is found only in the northern part of Omdurman and Khartoum close to the river, while in the south part of Omdurman area it is more complex. The possible explanations for this variation is that may be those areas have complex structure underground.

Figure 3.30 shows the map of the spatial distribution of the amplification factor in the study area. In hard rock sites (Basement complex as granite rock and occurring in the southern and northern area and Basalt at central), the amplification factor is expected to be a flat response or smaller values, according to the concept of the method mentioned in section 3.1.1. But if compares the amplification in the sedimentary site with the amplification in the hard rock, it has the same values. For this reason we believe that the amplification in hard rock is not accurate. The possible reason for this is that these sites might have thinning layers giving this amplification. In the sediment formations, since where majority of those sites have different amplification factor. In some area it is possible to distinguish the sediment formations by using the amplification observation. An example of that is when the amplification factor has similar boundaries of the recent alluvial formation (Figure 3.4). But inside this formation there some point that have high amplification as shown in at sites M59, M60 and M61. This may be due to thickness of the sediment contain high percent of clay, and classified by Hussein (1992) as basin. Generally the amplification factor is increasing toward the river. In addition, the amplification is higher on the western river bank than in the eastern one. The thickness and consolidation of the rock may case of this variation of amplification, as we seen in recent alluvial deposits. But in some parts located on thick sediment, high amplification factor is not observed. Example of that is the area occurring on the north, the south Omdurman and the north river bank in Khartoum area. The study area has more than one formation with different types and the underground structures are complex. Therefore, to estimate the amplification it might be difficult. We believe that the spatial distribution of amplification does not represent a real site amplification factor.

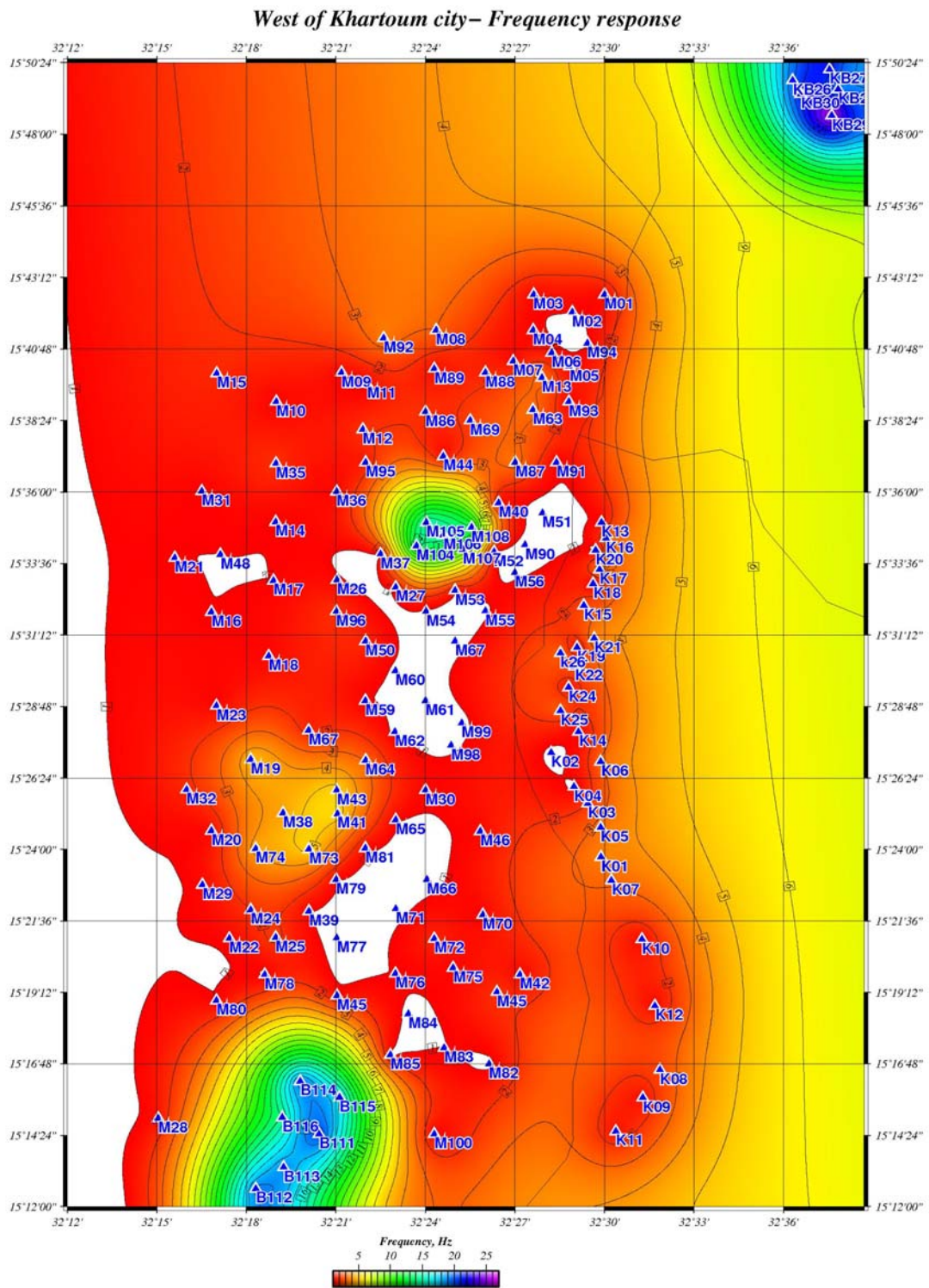


Figure 3.29: Map of the spatial distribution of the fundamental frequency of the study area Omdurman site (M), basement complex rock in Omdurman site (B), Khartoum sites (K), M104 to M108 are site of basalt area and basement complex in Khartoum site (KB).

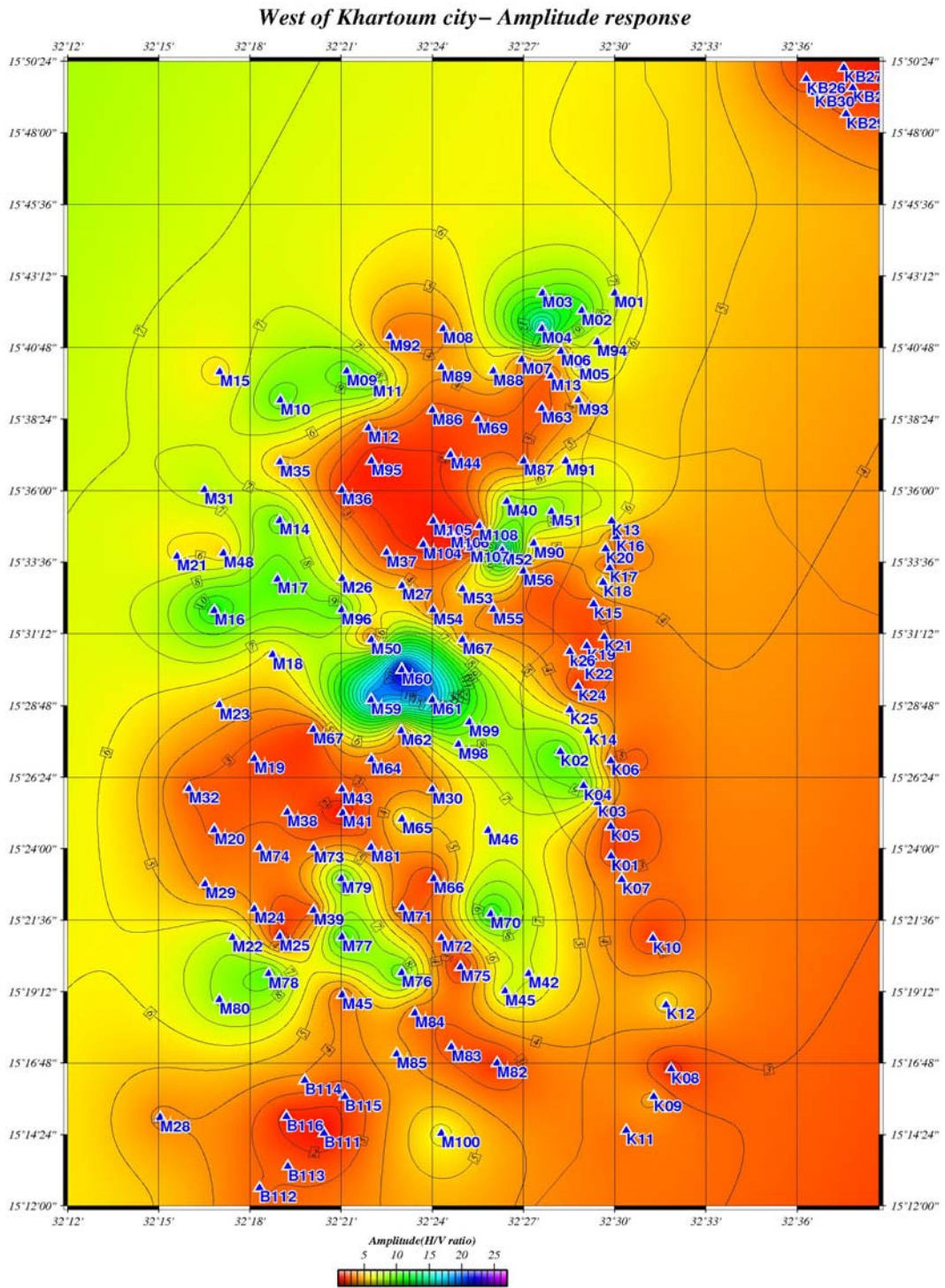


Figure 3.30: Map of the western Khartoum, showing the spatial distribution of the amplification factor. Omdurman site (M), basement complex rock in Omdurman site (B), Khartoum sites (K), sites from M104 to M108 are basalt area and basement complex in Khartoum site (KB).

### 3.2.2 Analysis of earthquake data for estimating local site effects

As we mentioned earlier in the local seismic section 1.3.2, the local earthquake around Khartoum area may have caused of the local site effects. However, in this section, local earthquake data are used to calculate the local site effects in the Khartoum area. There are two methods are conducted; First method, the H/V ratio or Nakamura technique and second method, the Standard Spectral Ratio (SSR). SESAN software is used to analyze data (Havskov and Ottemöller, 2005). Full description about these methods has been discussed in section 3.1.

#### Analysis of the H/V ratio for the noise and S-wave records of weak motion

Local earthquakes and the distribution of stations are discussed in section 3.1.2. Two stations (SLAT and MRKH) data are used and they have factors to be interesting in assumption of the SSR method. The factors are these stations are close to each other compared to earthquake sources and deployed on two different formations. However, noise and S-wave records of two datasets earthquake in two stations are used. H/V ratio and SSR method are conducted by using the SPEC program part of SEISAN software. The process of analysis of the H/V ratio is the same as the ambient noise records estimation and described in section 3.2.1. The parameters are concerned in program that can able to process data and displays results are given in appendix B. Table 3.2 contain some information about the local earthquakes. Two groups of earthquakes are analyzed. Group one contains two earthquakes named *EQ10* and *EQ6* and analysis of the noise and S-waves parts of the earthquake records are analyzed separately by using both horizontal components (N-S or E-W) with vertical component (S-Z) are given (Figure 3.31). Group two contains four earthquakes named *EQ2*, *EQ3*, *EQ4* and *EQ8* and analysis are given (Figure 3.32). In order to merge the error and to compare between the spectra of earthquakes, the summations of these spectra ratio are made. The summation of the spectra of each horizontal component over vertical component of all earthquake records together in each station is made.

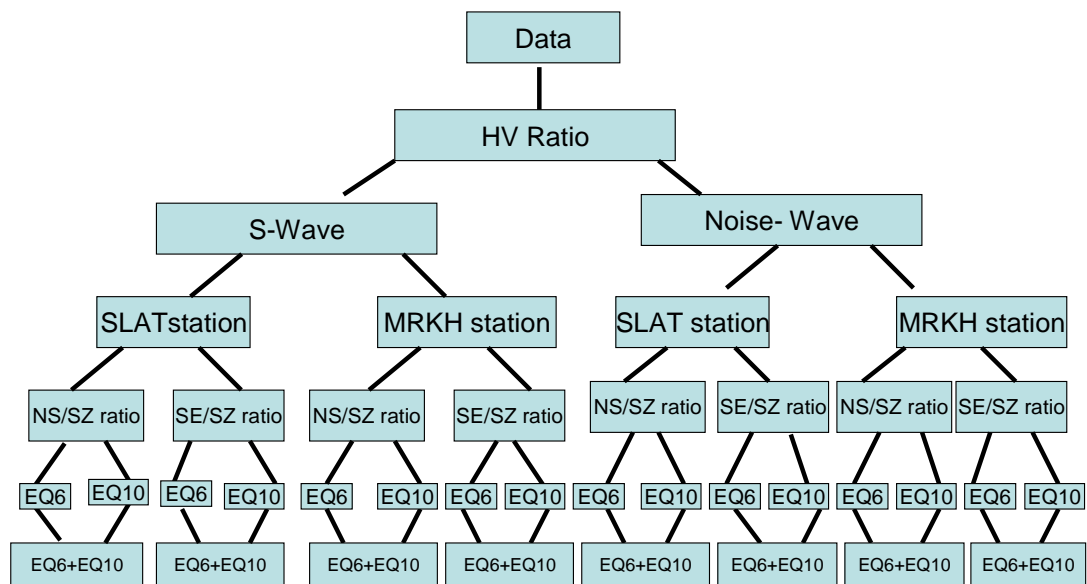


Figure 3.31: Sketch shows the structure of H/V ratio analysis in two stations records using the S-wave and Noise recording part of group one of earthquake dataset. It consists two earthquakes data number EQ10 and EQ6. NS and SE earthquake spectral of horizontal components. SZ earthquake spectral of vertical component.

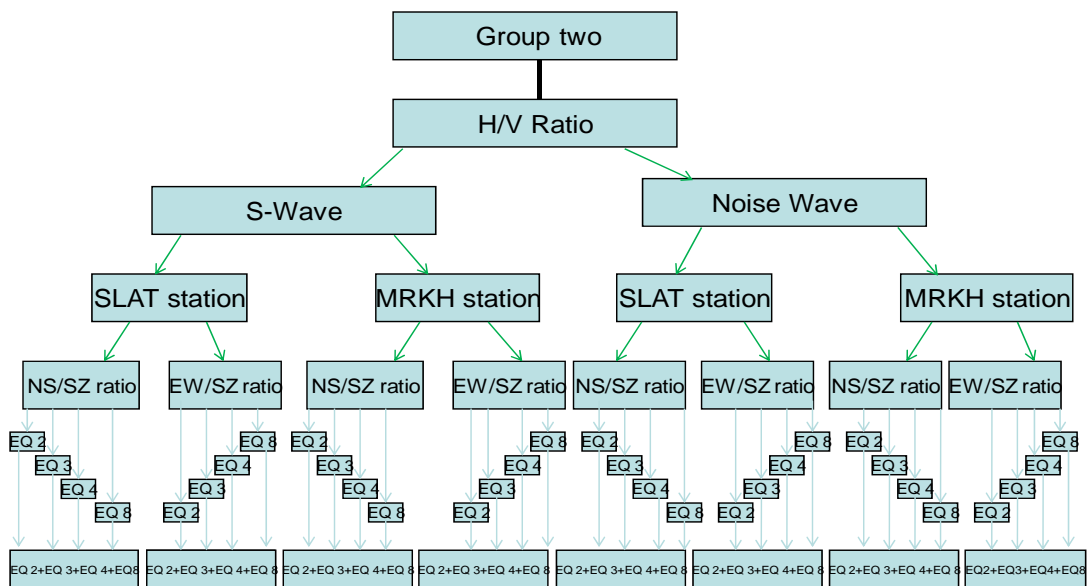


Figure 3.32: Sketch shows the structure of H/V ratio analysis in two stations records using the S-wave and Noise recording of group one of earthquake dataset. It consists two earthquakes data number EQ2, EQ3, EQ4 and EQ8. NS and SE earthquake spectral of horizontal components. SZ: earthquake spectral of vertical component.

Table 3.4: H/V ratio of two stations computed at MRKH and SLAT station, using the noise and S- wave for four earthquakes EQ10+EQ6. S is the transfer function of horizontal components and has direction of N-S and E-W and SZ: vertical component

Earthquake	H/V ratio with Components using	Fundamental frequency	Amplification factor
<i>EQ10+EQ6</i> (MRKH S -wave)	S MRKH N -S / S MRKH SZ	2.57	3.69
<i>EQ10+EQ6</i> (MRKH S -wave)	S MRKH E-W / S MRKH SZ	2.52	3.54
<i>EQ10+EQ6</i> (MRKH) (noise)	S MRKH N -S / S MRKH SZ	1.10	2.66
<i>EQ10+EQ6</i> (MRKH) (noise)	S MRKH E-W / S MRKH SZ	0.96	1.87
<i>EQ10+EQ6</i> (SLAT)(S -wave)	S SLAT N -S / S SLAT SZ	1.02	4.00
<i>EQ10+EQ6</i> (SLAT)(S- wave)	S SLAT E-W / S SLAT SZ	0.98	3.06
<i>EQ10+EQ6</i> (SLAT) (noise)	S SLAT N -S / S SLAT SZ	1.12	1.90
<i>EQ10+EQ6</i> (SLAT) (noise)	S SLAT E-W / S SLAT SZ	1.16	2.56

The fundamental frequency and amplification factor are estimated from two groups of earthquake dataset. In group one, the H/V (NS/SZ and EW/SZ) ratio of two earthquake dataset records in two stations (MRKH and SLAT) are computed by using noise and S-wave records. Table 3.4 shows the result of the H/V ratio analysis. The spectra of the H/V ratio computed in MRKH station record show the average amplification of the S –wave about 3.6 at 2.5 Hz. Figure 3.33 and figure 3.34 show the site response spectra of H/V (NS/SZ and EW/SZ) ratio of the S-wave computed in MRKH station. The average amplification of noise wave computed in MRKH station is 2.2 at 1 Hz. The spectra of H/V (NS/SZ and EW/SZ) ratio of noise wave computed in MRKH station records are given in figure 3.35 and figure 3.36 separately. In SLAT station, the spectra of both horizontal components computed from S-wave have amplification of 3.5 at 1 Hz. The responses spectra of S-wave are computed in SLAT are given in figure 3.37 and figure 3.38. Whereas, the noise wave is used, the average amplification factor of 2.2 at 1.1 Hz. The noise spectra computed in SLAT station are given in figure 3.39 and 3.40. In general the S-wave shows high amplification compared to noise wave. MRKH station has high amplification of S-wave at high frequency compared to SLAT station.

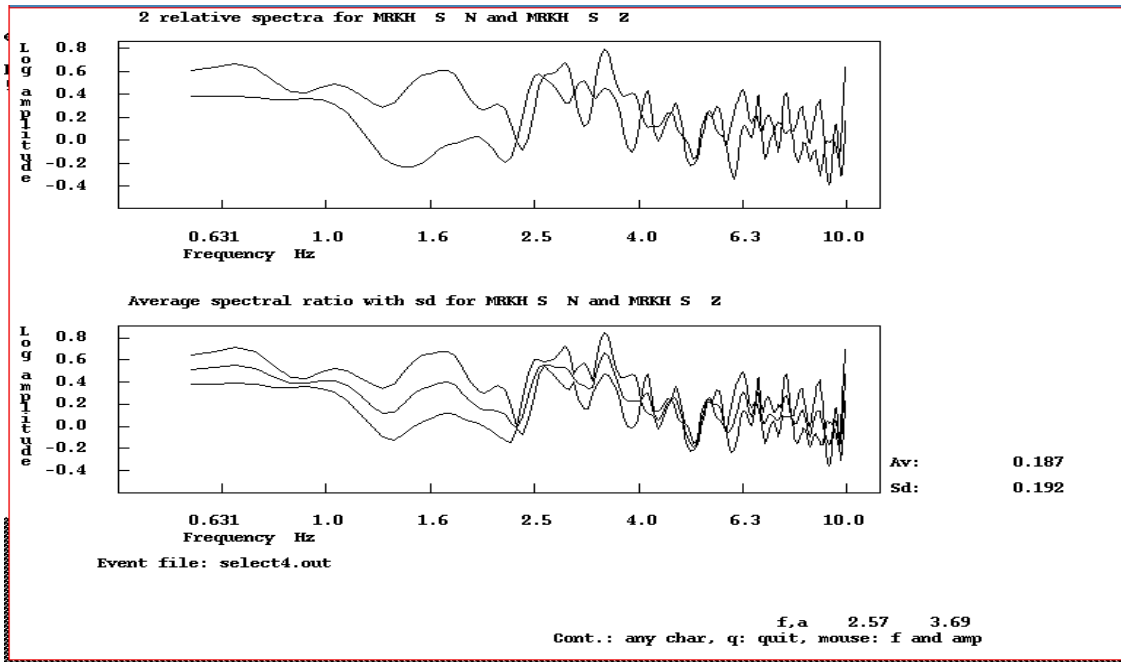


Figure 3.33: The  $H(NS)/V(SZ)$  ratio of  $S$ - wave earthquakes (EQ10+EQ6) records computed in SLAT station. Two relative spectral of two earthquakes are show in the top. NS: spectral horizontal component, SZ: spectral vertical component. The average spectral ratio shows in the bottom. The amplification factor is 4 at 3 Hz.

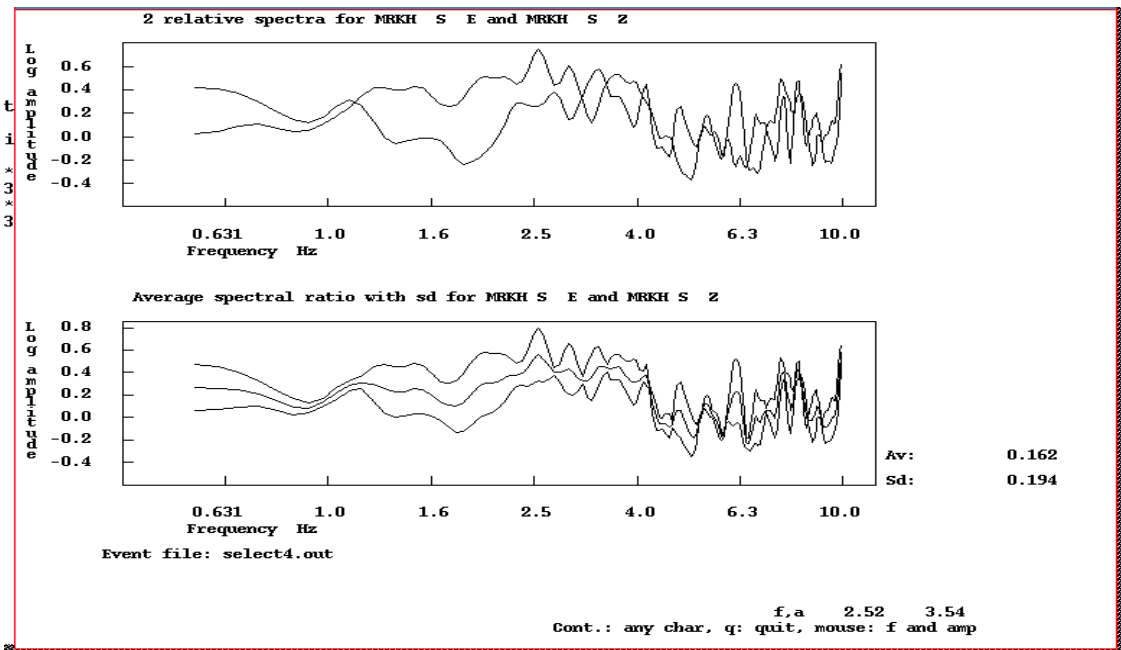


Figure 3.34: The  $H(ES)/V(SZ)$  ratio of  $S$ -wave earthquakes (EQ10+EQ6) records computed in MRKH station. Two relative spectral of two earthquakes are show in the top. ES: spectral horizontal component, SZ: spectral vertical component. The average spectral ratio shows in the bottom. The amplification factor is 4 at 3 Hz.

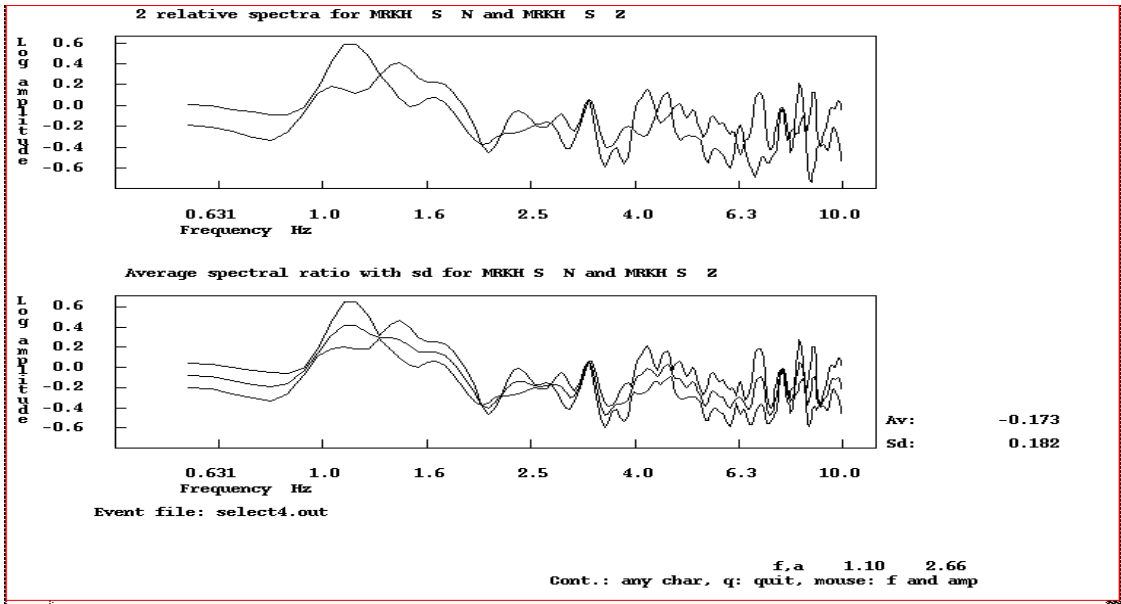


Figure 3.35: The  $H(NS)/V(SZ)$  ratio of noise wave earthquakes (EQ10+EQ6) records computed in MRKH station. Two relative spectral of two earthquakes are show in the top. NS: spectral horizontal component, SZ: spectral vertical component. The average spectral ratio shows in the bottom. The amplification factor is 3 at 1 Hz.

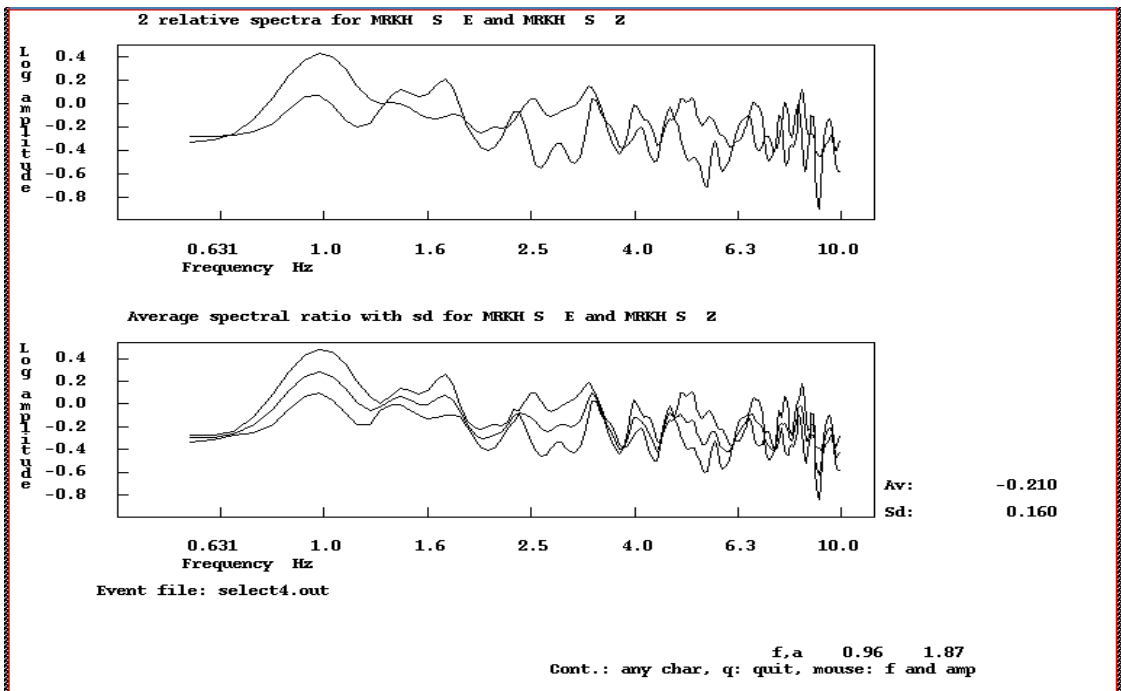


Figure 3.36: The  $H(ES)/V(SZ)$  ratio of noise wave earthquakes (EQ10+EQ6) records computed in MRKH station. Two relative spectral of two earthquakes are show in the top. ES: spectral horizontal component, SZ: spectral vertical component. The average spectral ratio shows in the bottom. The amplification factor is 2 at 1 Hz.



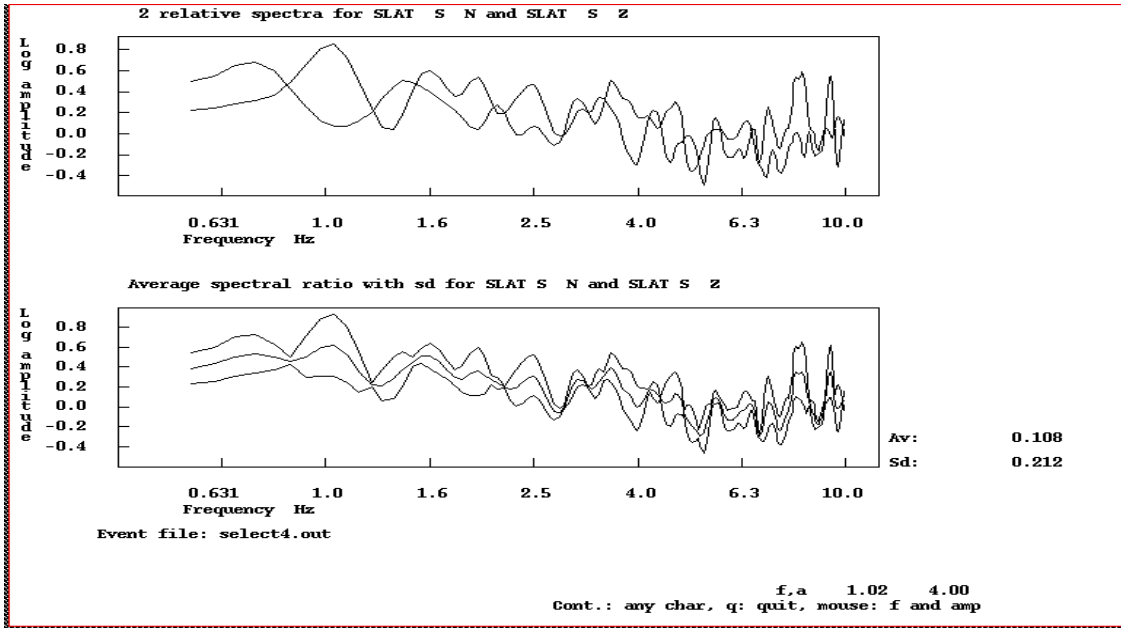


Figure 3.37: The  $H(NS)/V(SZ)$  ratio of  $S$ -wave for two earthquakes (EQ10+EQ6) records computed in SLAT station. Two relative spectral of two earthquakes are show in the top. NS: spectral horizontal component, SZ: spectral vertical component. The average spectral ratio shows in the bottom. The amplification factor is 4 at 1 Hz.

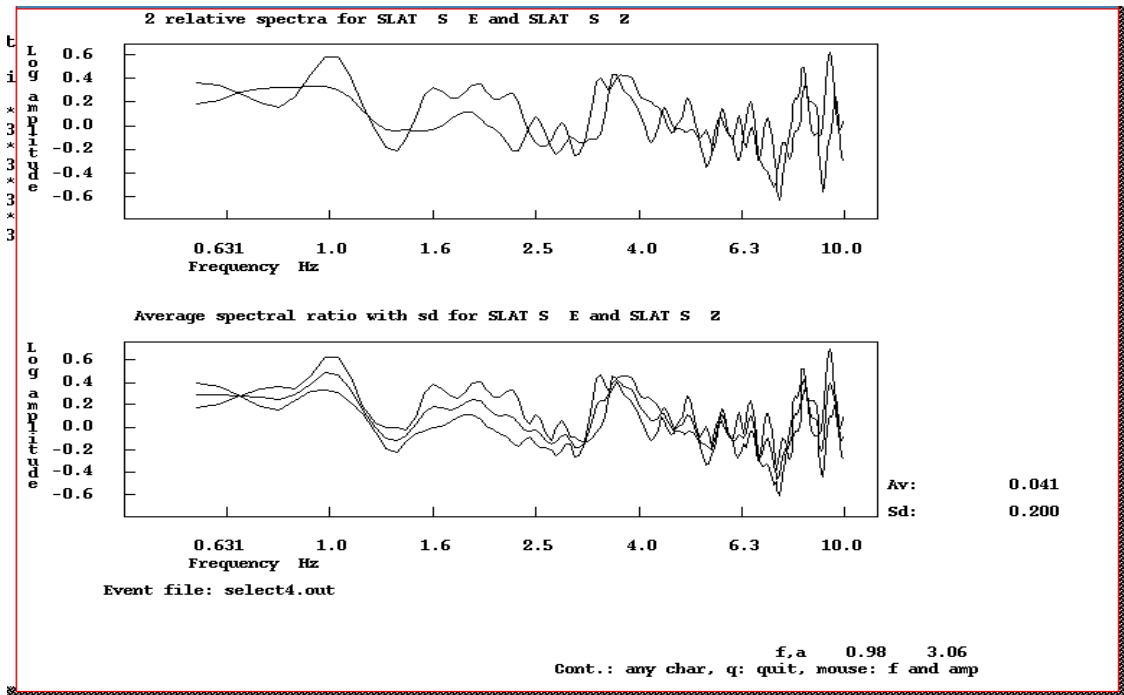


Figure 3.38: The  $H(ES)/V(SZ)$  ratio of  $S$ -wave for two earthquakes (EQ10+EQ6) records computed in SLAT station. Two relative spectral of two earthquakes are show in the top. ES: spectral horizontal component, SZ: spectral vertical component. The average spectral ratio shows in the bottom. The amplification factor is 3 at 1 Hz.

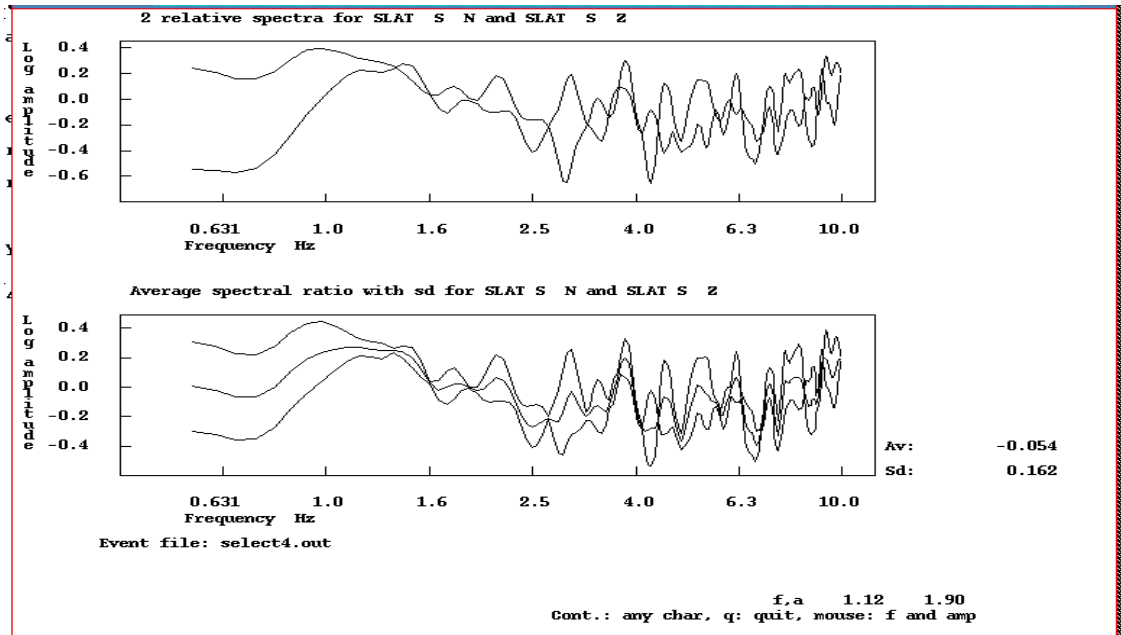


Figure 3.39: The  $H(NS)/V(SZ)$  ratio of noise wave for two earthquakes (EQ10+EQ6) records computed in SLAT station. Two relative spectral of two earthquakes are show in the top. NS: spectral horizontal component, SZ: spectral vertical component. The average spectral ratio shows in the bottom. The amplification factor is 2.0 at 1 Hz.

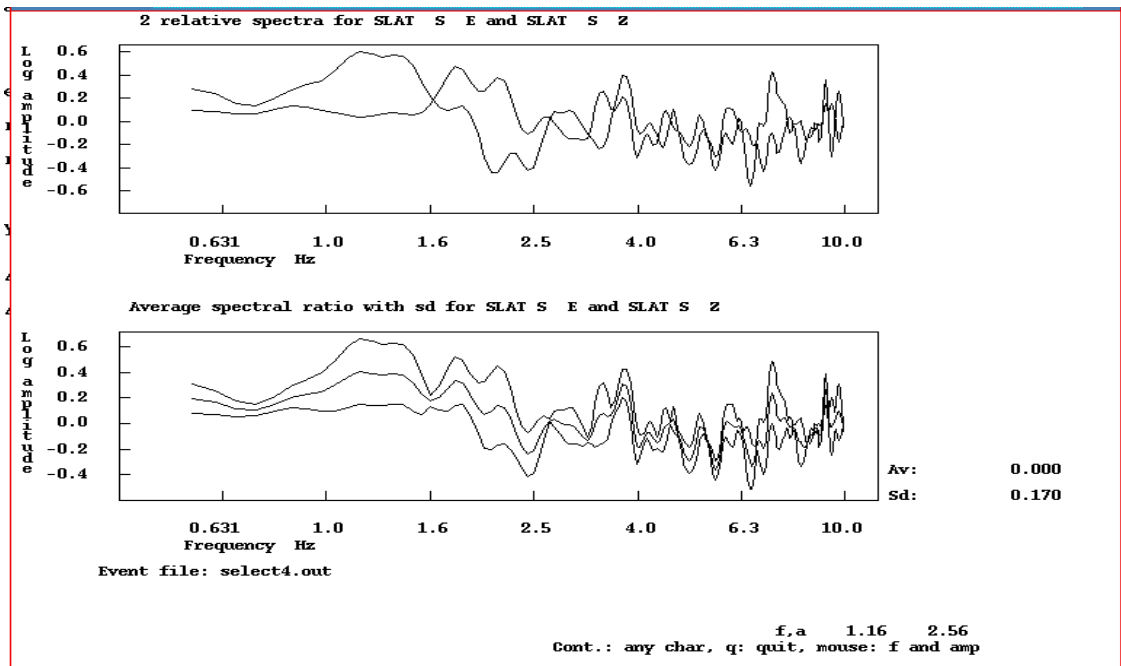


Figure 3.40: The  $H(ES)/V(SZ)$  ratio of noise wave for two earthquakes (EQ10+EQ6) records computed in SLAT station. Two relative spectral of two earthquakes are show in the top. ES: spectral horizontal component, SZ: spectral vertical component. The average spectral ratio shows in the bottom. The amplification factor is 2.5 at 1 Hz.

Table 3.5: H/V ratio of two stations computed at MRKH and SLAT station, using the noise and S- wave for four earthquakes EQ2+EQ3+EQ4+EQ8. S is the transfer function of horizontal components and has direction of south to north / east to west with vertical component (SZ) of two stations.

Earthquake	H/V ratio with Components using	Fundamental frequency	Amplification factor
EQ2+EQ3+EQ4+EQ8 (MRKH S -wave)	S MRKH n -s / S MRKH sz	3.56	321.2
EQ2+EQ3+EQ4+EQ8 (MRKH S -wave)	S MRKH e-w/ S MRKH sz	3.61	269.84
EQ2+EQ3+EQ4+EQ8 (MRKH noise -wave)	S MRKH n -s / S MRKH sz	3.53	21.60
EQ2+EQ3+EQ4+EQ8 (MRKH noise- wave)	S MRKH e-w/ S MRKH sz	1.67	14.33
EQ2+EQ3+EQ4+EQ8 (SLAT S -wave)	S SLAT n -s / S SLAT sz	0.70	2.80
EQ2+EQ3+EQ4+EQ8 (SLAT S -wave)	S SLAT e-w/ S SLAT sz	0.71	3.13
EQ2+EQ3+EQ4+EQ8 (SLAT noise-wave)	S SLAT n -s / S SLAT sz	1.92	1.49
EQ2+EQ3+EQ4+EQ8 (SLAT noise- wave)	S SLAT e-w/ S SLAT sz	2.87	1.66

In group two, the result of two types of the H/V ratio (noise and S-wave) are computed based on four earthquake datasets recorded in two stations MRKH and SLAT. The results are given in Table 3.5. The display of the spectra and more details are given in Appendix C. Procedures are the same as the H/V ratio of the previous two earthquake analysis. The amplification of S-wave using four earthquake records in MRKH station of both horizontal components is unrealistic high. In general the MRKH station has higher amplification of the wave at high resonance frequency than SLAT station.

### Analysis of Standard Spectral Ratio (SSR method) of weak motion

SSR method is simple, since it is based on the relative of two horizontals in two stations, one use as reference station and second station used as the site under investigation. This method was discussed in section 3.1.1. The critical conditions for this method are the distance between the two stations and location of the sources (epicenter) which should satisfy the far- field approximation. Example, the earthquakes are sufficiently far away from the stations, such that the azimuth and distance can be considered the same. For processing data, the SPEC program in SEISAN software is

used. More information about the parameters and program are given in Appendix C. However, in following sections, the same cases in pervious methods (SSR method using weak motion) of the same two stations (MRKH and SLAT) and the same two groups of earthquakes are used.

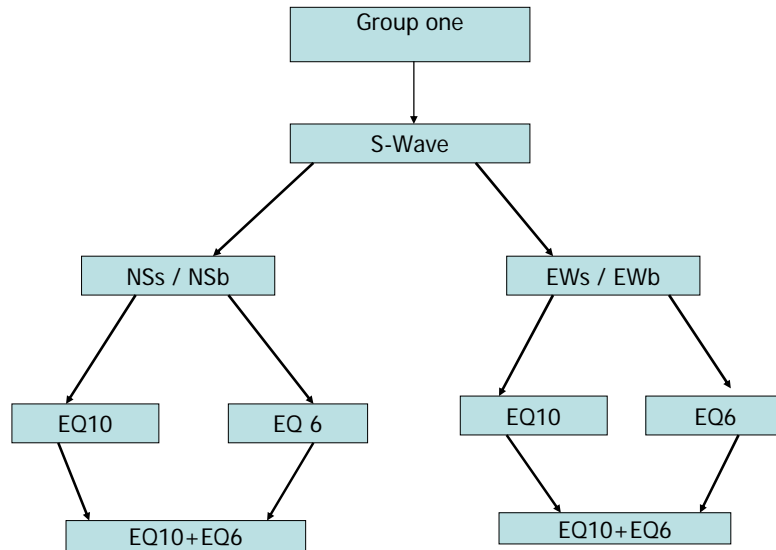


Figure 3.41: Sketch shows the structure of analysis of  $H_s/H_b$  standard spectral ratio of the S-wave recording from two earthquakes EQ10 and EQ6.  $H_s/H_b$  is the ratio of the horizontal components two stations. S: sediment, b: bedrock, N: N-S component and E: E-W component. The horizontal components at MRKH ( $H_s$ ) relative to the horizontal component at SLAT ( $H_b$ ).

For each group of earthquake, the standard spectral ratio of station MRKH (s) sediment and SLAT bedrock (b) with two relative spectral of horizontal components Earthquake spectrum of sediment E-W/ Earthquake Spectrum of bedrock E-W or Earthquake spectrum of sediment N-S/ Earthquake Spectrum of bedrock N-S using with S-wave part of earthquakes records ( $H_s/H_b$ ) are calculated. In each, relative spectra of the horizontal components of the two stations are given. The standard spectral ratio using two groups of earthquakes is analyzed separately.

In group one, the structure of data analysis is given as sketch in Figure 3.41. The results of all spectral ratios computed from two earthquake analysis are given in Table 3.6.

Table 3.6 Standard spectral ratio result of S-wave of group one. Spectral ratio of the horizontal components of sediment (MRKH) to bedrock (SLAT) using two earthquakes (EQ10+EQ6) recorded.

Earthquake	Relative stations	Fundamental frequency on spectral ratio	Amplification on spectral ratio
EQ10+EQ6 (S-wave)	S MRKH s-n/S SLAT s-n	0.98	2.88
EQ10+EQ6 (S-wave)	S MRKH e-w/S SLAT e-w	1.32	6.12

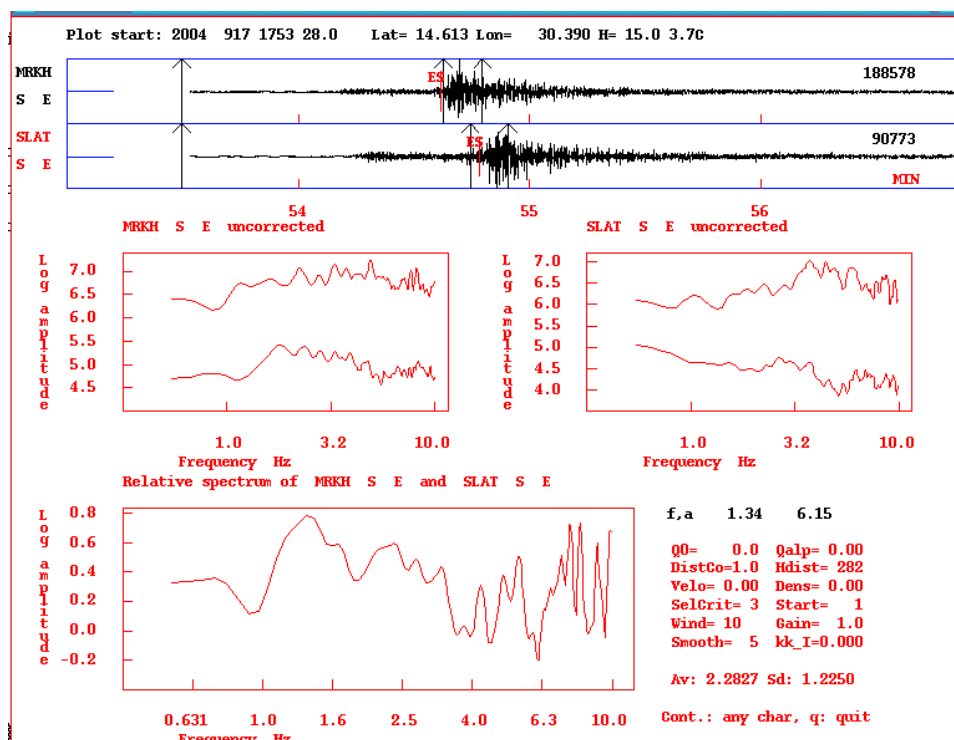


Figure 3.42: The waveforms (top), spectral ratio (middle) and spectral ratio (bottom) of horizontal components (EW) of the S-wave part of earthquake on 2004. In the upper plot we see the two records for the earthquake of 2004 in two stations MRKH and SLAT. In the bottom of the figure to the left is the spectrum of the MRKH and to the right is the spectrum of the SLAT. Below is the ratio of horizontal component MRKH to that of the horizontal component of SLAT. Here we can see the fundamental frequency around 1.3Hz with amplification factor of 6.2.

During the analysis we observed that two different earthquakes have the same spectra of Hs/Hb ratio. Both spectra have the same frequency and amplification factor. Figure 3.42 and 3.43 shows the similarity of these two case. The sandstone formation where the MRKH station is located has an amplification factor about 6.2 at frequency

around 1.3Hz. This result by this method is the same as one obtained by H/V ratio using noise records. This observation led to deeper investigations about why these two earthquake have such a similarity. There are two observations that can be distinguished between these two spectra. First, is the spectrum of the SLAT station at right hand side in figure 3.43, the distribution of earthquake energy through the frequency range from 1 to 10 Hz is different than the one obtained in figure 3.42. Second by the similarity of spectra of two earthquakes is only observed on north- south component (Figure 3.45).

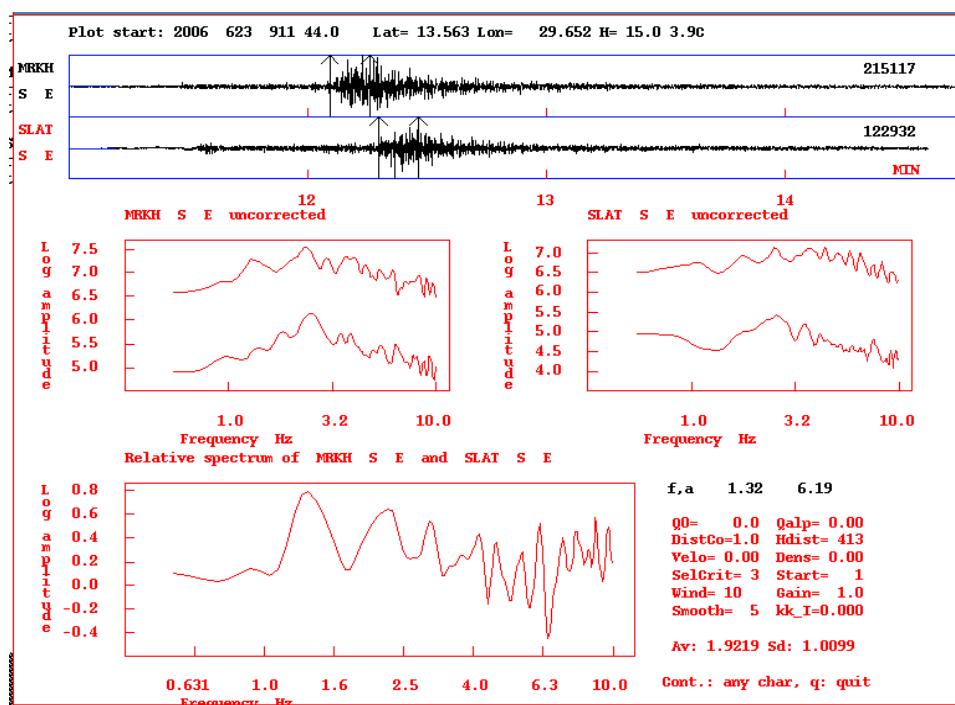


Figure 3.43: The waveforms (top), spectral ratio (middle) and spectral ratio (bottom) of horizontal components (EW) of the S-wave part of earthquake on 2006. In the upper plot we see the two records for the earthquake of 2006 in two stations MRKH and SLAT. In the bottom of the figure to the left is the spectrum of the MRKH and to the right is the spectrum of the SLAT. Below is the ratio of horizontal component MRKH to that of the horizontal component of SLAT. Here we can see the fundamental frequency around 1.3Hz with amplification factor of 6.2.

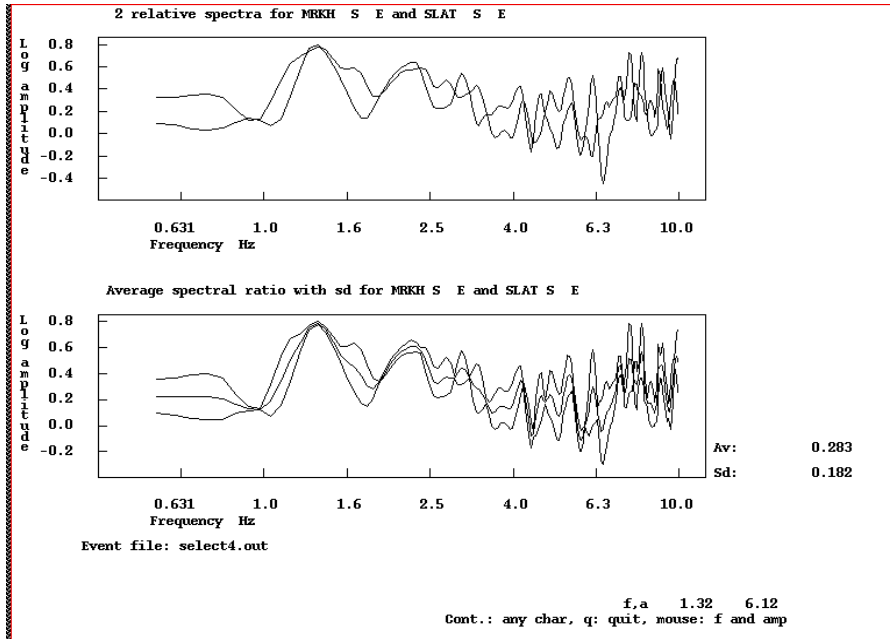


Figure 3.44: The standard spectral ratio  $H_s/H_b$  (EW/EW) ratio of S- wave of two horizontal component (EW) of sedimentary rock ( $H_s$ ) and bedrock ( $H_b$ ) for two earthquakes (EQ10+EQ6) in the top. The average spectral ratio with its spectral is shown in the bottom the amplification of that wave is about 6 at low frequency around 1Hz. Here we see clear by that the two relative spectra have the same shape.

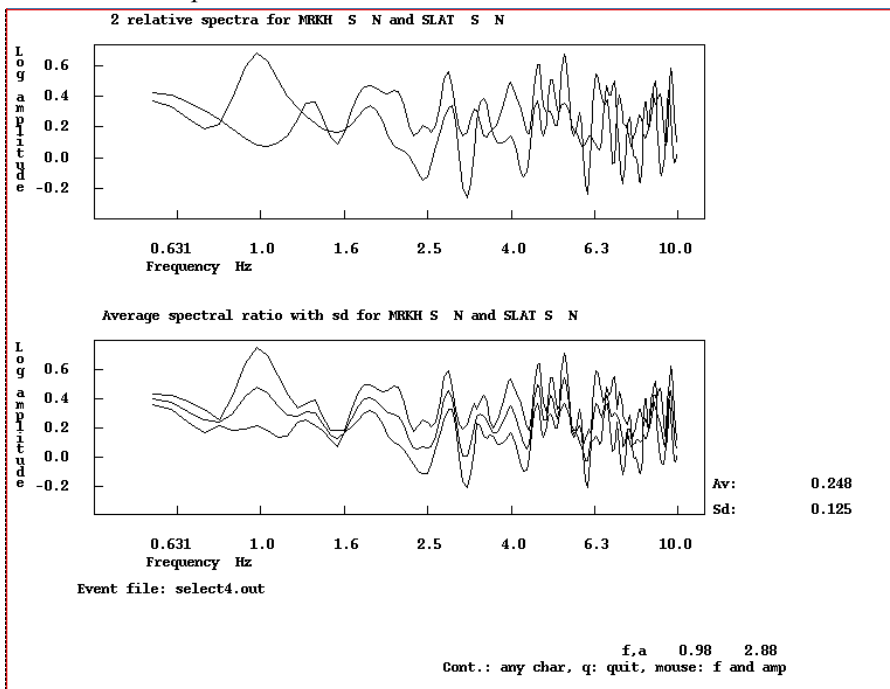


Figure 3.45: The standard spectral ratio  $H_s/H_b$  (SN/SN) ratio of S- wave of two horizontal component (SN) of sedimentary rock ( $H_s$ ) and bedrock ( $H_b$ ) for two earthquakes (EQ10+EQ6) in the top. The average spectral ratio with its spectral is shown in the bottom the amplification of that wave is about 2.9 at low frequency around 1Hz. In the upper of the figure we see the two spectra of two station are no the same.

Group two contains four earthquakes. The processing of data analysis of standard spectral ratio is given as sketch in figure 3.46. The results of all spectral ratios computed from four earthquake analysis are given in Table 3.7. Both spectral ratios have the same frequency and amplification factor, but they have different shape of spectral. Figure 3.47 and 3.48 shows the different of two average spectral ratios shape. There are two observations that can be distinguished between these two spectra. First, the four relative spectra for those two horizontal components are quite different in both spectra. There are three spectra of earthquakes which have the same shape and show the amplification between frequencies from 1.0 Hz to 1.6 Hz. Second, the shape of spectral ratio broader between frequencies range from 1 to 2.5 Hz is only observed on east-west component in figure 3.47.

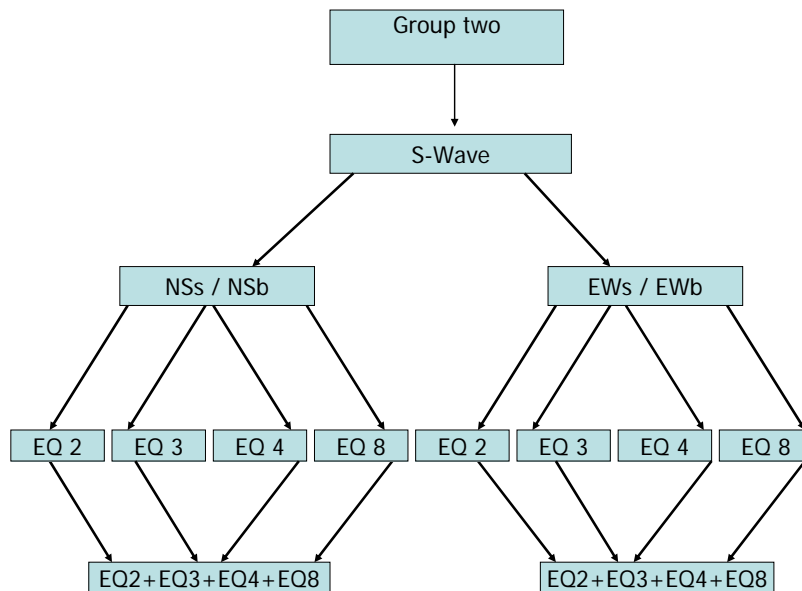


Figure 3.46: Sketch shows the structure of analysis of  $H_s/H_b$  standard spectral ratio of the S-wave recording from two earthquakes EQ2, EQ3, EQ4 and EQ8.  $H_s/H_b$  is the ratio of the horizontal components two stations, s: sediment, b: bedrock, N: N-S component and E: E-W component. The horizontal components at MRKH ( $H_s$ ) relative to the horizontal component at SLAT ( $H_b$ ).



Table 3.7: The standard spectral result of S-wave of group two. Spectral ratio of the two horizontal components of sediment (MRKH) to bedrock (SLAT) using four earthquakes (EQ2, EQ3, EQ4 and EQ8). The result obtained fundamental frequency and amplification factor of the S-wave.

Earthquake	Relative station	Fundamental frequency on spectral ratio	Amplification on spectral ratio
EQ2+EQ3+EQ4+EQ8 (S- wave)	S MRKH <sub>N-S</sub> /S SLAT <sub>N-S</sub>	1.86	1.40
EQ2+EQ3+EQ4+EQ8 (S- wave)	S MRKH <sub>E-W</sub> /S SLAT <sub>E-W</sub>	1.85	1.41

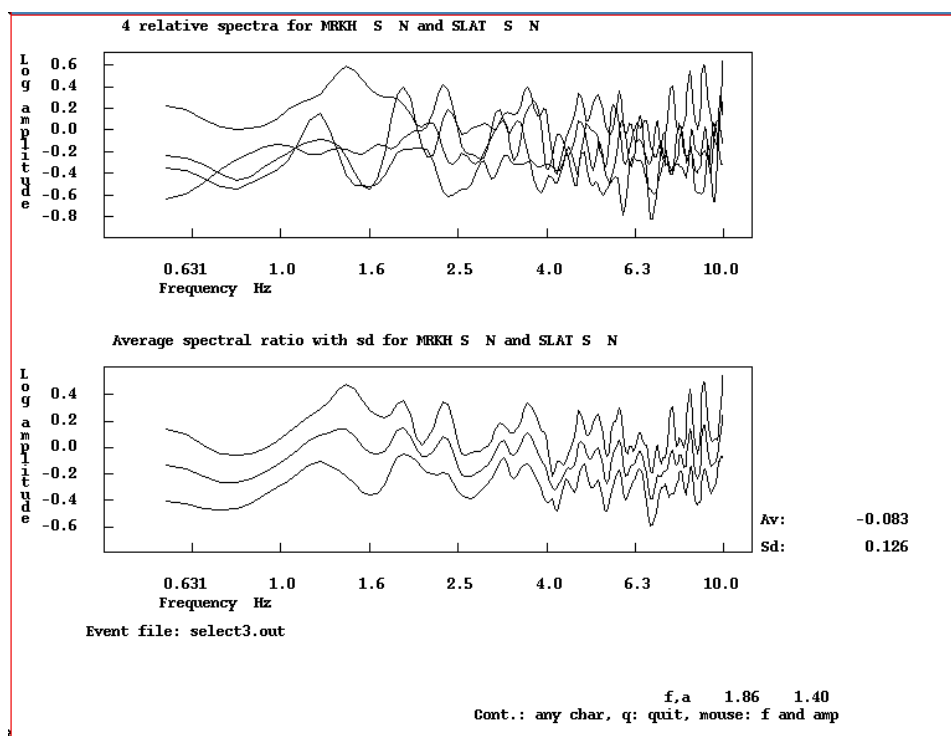


Figure 3.47: The standard spectral ratio  $H_s/H_{sb}$  ratio of S- wave of two horizontal components of sedimentary rock ( $H_s$ ) divide to bedrock ( $H_b$ ) for group two. Group two contain four earthquakes (EQ2+EQ3+EQ4+EQ8). The amplification is about 1.4 at frequency of 1.9Hz. In the upper part of the figure we see all four earthquake spectra.

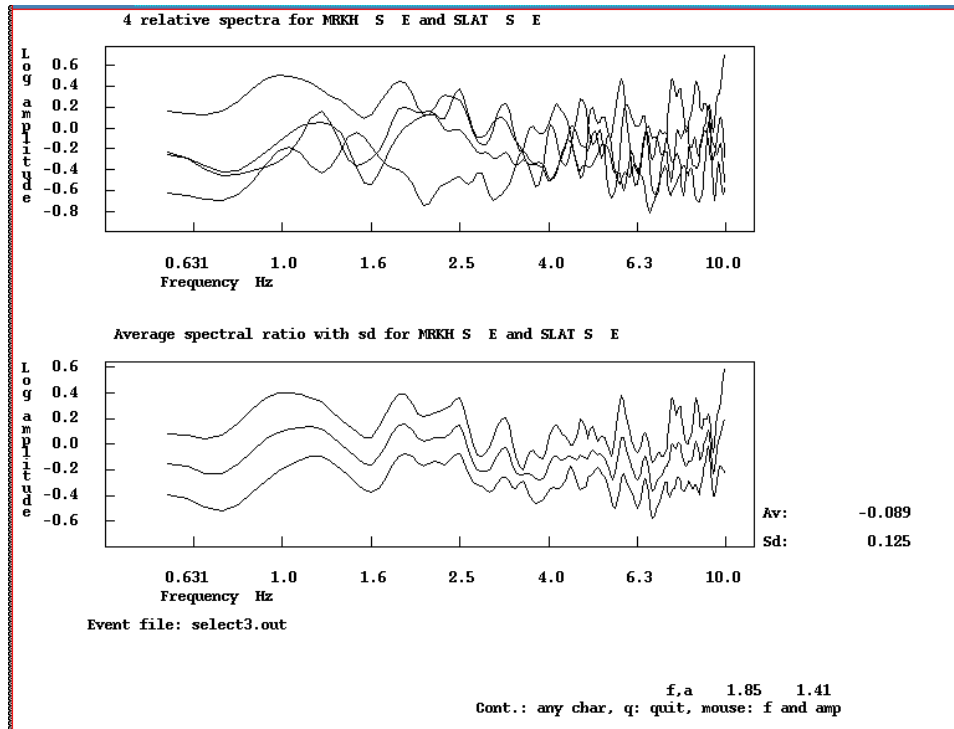


Figure 3.48: The standard spectral ratio  $HSEs/HSEb$  ratio of  $S$ - wave of two horizontal component of sedimentary rock ( $Hs$ ) and bedrock ( $Hb$ ) for group two. Group two contain four earthquakes ( $EQ2+EQ3+EQ4+EQ8$ ). The amplification of that wave is about 1.4 at around 1.9Hz. In the upper part of the figure we see all four earthquakes spectral.

### 3.3 Discussion of the local site effects

#### 3.3.1 Description of the H/V ratio results with respect to geological units

In section 3.2.1 two maps were produced showing the distribution of fundamental frequency and amplification factors (Figure 3.29 and 3.30). The result shows a clear relation between the fundamental frequencies and the type of geological units. Furthermore, within the same geological units there are different site responses. In this section we will discuss the average of our result for spectral ratios vary all the formations in the study area. Spectral attention is given to the fundamental frequency and the underlying geological units. The measurements are based on ambient noise records. H/V spectral ratios are divided into two major groups' of sedimentary units and hard rock based on the geological map (Figure 3.4) and our observations (Figure 3.3). All the site

spectra are within the frequency range from 1 to 10 Hz. The reason of choosing this range of frequency is that the most site measurements consist of this range.

Figure 3.49 shows eight spectral ratios for all the formations in the study area. To simplify the results we divide them in two groups; first group showing the spectra of the hard rock sites (Basement Khartoum, Basement Omdurman and Basalt Omdurman site are named **A**, **B**, **C** respectively) and the second group contains the spectra of the sedimentary units (Cretaceous sandstone Omdurman site, Gezira formation Omdurman site, Older alluvium Khartoum site, Recent alluvial Omdurman site and recent alluvial Khartoum site are named **D**, **E**, **F**, **G** and **H** respectively). In the following paragraphs we will discuss the H/V ratio of these two groups.

The H/V spectral ratios on hard rock sites (**A**, **B** and **C**) do not show a flat response as expected in an area with one unit of rock. Both **A** and **B** have almost the same spectra which is close to flat spectra but they have amplification at low frequency range while the **C** shows amplification of 1.4 at a frequency around 5.5 Hz. In both cases the amplification factor is more than 1.4. The reason for that, is either those areas have thinner layers underlying site measurements as identified by high frequencies (Figure 3.19, 3.20 and 3.21) or that these sites such as Basement rock in Khartoum and Basalt rock in Omdurman area are affected by surface mining activities. There is a dam in **B** area which may have some effect on amplification as well.

The second group shows the spectral ratios of the sedimentary formations (**D**, **E**, **F**, **G** and **H**). Four spectra **D**, **E**, **G** and **H** show peak of amplification at low frequencies around 1 to 2 Hz, and the **F** spectrum shows a peak amplitude at a frequency around 3.8 Hz. A high amplification factor, approximately of 9, with a low fundamental frequency of 0.9 Hz was observed on the spectrum **H**. These sites were located on unconsolidated sediments mainly clay with sandstones, which has thickness more than 400 m (Mohammed et al., 2002). This result is consistent with what is expected from a thick sediment layer (Reiter, 1990). All these sites are placed close to the White Nile River which has a thick sediment layer. The sharp contrast between the sediment and the underlying bedrock gives a clear peak of amplification. The average of site response on the Cretaceous sandstone of the Omdurman formation is shown in spectrum **D**, it gives a maximum amplification factor of 4 at frequency around 1.5 Hz. Most of the study area is

covered by this unit. There is no difference in frequency values that obtained in figure 3.29. The variation of the thickness of uppermost layers and consolidation of upper mudstone rock may have little difference than average shown in spectrum **D**. The topography of the area at western Omdurman town probably affects the result.

The **G** spectral shows the site response on recent alluvial stone of Omdurman site. The peak amplitude is at less than 1 Hz and reaches an amplification factor of 3.2. From our survey, it is seen that the topmost layer of soil is compact when compared to underlying unconsolidated sediment which is more than 500 m (Mohammed et al., 2002). If we compare this case with **D**, it is seen that the amplification dramatically changes with frequency depending on the thickness of the layers underneath. Since the areas between **D** and **G** have the same topography, the site effect change is probably by associated with thickness of the underlying layers.

In figure 3.49 the spectra shown in **E** and **F** have a similar shape with average amplification around 2.7, but both spectra have two peaks at two frequencies. **E** has two peaks, one with high amplification at low frequency around 1 Hz while the second peak is at 4 Hz with low amplification. Here, the shape of the spectral ratio is the same as in Omdurman (**D**, **G** and **H**). The available geological map (Figure 3.4) and borehole data reveals that this area has a complex pattern of clay lenses overlain by a thin sandstone layer at surface, which could be reason to have these peaks at low frequency. The second peak at 3.5 Hz probably reflects the thin layer of consolidated sandstone. Recently constructed buildings in this area have stability problems, which may be due to site response. The spectral ratio **F** show the same site response as given in **E**, but with opposite peaks occurring at frequency range from 1 to 4Hz. The high peak occurs at high frequency relative to low peaks. In this case, according to geological observation that, two most upper layers is exactly opposite at Omdurman area have site response given in spectrum **E**. As mentioned earlier in section 1.5.2, these two sites have similar formations according to the map made by GRAS (1988 and 2006), but were located at different sides on the eastern and western part of the White Nile River. For these two cases the response spectral is looks have similar frequency and amplification but they have different shape. For these two cases, the topmost layers are different. This could be due to the topmost

layers of the mudstone of the Gezira formation on Omdurman is highly compacted where compare with the older alluvium at Khartoum sites (F).

In conclusion, the last five sedimentary formations show a good correlation between the geology and the site response. The H/V spectral ratio in this case seems to successfully estimate the frequencies on which sediment amplification occur.

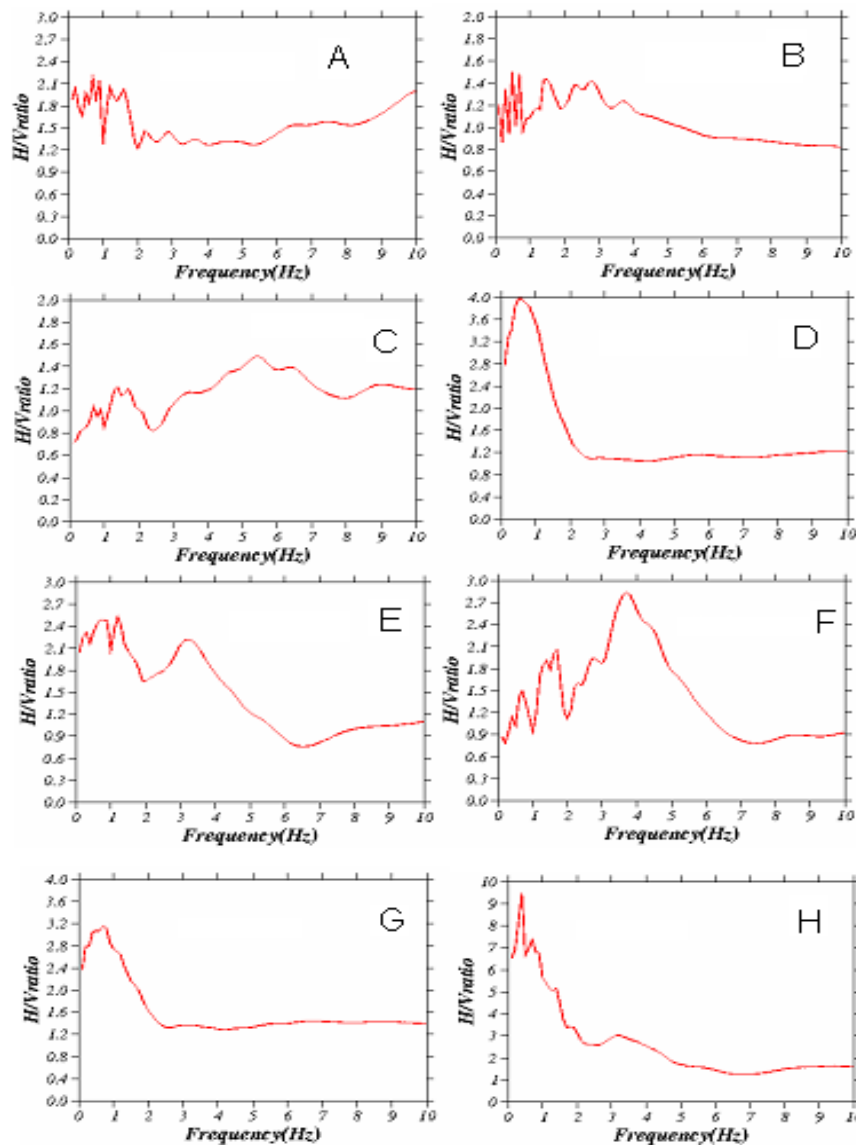


Figure 3.49: Eight H/V average spectral ratios representing the eight formations in study area. Basement complex Khartoum (A), Basement complex Omdurman (B), Basalt rock Omdurman (C), Cretaceous sandstone Omdurman formation (D), Gezira formation Omdurman (E), Older alluvium Khartoum (F), Recent alluvial Omdurman (G) and Recent alluvial Khartoum (H).

### 3.3.2 Description of the H/V ratio result with respect to subsurface layers

In the following paragraphs, we correlate the thickness of various formations with the H/V spectral ratios. In figure 3.29 and 3.30 the distribution of the fundamental frequency and amplification factor respectively in the study area show a number of anomalies. From the previous papers, three cross-sections in study area based on the borehole data are constructed by Farah et al, 1997. Here we used these three cross-sections which are shown in figure 3.4. These three cross-sections with the sites of measurement are given in figure 3.51. From this figure, it is clear that strong lateral and vertical variations exist in the three cross-sections. More information about these sites on those cross-sections is given in Appendix B.

Below, the H/V spectral ratio results for each of three cross-sections through the sites that fall along them are discussed.

**Section A- A<sup>1</sup>** is crossing the area along the White Nile river at the western bank, trending north-south. The H/V spectral ratios of sit M42 is given in appendix C and also seen from the two figures 3.29 and 3.30. The fundamental frequency is around 1.2 Hz with amplification around 5. The sediments under this point have alternating layers of mudstone and sandstone. The thick of the sandstone layer is approx 12 m. We expected that this site have two subsurface layers and may reflect two or more peaks in the spectrum. This is exactly what we see in the spectrum computed from the site M42. Sites M56, M90, M51 and M91 are the same response with having amplification around 4 at a frequency less than 1Hz. That could be reasonable for these points since we can see that these sites are underlain by thick layers.

Sites M03, M05 and M93 show peaks at a low frequency around 0.8 to 0.9 Hz with high amplification about 16 to 18, while site M93 has lower amplification around 1.5. It's the possible explanation for this variation is due to the thickness of the layers under these points. We could see that both sites M03 and M05 have low frequency which may be due to the thickness of the mudstone layer, while the site M93 has a wide band peak with less amplification. This can be explained as the site M93 was located on thick sandstone layer with high degree of consolidation. Since the areas are flat along this section, and acoustic impedance contrast between mudstone and sandstone layers is high,

we believe that the majority of the H/V spectral ratios from these sites have a good agreement with subsurface layers.

**Section B-B<sup>I</sup>** as we observed from figure 3.29 and 3.30, four anomalies of frequencies and amplification factors are present in this section. We would like to have explanation for these anomalies, since the majority of these points on the section are located in one formation (Cretaceous sandstone formations). The spectrum of site response at site M82, as we could see, has peak amplification around 0.7Hz with amplification factor around 2. As we observed before in **section A- A<sup>I</sup>**, those points are located on mudstone and have the same frequency spectrum as M82, have less amplification when correlated with those points at **section A- A<sup>I</sup>**. We can explain that those points on **section A- A<sup>I</sup>** are located inside the city with more noise which might generate higher amplitudes, where point M82 is far away, in a quiet place. Therefore, we believe that those points have a reliable H/V ratio. Sites M99 and M98 show peaks at a low frequency around 1 Hz, as we could expect in an area which has a basin or thick sedimentary layers under these sites. That is exactly what we observed in our section **B-B<sup>I</sup>**. The amplification factor seems to be the same in both site M99 and M98, while this amplification is higher than shown in site M55. If we consider the stratigraphy of these layers underneath this variation of amplification can be expected. Furthermore, the layers under these sites are characterized by single layer of sandstone. This may explain why these spectra should have a low frequency. The spectra ratio computed from points M87, M63 and M13 show gradual increase in the frequencies when the depth of mudstone is increasing. We expect that the fundamental site frequency decrease from the hills to river (White Nile) based on Equation 3.10 (Reiter, 1990). Another explanation for that could be that this area is highly inhabited the ground water level is shallow. The remaining sites in this section have the same effects until site M03, which shows again many peaks, which is a reflection of more than one layer under this site.

**Section C - C<sup>I</sup>** crosses most formations in the study area with variation of the layers at depth. The site response spectrum computed for the site M115 is mostly flat, except from a peak at about 14Hz with low amplification. That may be due to thinner layer under this site. Site M77 shows the site response spectrum with low frequency around 0.9 Hz which could be reasonable if we consider the thickness of the layer under this point. At sites

M38 and M59 there are high frequencies peak around 4Hz with a low frequency peak that may be due to the following observation; the sites are located on sandstone, which is a highly consolidated layer and has a flat topography. Furthermore, since these points are located on sandstone, we compared the spectra ratio from the sandstone formation (**D**), as we described in 3.3.1 in part (site response with geological formation) with a second spectrum obtained from these points which have high frequency (**D\***). These two spectra ratios are given in figure 3.50. We recognize that both have a peak at low frequency around 1Hz, while these have different amplifications. The **D\*** has in addition a peak at high frequency, showing us more than one peak. Therefore, we believe that these points may reflect the sharp boundaries between two or more layers under these sites. The site has high amplification with frequency around 1.1Hz. This does not fit with subsurface layers which are located on thick sandstone layer. The sites M37, M36 and M10 represent frequency around 1.2Hz but with different amplifications. This variation could be due to topography, where the thickness of the layer is 34 meters above the surrounding of the flat area. The level increases gradually, which may be the reason for having high amplifications. We expected to see high frequency at spectrum of site M36 because it is located on a thinner mudstone layer.

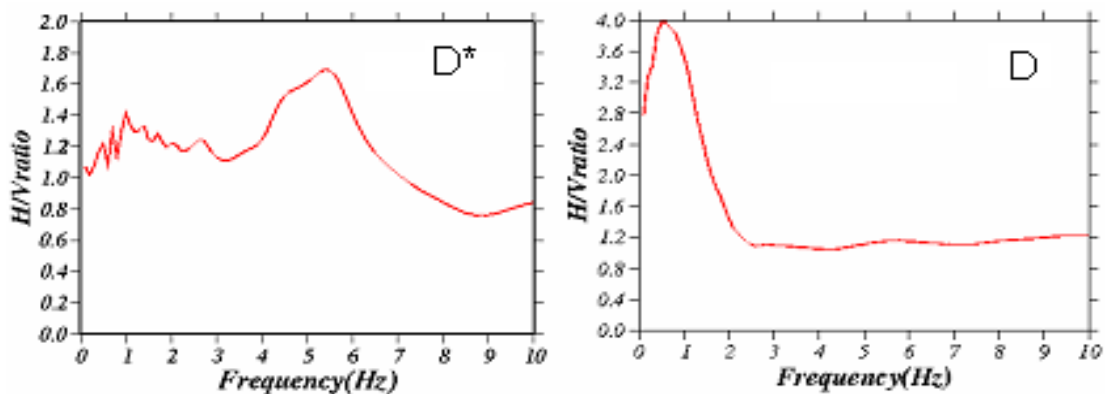


Figure 3.50: Two groups of the site response for Cetaceous Sandstone Omdurman formation, **D** is average site response of all sandstone sites and **D\*** is average of site response spectrum of cetaceous sandstone formation located southern Basalt area with high anomalies of frequency.

Most of site response from our data follow the expected relation between the fundamental frequencies and thickness of layer (Equation 3.10) (Reiter, 1990). The missing agreement between the distribution of the amplification factor at fundamental



site frequency and subsurface geology is probably related to the fact that the amplification factor is poorly constrained by the used empirical approach (Nakamura, 2000).

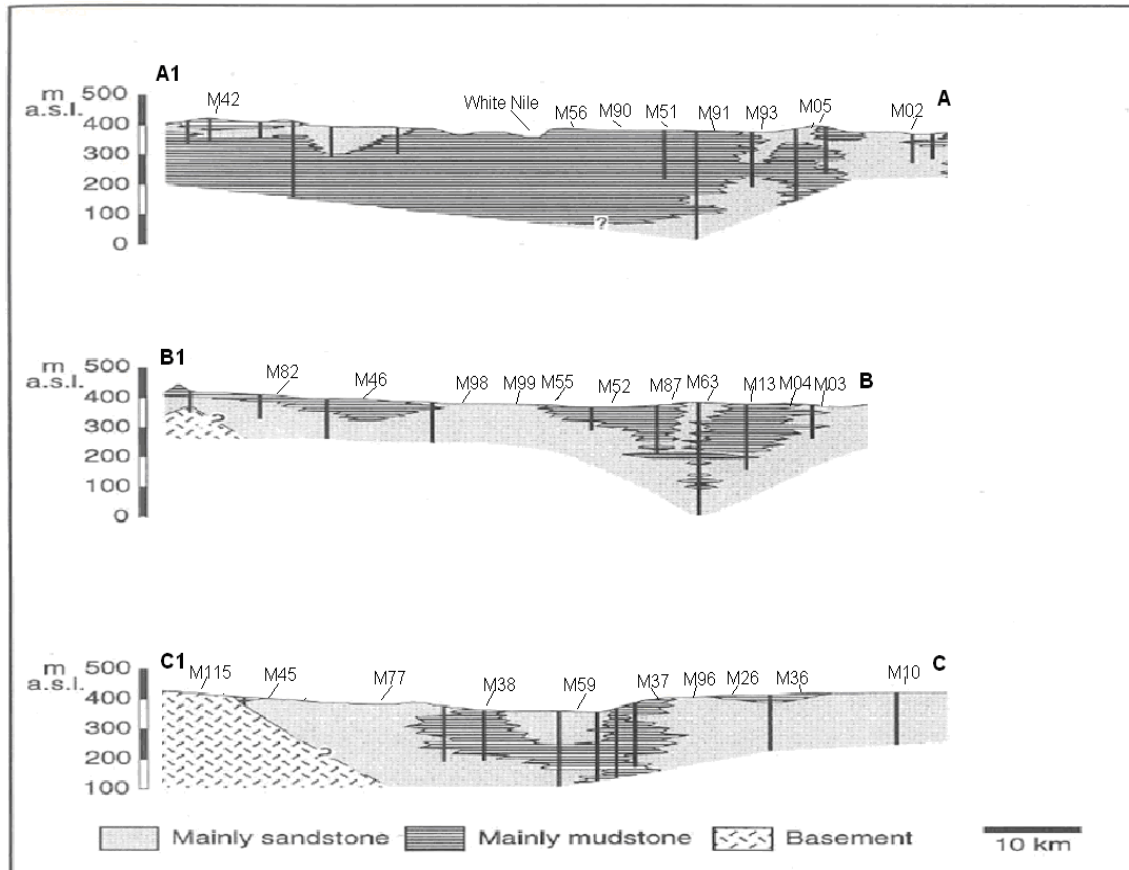


Figure 3.51: Three cross sections show the sedimentary sequence of the Omdurman area. The locations of these are shown in figure 3.4. On top of these sections shows the some sites from our measurements (Farah et al., 1997).

### 3.3.3 Description of the H/V ratio and Standard Spectral Ratio result using earthquake data

Two methods, H/V ratio and SSR, are used to analyze the earthquake data and estimate the local site effects in Khartoum area. The results are given in section 3.2.2. The results are discussed in terms of the quality of data and local site effects with respect to the geological units of the Khartoum area. In following paragraph we will describe H/V ratio and SSR method results separately.

At the first method, H/V ratio results are shown in table 3.4 and 3.5. Two groups of earthquake records with S-wave and noise wave parts are used in the analysis. In both two groups of earthquakes H/V ratios of S-waves' have the same sequence. They have amplification of MRKH station at frequencies 3 to 4 Hz with high amplification factor depending on the distance of earthquake groups' location. The closest group has higher amplifications than the group with a far location. The only explanation of that is the Cretaceous sandstone where station (MRKH) located has amplified wave. The H/V ratio with component north-south direction consists of high amplification wave than one have component east-west direction. This could be due to structure under this station as parallel to Khartoum basin (see Figure 1.5 and 1.8). In SLAT station, the H/V ratios of S-wave records in both groups have amplified at lower frequency compare to MRKH station with the less amplification.

In SLAT station we expected to have a flat response, since this station placed in basement unit which is granite rock. It has amplification at lower frequency. That probably due to station employed in exposed rock that the surface may contain numerous fractures and weathered patches, making it less compact. Such a site may have its own site response spectra that may not be flat. From two groups analysis used noise wave, there no systematically of amplification observed at both station MRKH and SLAT. in group one show the amplification at low frequency around 1 Hz, while in group two have amplification wave at high frequency relative to group one more than 1.5 Hz.

We observed relation between the earthquake groups location with the frequency is propotional, while with amplification factor is reverse. However, according to Equation 3.10 (Reiter, 1990) there are no consequences between the H/V ratios of S-wave and thickness of sediments underlying these two stations. It is opposite of what we expected. The thickness of sediment underlain MARK station is thickening than underlain of SLAT station. It is suppose to have lower frequency at MARK station. In other hand the frequency represented in H/V of noise waves in two stations are fit with concept of Equation 3.10.

At the second method, SSR, the results are divided in two earthquake groups. In these two group the standarl spectral ratio is consist of frequency range from 1 to 2 Hz, while the amplification factors are different. The amplification given by this method is

obtain amplified of S-wave in MRKH station, if SLAT station is considered as a reference station. In group one, the resonance frequencies are consist with high amplification shown in component on east-west direction, while on north-south direction is not obtained less amplification. This may be due to some factors; the structure underlying these stations, the geometrical of Khartoum basin, and the azimuth of those earthquakes relative to stations location. It is difficult to interpret by using these factors, because there are no focal mechanism available of those groups of earthquakes and there are no geological data available underlain those stations. In group two of earthquake given in Table 3.7, showing the fundamental frequency and amplification factors of two components are the same. The spectral show the high peak only component on north-south. We expected to have high amplification compare to group one, hence the source is close to stations, but this case does not observed. The only explanation is that, those earthquakes have small magnitude and their azimuths are different which cannot distinguish between these spectral component ratios. However, in order to check this method in right way at these groups earthquakes (group one and group two), we must have a flat response at bedrock station (SLAT). That mean the amplification should be 1 at bedrock station. For all calculation results have been done, either in H/V ratio (S-wave and noise wave) method or by using this method. They show amplification at SLAT station more than 1.5 and there are no flat response in SLAT station. In both methods do not have reliable amplification because the main assumption of far-field approximation is invalid.



# 4 Conclusions and future perspectives

## 4.1 Conclusions on the seismotectonics of Central Sudan

At following there is a summary of conclusion based on the seismotectonic analysis:

- 1- The focal mechanism for the 1966 earthquake obtained in the study indicates left-lateral faulting along a fault oriented NE-SW ( $17N^0$ )
- 2- The interpretation of this focal mechanism in the regional context is difficult. However, the proposed fault plane fits the orientation of the earlier zone of weakness associated with the White Nile Rift system.

## 4.2 Conclusions on the local site effect study applied in Western Khartoum

As discussed in chapter one and chapter three, the geology, tectonics of central Sudan in particularly the geology of Khartoum area, is expected to give local site effects. An important following conclusion can be drawn:

- 1- The obtained site response mainly based on H/V spectral ratio is in generally good agreement with the underlying geology.
- 2- The complexities of the subsurface sedimentary layers are partly reflected in the H/V spectral ratio results.
- 3- The eastern bank of the White Nile shows a low frequency peak with high amplifications.
- 4- The H/V ratio using noise has systematic comparisons with site spectrum obtain from H/V ratio using noise and S-wave part of earthquake records, found that the method reproduces very well as the shape of the site response, but underestimates the amplification level. Therefore conclude that H/V ratio, when applied to the S-

- wave signals, reveals the overall frequency dependence. In some cases we did find a good similarity in parameter as fundamental frequency and amplification factor but in a few other H/V ratios we were only able to identify the fundamental resonance frequency. Furthermore, it should be pointed out that this technique has good consistency when applied in soft soil sites only, and might not be valid for other kinds of site effects.
- 5- The standard spectral ratio results show poor correlation. This is probably due to the earthquake locations with respect to the recording stations that may not be ideal.

As it is seen in the previous chapters, the area between Jebel Dumbeir and Khartoum need to be studied in more detail, to understand the shallow earthquakes in that area. Therefore, it is important to install some stations around Jebel Dumbeir and Umm Ruwaba town.

For local sites effect, it seems that the Nakamura method (H/V ratio) is capable of estimating of the fundamental frequency. It's cheap and time efficient. We suggest that similar survey covering the whole city should be performed. We also suggest that other geotechnical methods must be used in parallel to give better constraint of exact amplification factors. Since the reference site (SLAT station) situated on rock may have some local effects. We suggest redeploying SLAT station again either in the area close to the Sabaloka Igneous Complex or western of Gili Oil refinery close to Nile River where the granites rock was exposed. These two places should be unaffected by topographies. Another alternative for a reference site could be in the basement rock to Awila dam in south of Omdurman town. Information about the fundamental site frequencies obtained from H/V spectral ratio and information about the exact amplification factors at several sites obtained by using SSR technique would give us a good knowledge about the expected damages from a future strong earthquake in Khartoum.

# 5 Acknowledgements

This work would not have been possible without my supervisors Professor Kuvvet Atakan and Professor Jens Haskov, thank you very much for your guidance, support and encouragement during the preparation of this thesis.

I want to say a “great thank you” to Ms. Nada Bushra and Dr. Osman for showing me the way to apply for graduate studies in the University of Bergen.

I would like to thank the Norwegian State Educational loan for funding me throughout my studies.

I would also like to thank the people in the Seismology Research Institute in Sudan for helping me in my field work. Special thanks go to Mr. Bader Eldeen for his efforts to help me during the survey. Many thank to Elena Vezzadini for correct language of text.

I wish to express my gratitude towards the people of the Sudanese Seismological Network, Geological Research Authority of Sudan (GRAS) for giving me data. Special thanks to Mr. Aladdin for fixing my instruments.

Many thanks go to Mohammed Rossi, Aleksandra kandilarov and Dr Mohamed Babekir for helping me in producing the maps with the final results. Many thanks also go to Louise Wedderkopp Bjerrum, Asude Arslan, Hlompho Malephane, Zoya Zarifi, Sajjad, Gerard and the people of Cake-Club.

Finally I want to thank my family, my parent- mother Taiba , father- Ahmed, brothers, sisters and my wife. Also thank my uncles and aunt. They have great support in my considerations and decision of extending my stay in Norway.





# 6 References

- Abdalla, A.E.O., 2006, Aquifer Systems in Kordofan, Sudan: Subsurface Lithological Model: South African Journal of Geology, v. 109, p. 445-458.
- Aki, K., 1988, Local site effect on ground motion, in Earthquake Engineering and Soil Dynamics. II: Recent Advances in Ground-Motion Evaluation, J. Lawrence Von Thun (Editor),: Am. Soc. Civil Eng. Geotechnical Special Publication, v. 20, p. 103-155.
- Almond, D.C., Ahmed, F., and Khalil, B.E., 1969, An excursion to the Bayda Volcanic field of northern Sudan: bulletin Volcanologique, v. 33, p. 544-565.
- Ambrasey, N.N., and Adams, R.D., 1986, Seismicity of the Sudan: Bulletin of the Seismological Society of America, v. 76, p. 483-493.
- Andrew, F.M., 1948, The geology of the Sudan: London, Oxford University.
- Atakan, K., Bard, P.-Y., Kind, F., Moreno, B., Roquette, P., and Tenta A., 2004, J-SESAME: A standardized software solution for the H/V Spectral Ratio Technique: Proceedings of the 13th World Conference on the Earthquake Engineering, v. 2270, p. 37.
- Atakan, K., Brandsdottir, B., P, H., and Fridleifsson, G.O., 1996, Site Response as a function of Near-Surface Geology in the South Iceland Seismic Zone: Natrual Hazards, v. 15, p. 139-164.
- Awad, M.Z., and Schrank, E., 1994, Paleoecology of late Jurassic to mid-Cretaceous of the central and western Sudan: Geoscientific Research in Northeast Africa. Balkema Rotterdam, , p. 369-374.
- Ayad, M., Elrasheid, A., AwadAlla, M., and Khalid, A., 2004, The Determination of abu Delieg Earthquake Intensity: Khartoum, Ministry of Science & Technology, The National Centre for Research, Seismological Research Institute.
- Barazi, N., and Berl, G., 1985, Sedimentologie und Stratigraphie des Abyad-Beckens (NW-Sudan): Abh., v. 64, p. 85.
- Bard, P.-Y., 2004, Effect of surface geology on ground motion: recent results and remaining issues paper presented at 10th Eurpoean Conference on Earthquake Engineering: Austria, Vienna.
- Bath, M., 1979, Introduction to seismology, 428 p.
- Binks, R.M., and Fairhead, J.D., 1992, A plate tectonic setting for Mesozoic rift of west and central Africa: Tectonophysis, v. 213, p. 141-151.
- Bireir, F.A., 1993, Sedimentological Investigations around the State of Khartoum and. on the Northern Central Part of the Gezira – Central Sudan: Khartoum, University of Khartoum.
- Bonnilla, L.F., Steidl, J.H., Lindley, G.T., Tumarkin, A.G., and Archuleta, R.J., 1997, Site amplification in the San Fernando valley, California: Bulletin of the Seismological Society of America, v. 87-3, p. 710-730.
- Borcherdt, R.D., 1970, Effects of local geology on ground motion near San Francisco bay: Bulletin of the Seismological Society of America, v. 60.

- Bosworth, W., 1992, Mesozoic and early Tertiary rift tectonic in East Africa  
Tectonophysics, v. 209, p. 115-137.
- Browne, S.E., and Fairhead, J.D., 1983, Gravity study of the Central African Rift: a  
model of continental disruption Tectonophysics, v. 94, p. 187-203.
- Chapol, I., 1997, State of stress in East and southern Africa and seismic Hazard analysis  
of Malawi: Bergen, M.Sc thesis, Institute of Soil Earth Physics, University of  
Bergen
- Chavez-Garcia, F.J., Sanchez, L.R., and Hatzfeld, D., 1996, Topographic site effects  
and HVSR. A comparison between observations and theory: Bulletin of the  
Seismological Society of America, v. 86-5, p. 1559-1573.
- Clark, R.A., and Browne, S.E., 1987, The Kordofan earthquakes, central Sudan: Journal  
of African Earth Sciences, v. 6, p. 573-581.
- Dawoud, A.S., and Abdelati, A.S., 1988, Structural and Gravity Evidence for an Uplifted  
Pan-African Granulite Terrain in the Sabaloka Inlier: Journal of African Earth  
Sciences, v. 7, p. 789-794.
- Dong, and Shah, 2005, Assessment of Global seismic loss Based on Macroeconomic  
indicators: Natural Hazard v. 17, p. 269-283.
- Ebinger, C.J., and Ibrahim, A., 1994, Multiple episodes of rifting in Central and East  
Africa: A re-evaluation of gravity data.: Geol Rundsch, v. 83, p. 989-702.
- Eltahir, N., B., 2001, A Seismic Noise Study and the Earthquake Hazard in Sudan And  
The Crustal Structure of NE Africa: M.Sc,thesis, Institute of Solid Earth Physics,  
University of Bergen.
- Fairhead, J.D., 1988, Mesozoic plate tectonic reconstructions of the central South  
Atlantic ocean, the role of the West and Central African Rift System:  
Tectonophysics, v. 155, p. 181-191.
- Farah, E.A., Abodullatif, O.M., Kheir, O.M., and Barazi, N., 1997, Groundwater resource  
in a semi-arid area: a case study from central Sudan: Journal of African Earth  
Sciences, v. 25, p. 453-466.
- Farwa, A.G., 1978, Geology and Structure of the Gezira as Deduced from Gravity  
Measurement, M.Sc, thesis. Department of geology. University of Khartoum.
- Giardini, D., and Beranzoli, L., 1992, Waveform modelling of May 20,1990 Sudan  
Earthquake: Tectonophysics, v. 209, p. 105-114.
- GRAS, 1988-2006, GEOLOGICAL MAP OF THE SUDAN, The Geological Research  
Authority of The Sudan
- Hasancebi, N., and Ulusay, R., 2006, Evaluation of site amplification and site period  
using different methods for an earthquake-prone settlement in Western Turkey  
Engineering Geology, v. 87, p. 85-104.
- Havskov, J., and Alguacil, G., 2006, Instrumentation in Earthquake Seismology, 337 p.
- Havskov, J., and Ottemöller, L., 2005, SEISAN, the earthquake analysis software for  
Windows, Solaris, Linux and MacOSx: Bergen, 254 p.
- Hussein M, T., 1992, On the depositional framework of the Cretaceous Omdurman  
formation in Khartoum area, Sudan: Journal of African Earth Sciences v. 14, p.  
559-566.

- Ibrahim, A.E., 1993, Interpretation of Gravity and Magnetic Data from the Central African Rift System, University of Leeds U.K.
- ISC, 1993, Bulletin of the International Seismological Centre - List of events and associated observations October 1993  
Edinburgh, Scotland.
- Kennett, B.L.N., and Engdahl, E.R., 1991, Travel time for global earthquake location and phase identification.: *Geophys. J. Int.*, v. 105, p. 429-466.
- Khiralla, K.M., 1966, A study of the Nubian Sandstone Formation of the Nile Valley between Latitude 14-14.45 with reference to groundwater geology: Khartoum, M.Sc. thesis, Department of Geology, University of Khartoum.
- Lachet, C., Hatzfeld, D., Bard, P.-Y., Theodulidis, N., Papaioannou, C., and Savvaidis, A., 1996, Site effects and microzonation in the city of Thessaloniki(Greece): comparison of different approaches: *Bulletin of the Seismological Society of America*, v. 86, p. 1692-1703.
- Larson, E., 2006, Global CMT Catalog search, G. Ekstrom and N. Nettles.
- Mohamedzein, Y.E.-A., Aabdalla, J.A., and Abdelwahab, A., 2006, Site response and earthquake design spectra for Central Khartoum, Sudan: *Bullitin of Earthquake Engineering*, v. 4, p. 277-293.
- Mohammed, I.A., Jiaying, W., Tianyou, L., and Farwa, D.G., 2002, Sedimentary Basins in the Western White Nile, Sudan, as Indicated by a Gravity Survey *Journal of China University of Geosciences*, v. 13, p. 289-296.
- Mula, A., AwadELLAH, and Alrasheed, 2006, Earthquake activity in abu deleig region as delineated by remote sensing techniques, International conference of space technologies applications khartoum -Sudan.
- Mula, A.H., 1971, A geophysical survey of the J.Aulai region and a study of the fault solution of gravitational anomalies: khartoum, University of Khartoum.
- Nakamura, Y., 1989, A method for dynamic characteristics estimation of subsurface using microtremor on the ground surface.: *Quarterly Report of RTRI*, v. 30, p. 25-33.
- , 2000, Clear identification of fundamental idea of the Nakamuras technique and its applications, 12th World Conference on Earthquake Engineering. Auckland, New Zealand paper 2656.
- Nogoshi, M., and Igarashi, T., 1971, On the amplitude characteristics of microtremor: *Jour.seism.*, v. 24, p. 26-40.
- Özel, Cranswick, E., Meremonte, M., Erdik, M., and Safak, E., 2002, Site Effects in Avcilar, West of Istanbul, Turkey, from Strong - and Weak- Motion Data: *Bulletin of the Seismological Society of America*, v. 92, p. 499-508.
- Pedersen, H., LeBrun, B., Hatzfeld, D., Campillo, and Bard, P.-Y., 1994, Ground motion amplitude across ridges: *Bulletin of the Seismological Society of America*, v. 84, p. 1786-1800.
- Qureshi, I.R., Almond, D.C., and Sadig, A.A., 1966, An unusually shaped basalt intrusion in the Sudan *journal of Geology.Teor*, v. 8, p. 151-160.
- Qureshi, R., and Sadig, A., 1967, Earthquake and associated faulting central Sudan: *NARURAL*, v. 251.
- Reiter, L., 1990, Earthquake hazard analysis *Issues and Insights* p. 254.

- Salama, R.B., 1985, Buried troughs, grabens and rifts in Sudan: *Journal of African Earth Sciences*, v. 3, p. 381-390.
- Sambridge, M.S., and Kennett, B.L.N., 1986, A novel method of hypocentre location *Geophys.astr.Soc.*, 87 p. 679-697.
- Schnabel, P.B., Lysmer, J., and Seed, H.B., 1972, SHAKE: a computer program for earthquake response analysis of horizontally layered sites: Department of Civil and Environmental Engineering, Earthquake Engineering Research Center, Univ. California, Berkeley
- Schrank, E., and Awad, M., 1990, Palynological evidence for the age and depositional environment of the Cretaceous Omdurman Formation in the Khartoum area, Sudan *Berl geowiss Abh A*, v. 120.1, p. 169-182.
- Schull, T., J., 1988, Rift basins of interior Sudan. *Petroleum exploration and discovery The American Association of Petroleum Geologists (AAPG)*, v. 11721, p. 1128-1142.
- Singh, S.K., Reichle, M., and Havskov, J., 1980, Magnitude and epicenter estimatons of Mexican earthquake from isoseismic maps: *Geofisica Internacional*, v. 19.
- Snoke, J.A., J.W. Munsey, Teague, A.G., and Bollinger, G.A., 1984, A program for focal mechanism determination by combined use of polarity and SV -P amplitude ratio data: *Earth quake notes*, v. 55, p. 15.
- Stein, S., and Wysession, M., 2003, *An Introduction to Seismology, Earthquakes, and Earth Structure*, Blackwell Publishing, 498 p.
- Theodulidis, N., Bard, P.-Y., Archuleta, R., J , and Bouchon, M., 1996, Horizontal to vertical spectral ratio and geological conditions: the case of Garner Valley downhole array in Southen California *Bulletin of the Seismological Society of America*, v. 86, p. 306-319.
- Utheim, T., Havskov, J., and Natvik, Y., 2001, Seisolog data Acquisition systems: *Seimological Research Letter*, v. 72, p. 77-79.
- Vail, J.R., 1978, Outline of the Geologyand Mineral deposits of the Democratic Republic of the Sudan, and adjacent areas, : *overseas Geol. Mineral. Resource*, v. 49, p. 1-67.
- Wen, K.-L., Chang, T.-M., Lin, C.-M., and Chiang, H.-J., 2006, Identification of Nonlinear Site Response Using the H/V Spectral Ratio Method: *TERRESTRIAL ATMOSPHERIC AND OCEANIC SCIENCES* v. 17, p. 533-546.
- Whiteman, A.J., 1971, *The Geology of the Sudan Republic*: Oxford, Claredon press.
- Wiechert, E., 1907, Über Erdbebenwellen. Theroretisches über die Ausbreitung der Erdbebenwellen. *Nachrichten von der koniglichen Gesellschaft der Wissenschaften zu Göttingen*, : Mathematisch-Physikalische Klasse, 413-529 p.
- Wycisk, P., Kilitzsch, E., and Reynolds, 1990, Interactatonal sequence development and structural control of Phanerozoic Strata in Sudan- *Berliner geoss: Abh.*, v. 120, p. 45-86.

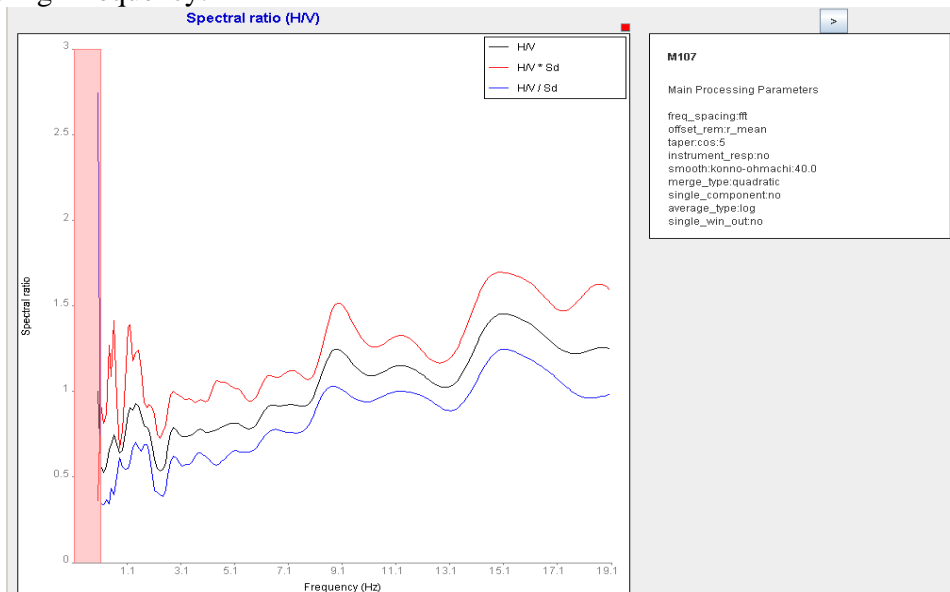
# Appendixes

- A.** *H/V ratio for ambient noise*
- B.** *H/V ratio with subsurface layers*
- C.** *Standard Spectral Ratio and H/V ratio using local earthquake records*

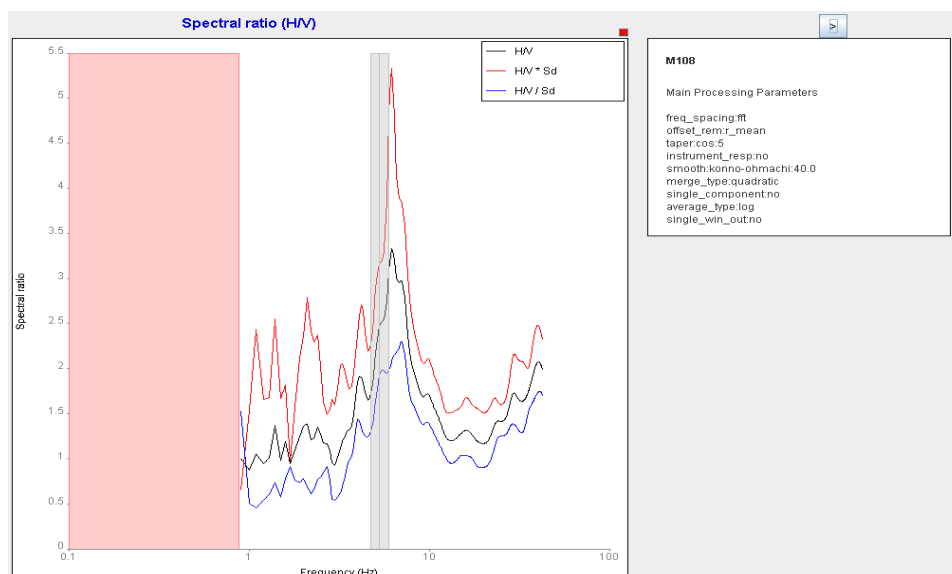


# Appendix A: H/V ratio for ambient noise

Example of Two sites are located on Basalt formation have influence of amplification at low and high frequency.



*This figure shows the site response spectrum computed at site M107, located in basalt rock in central of study area, all show high frequency around 15 Hz.*



*This figure shows the site response spectrum computed at site M108 located in basalt rock in central of study area, all show high frequency around 9 Hz.*

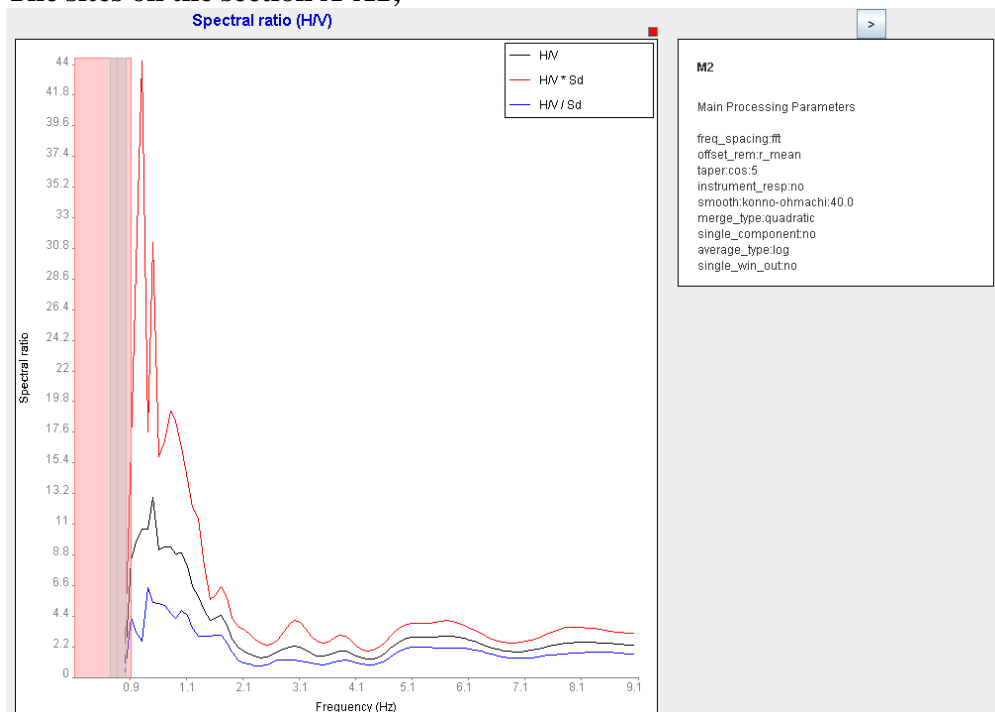


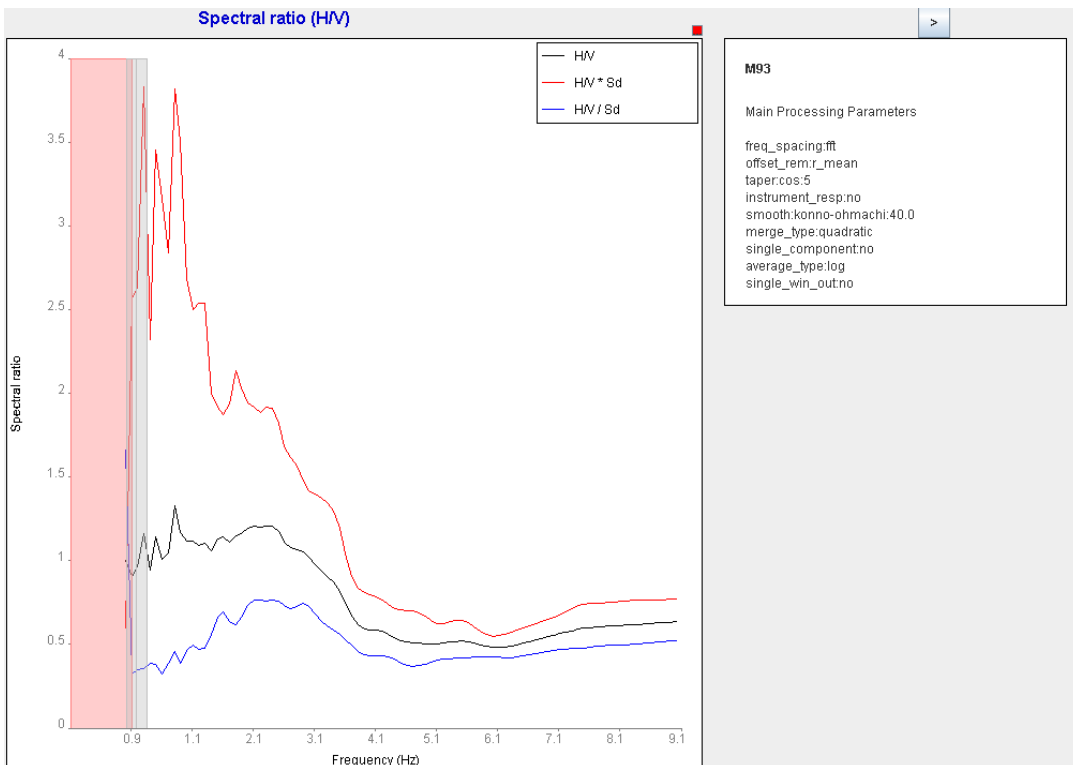
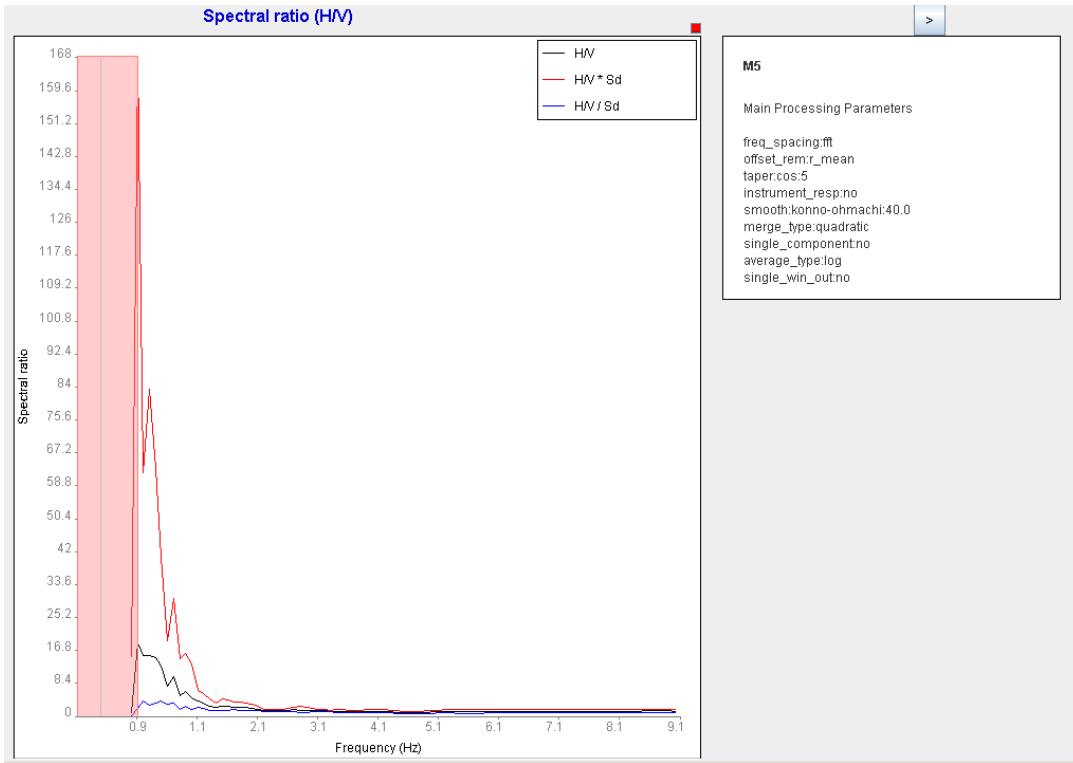


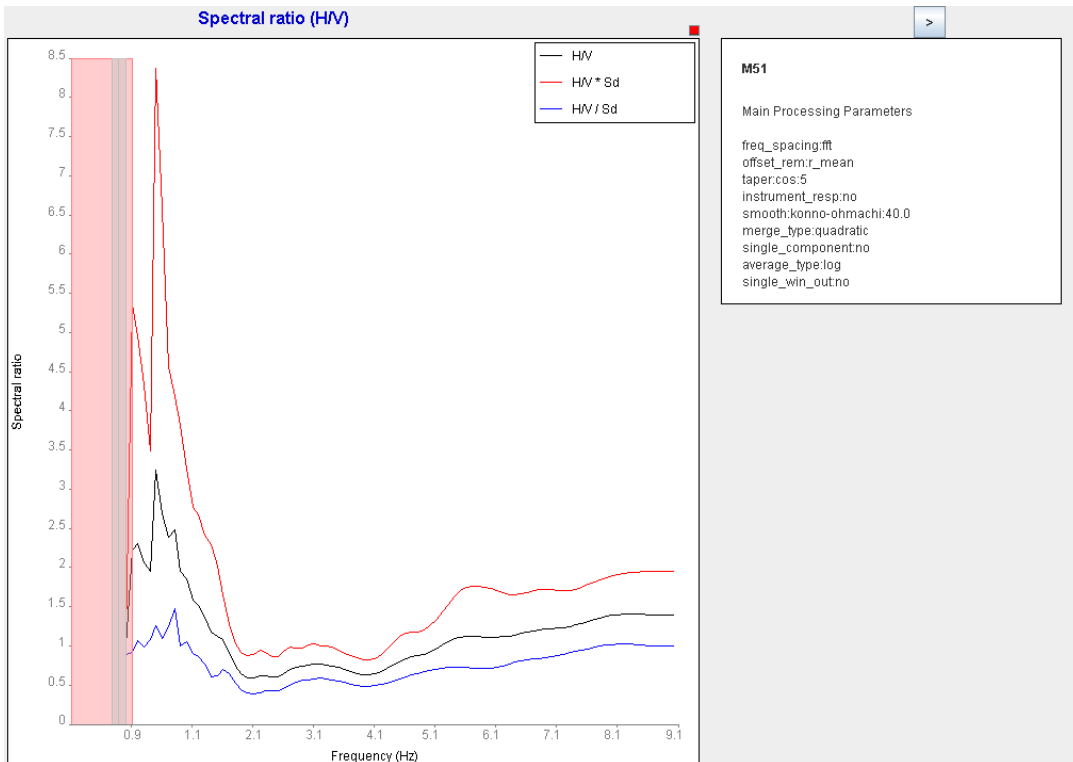
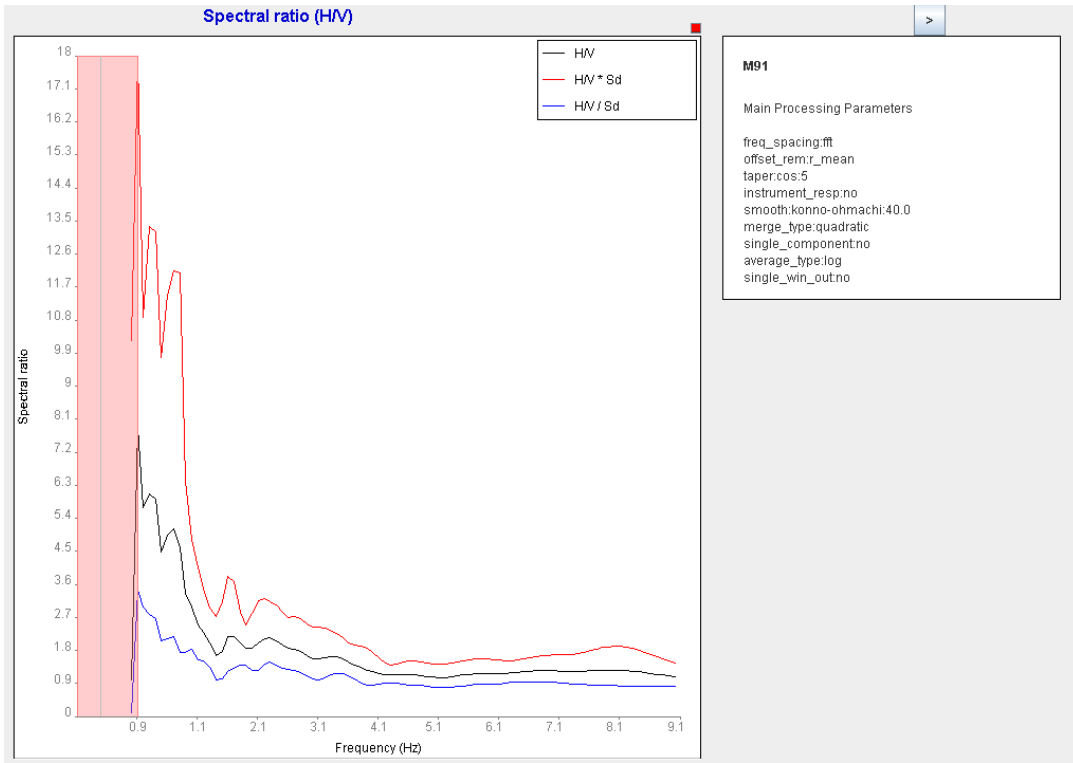
# Appendix B: H/V ratio with subsurface layers

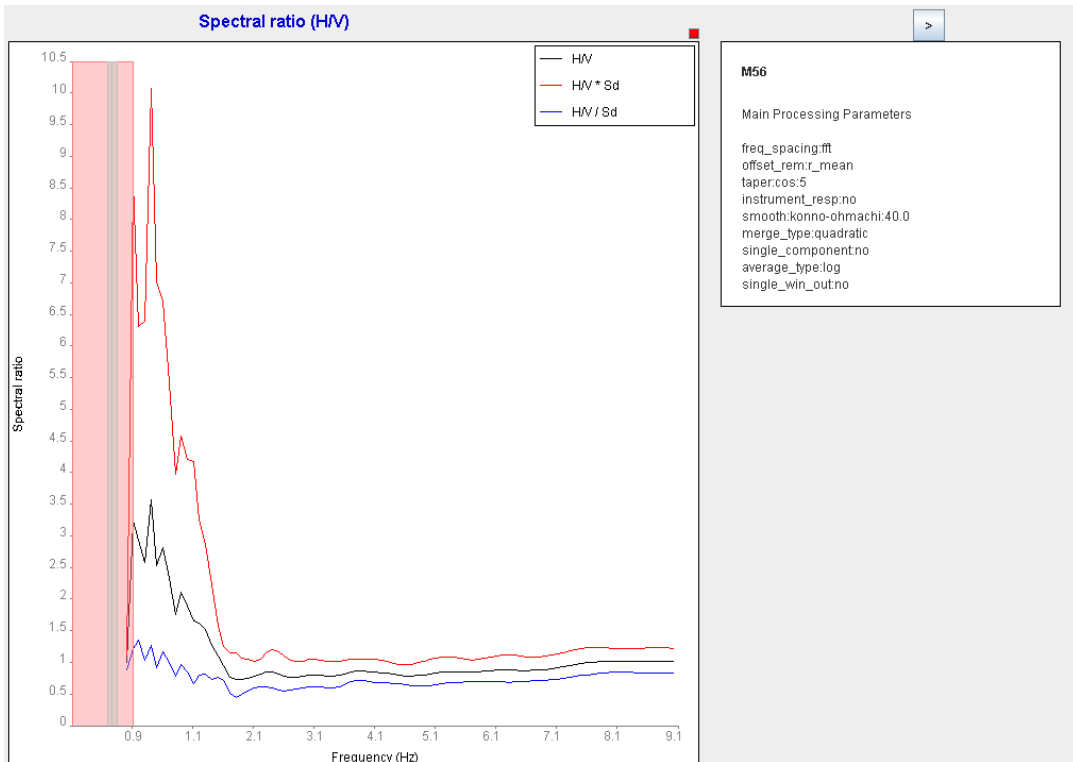
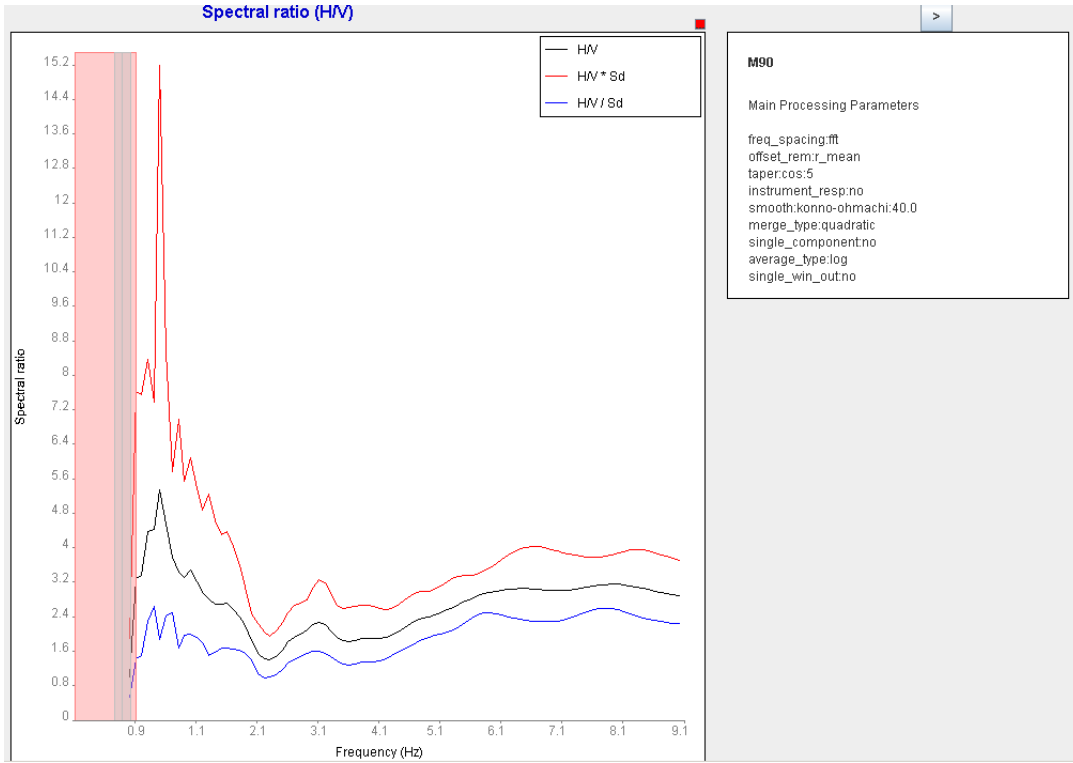
Three cross-sections (A-A1, B-B1 and C-C1) shown in figure 3.4. Each section has many sites that are obtained the local site effects respected to subsurface layers. Here the shape of the peaks of wave amplification may be reflected from underlying layers. The sites in each section started in following cross-sections from north to south.

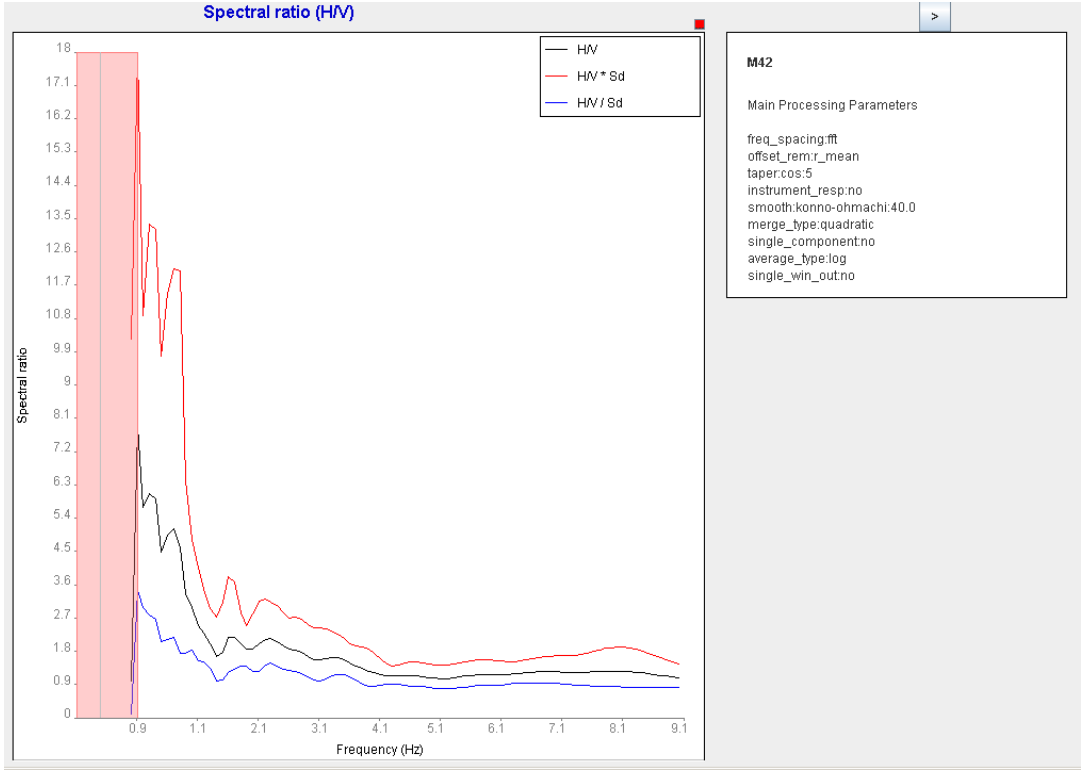
## The sites on the section A-A1;



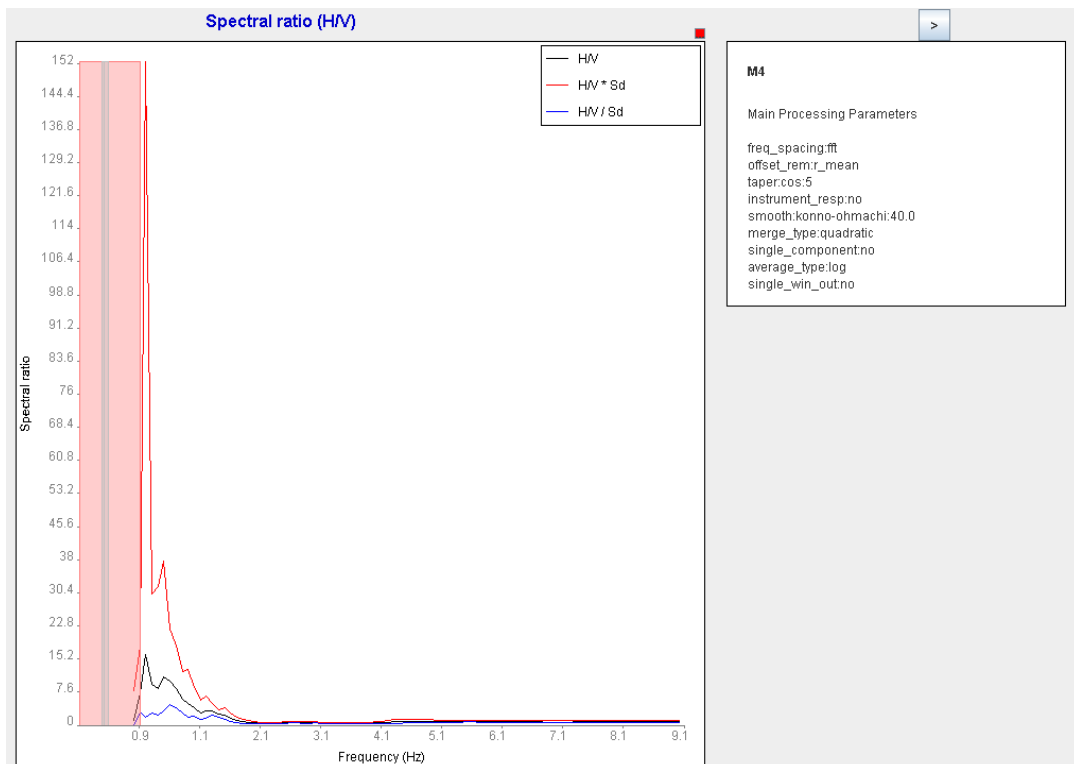
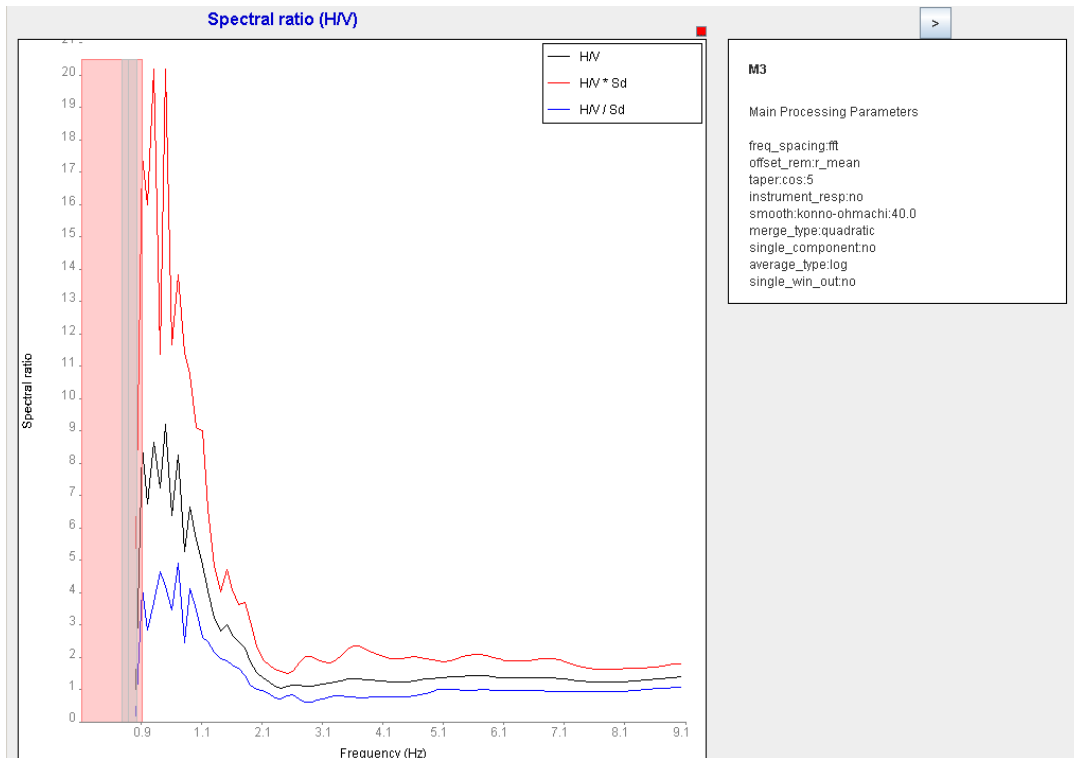


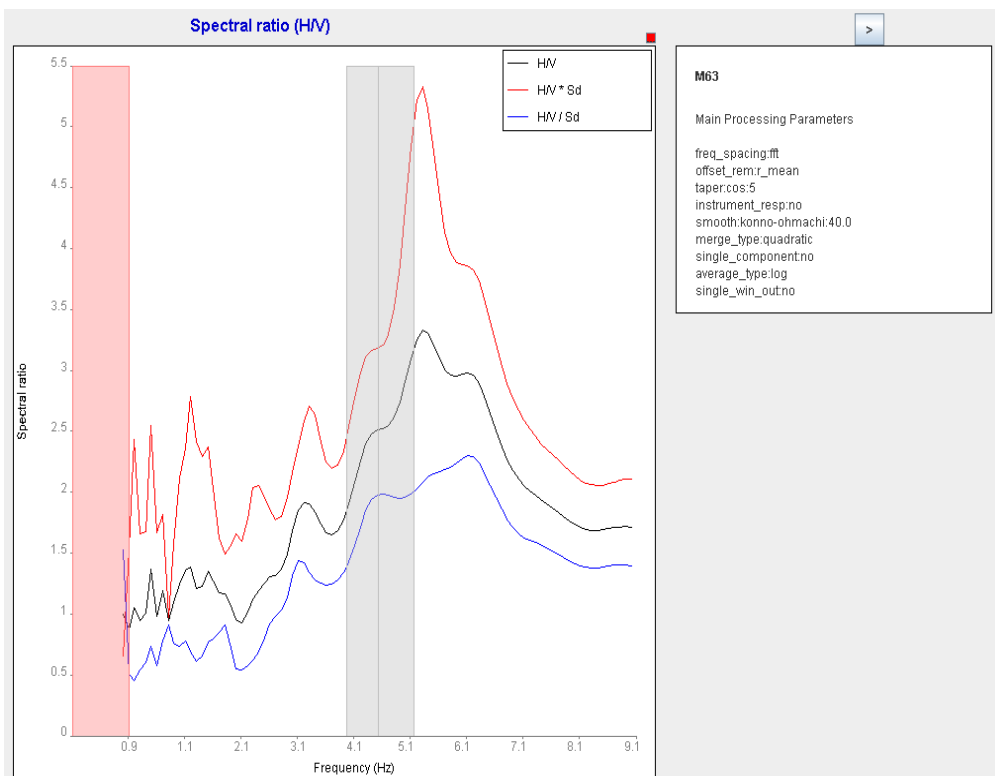
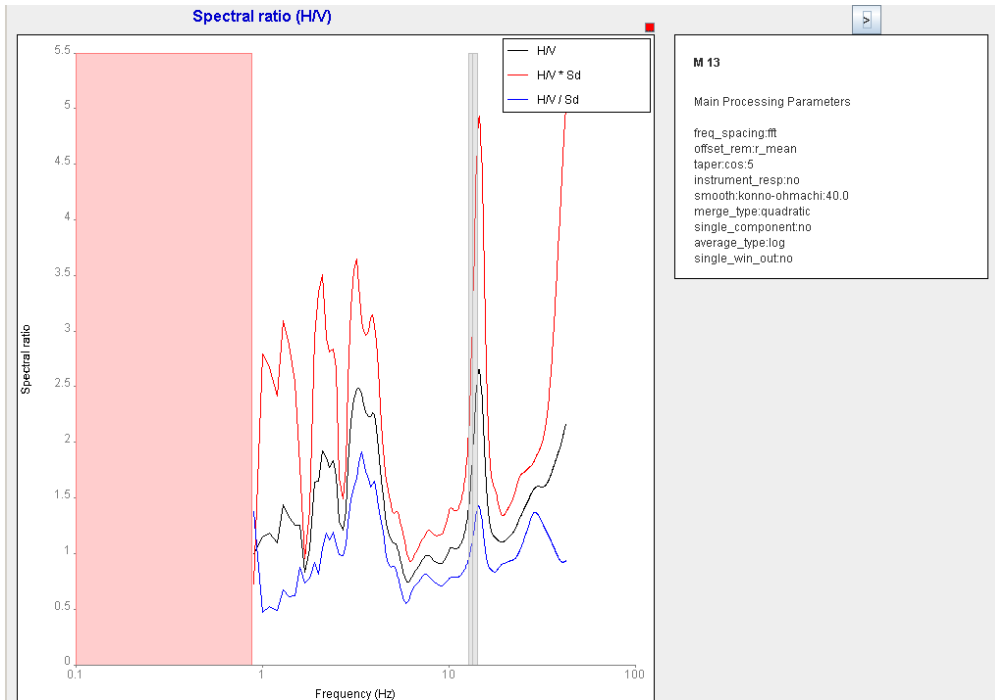


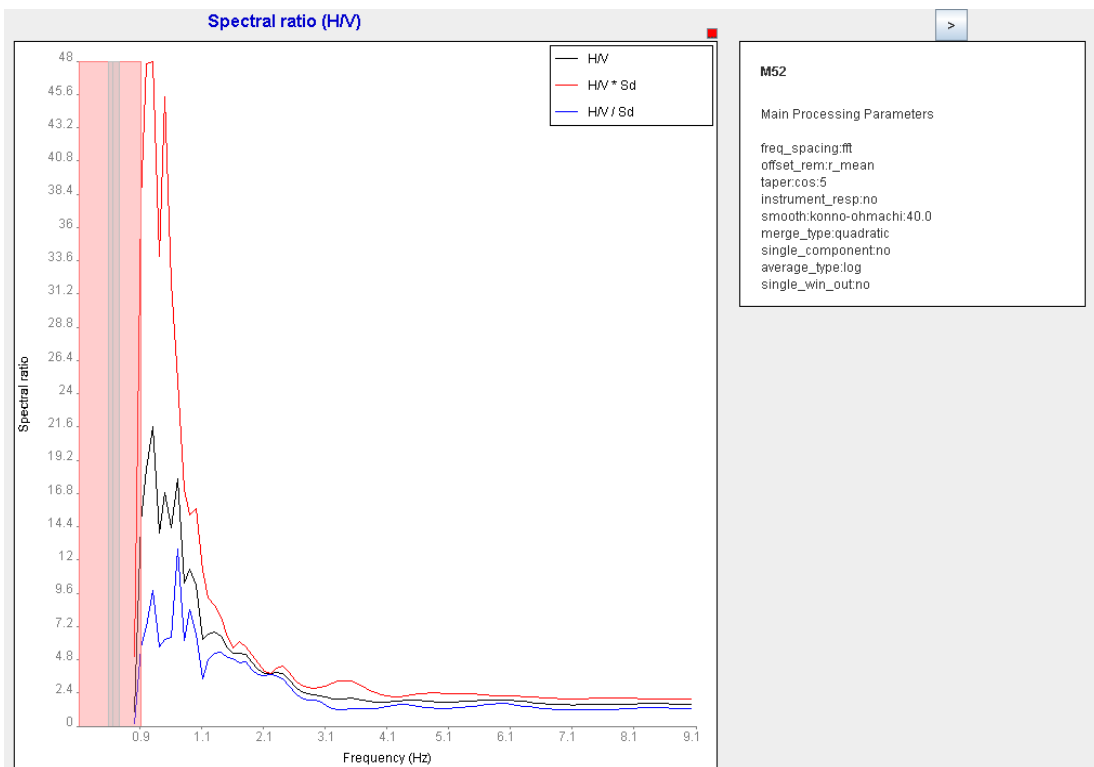
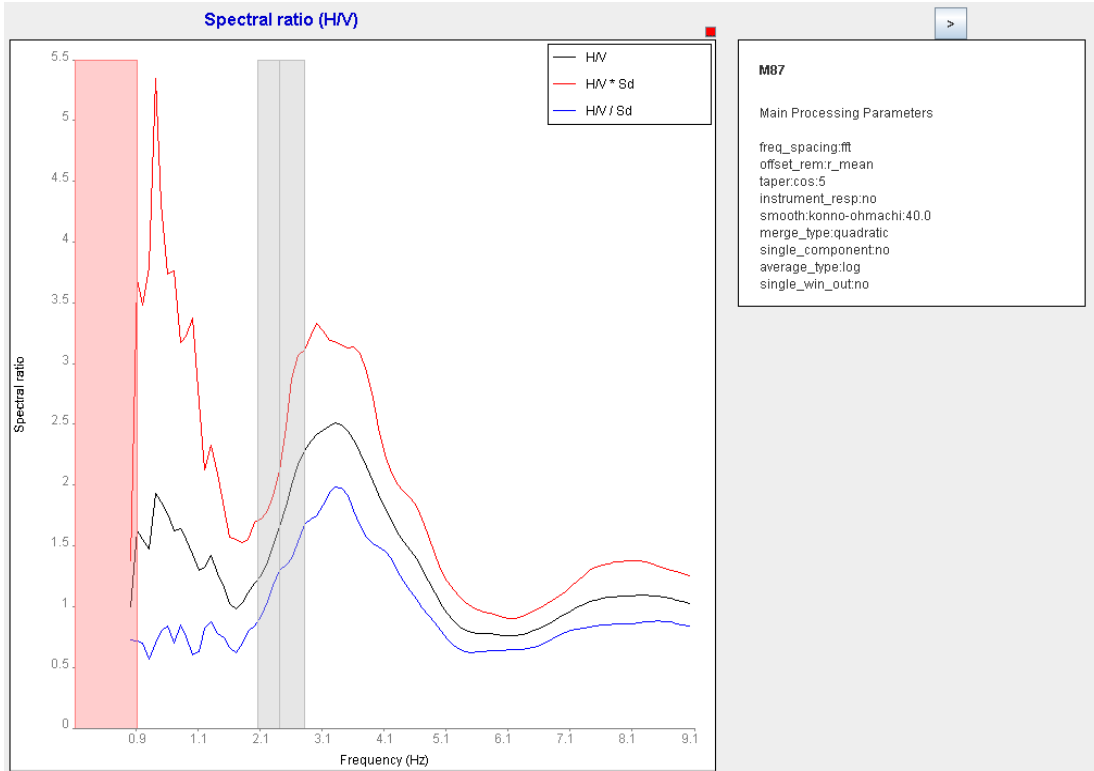




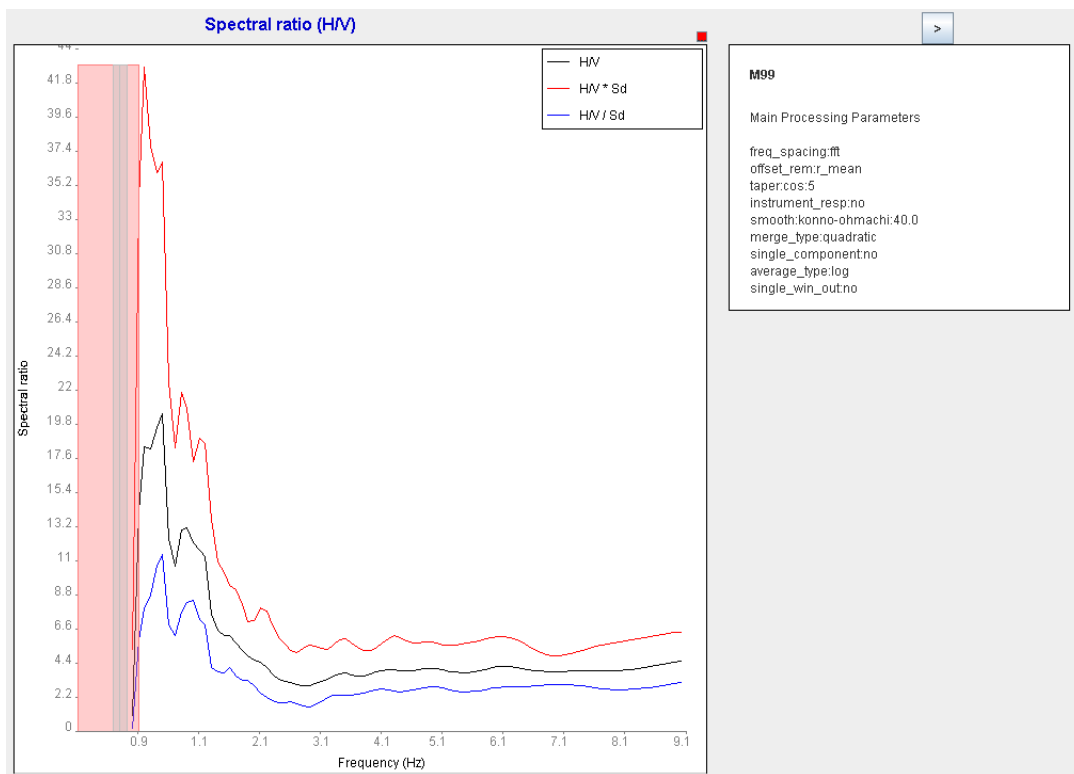
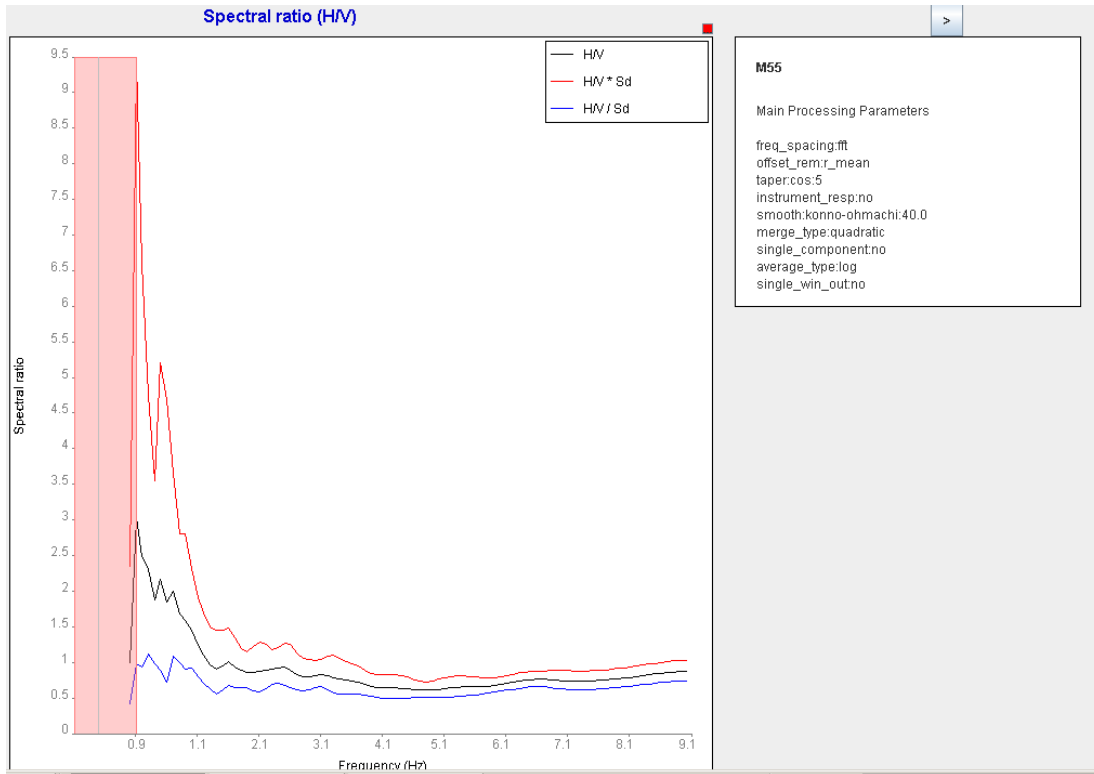
## Cross Section B-B1

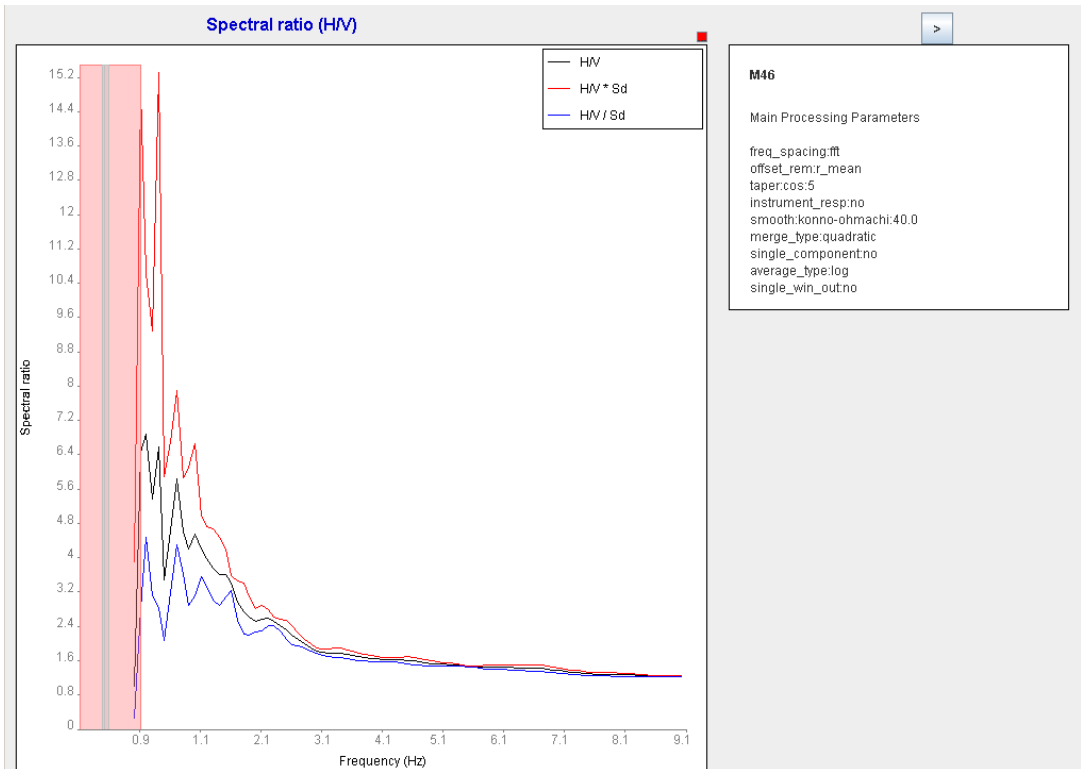
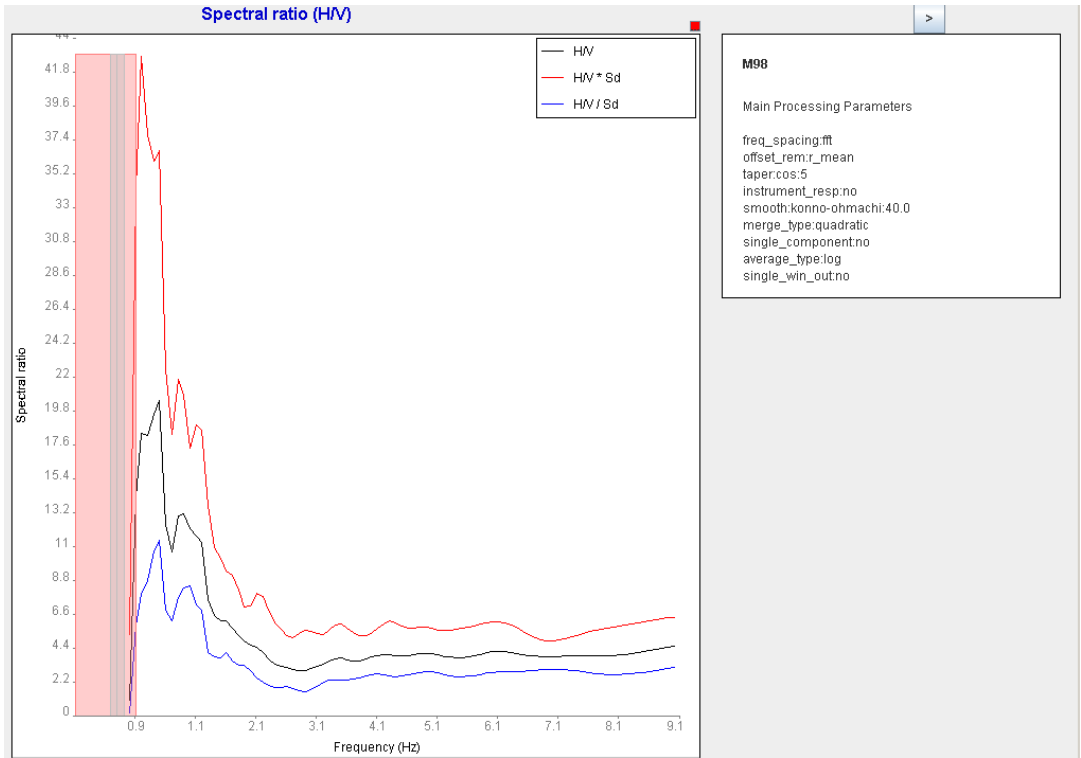


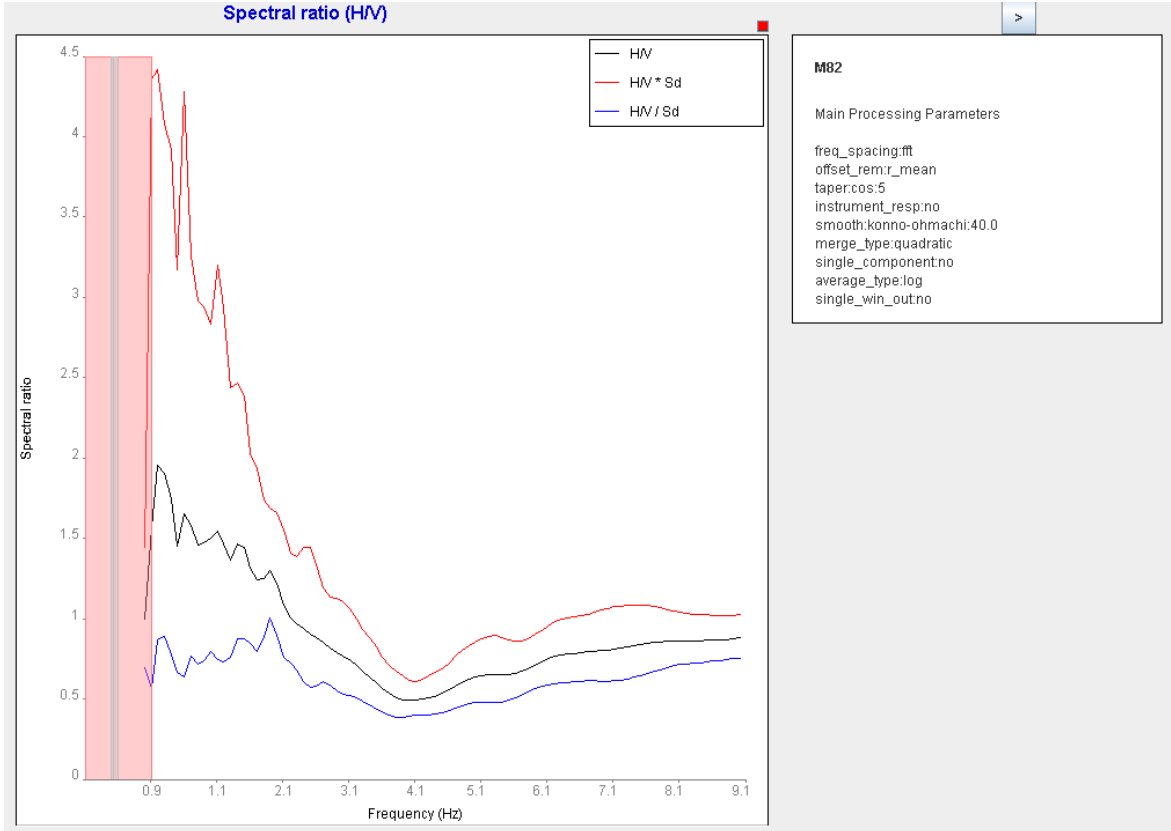




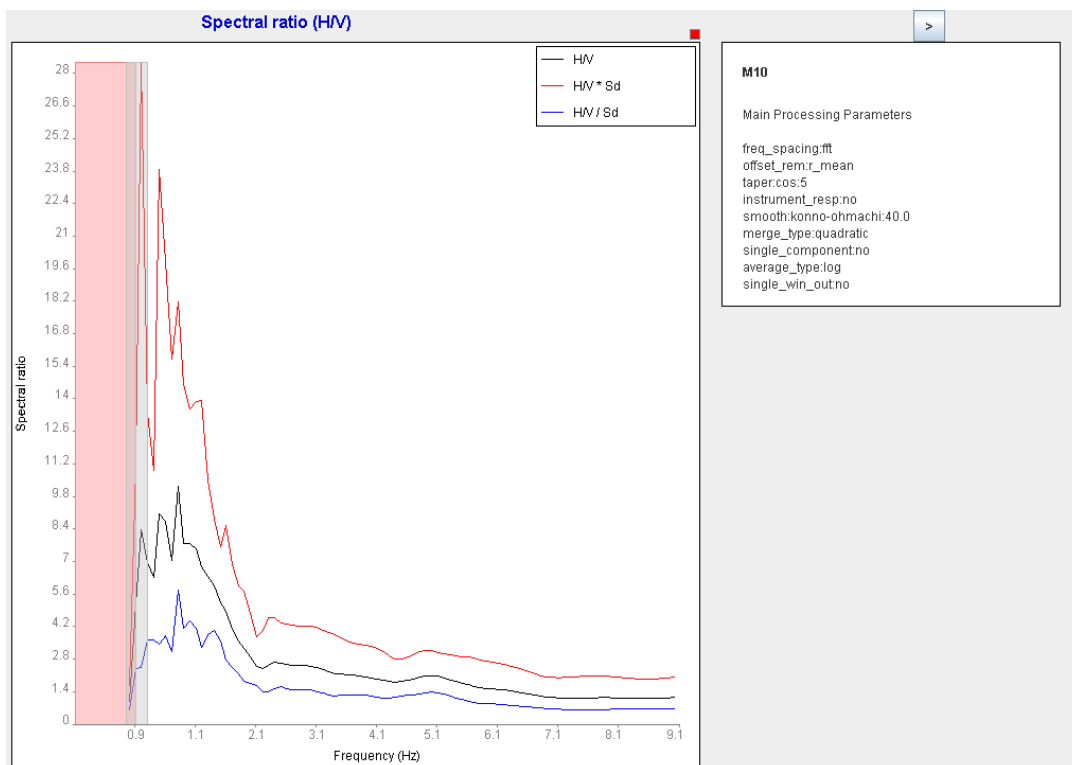
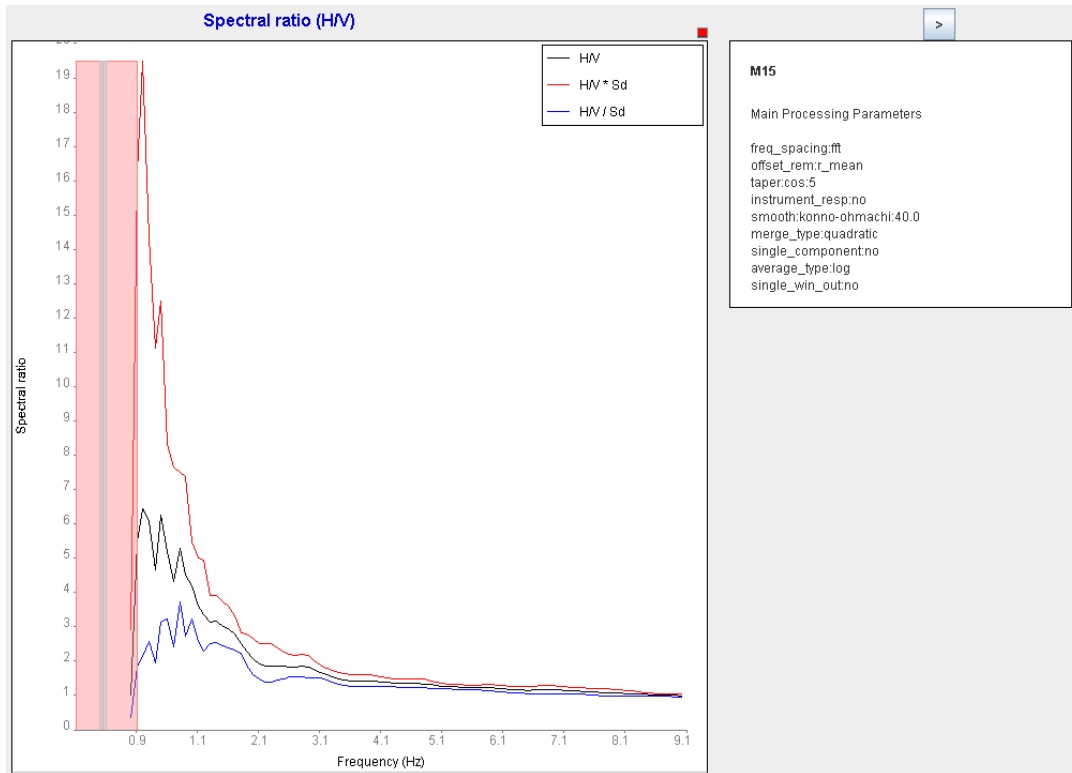


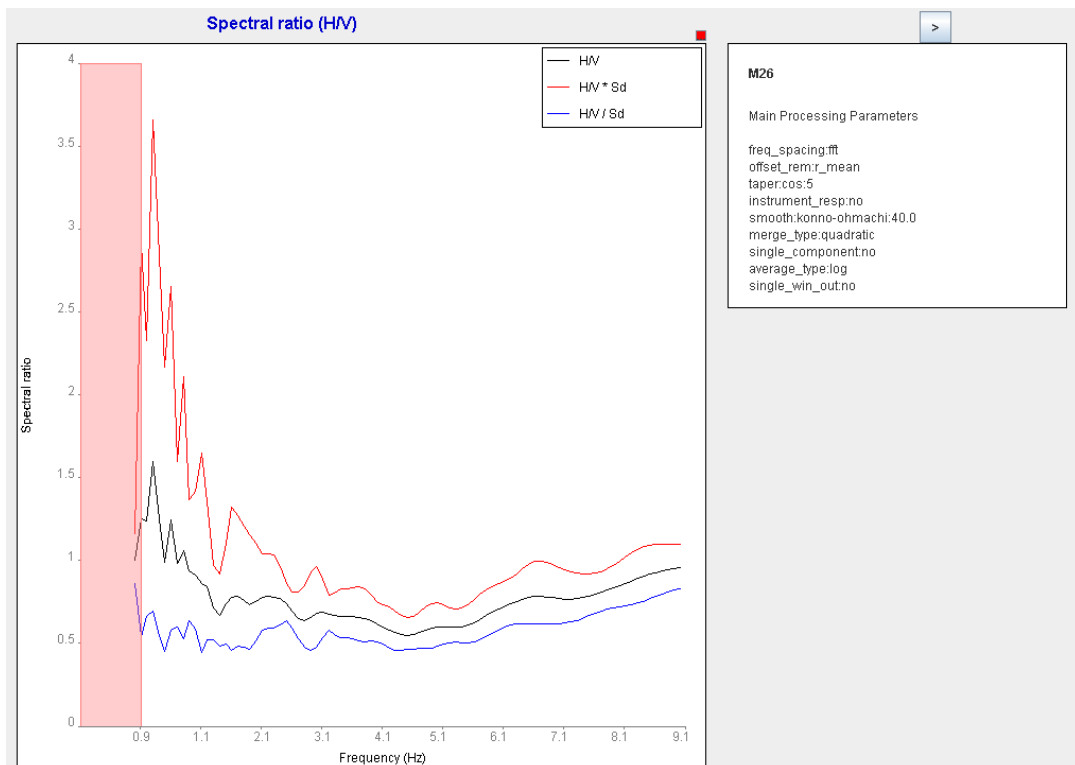
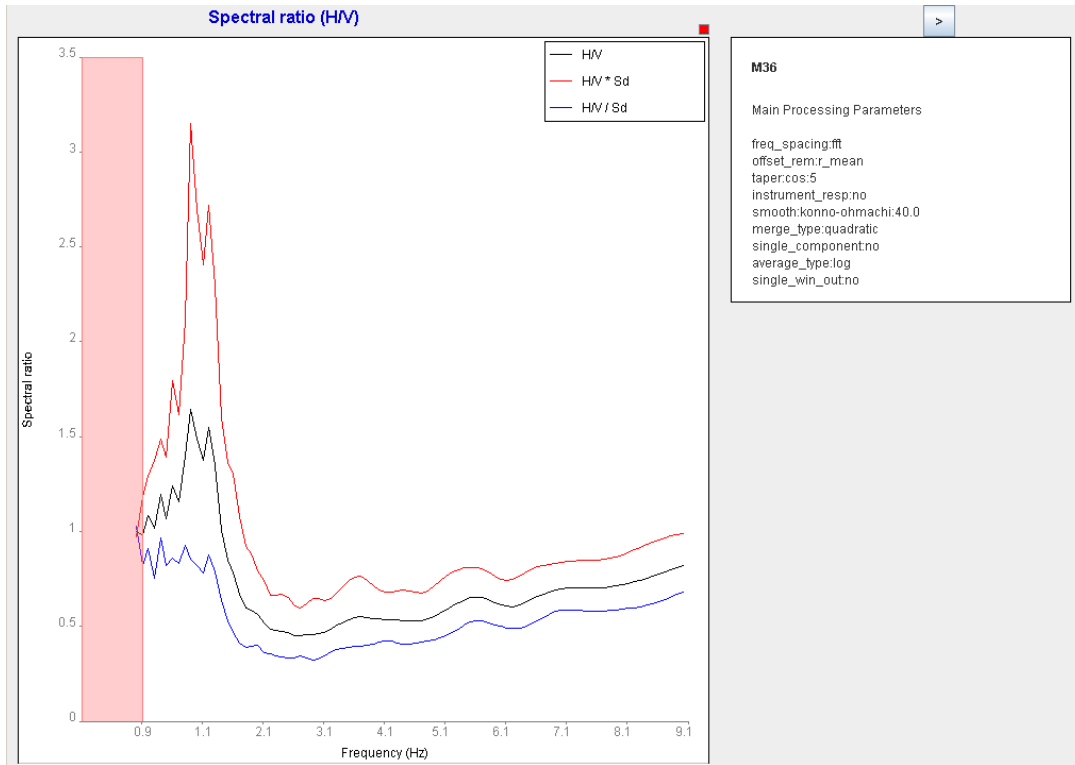


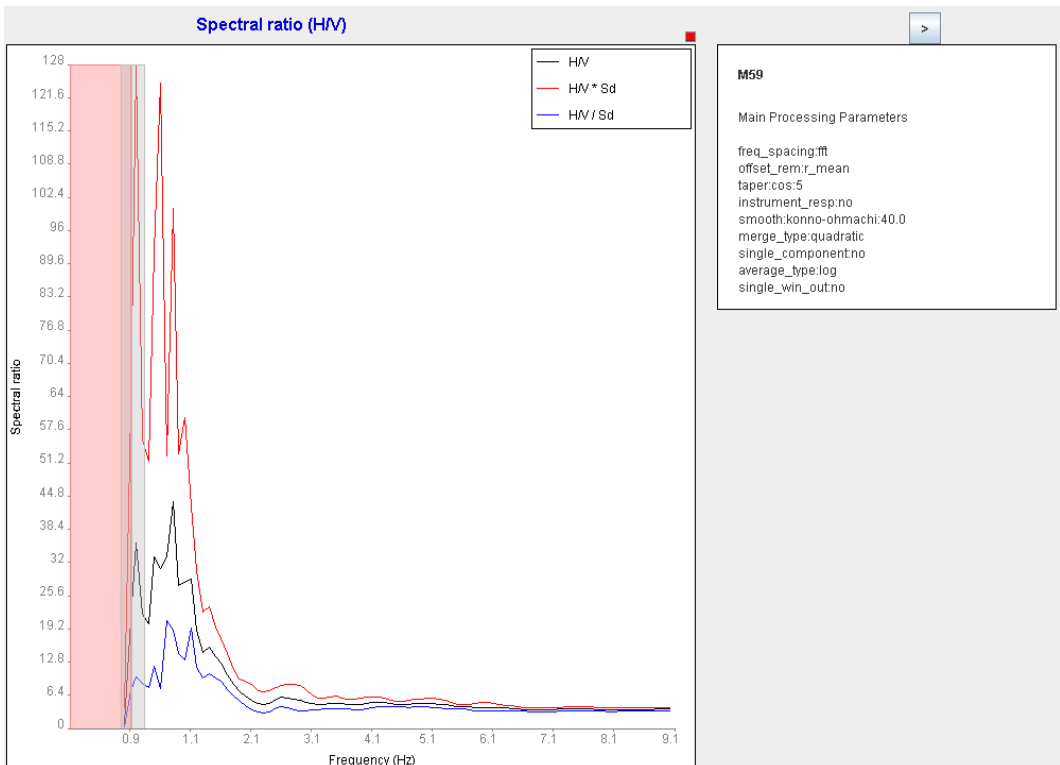
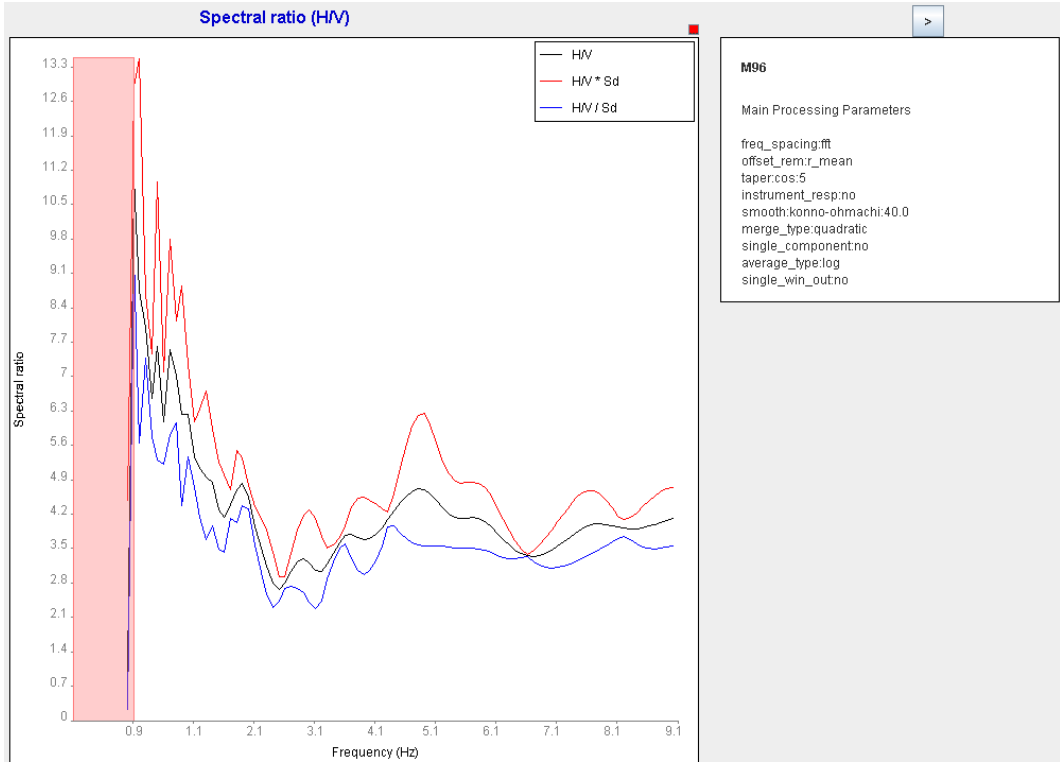


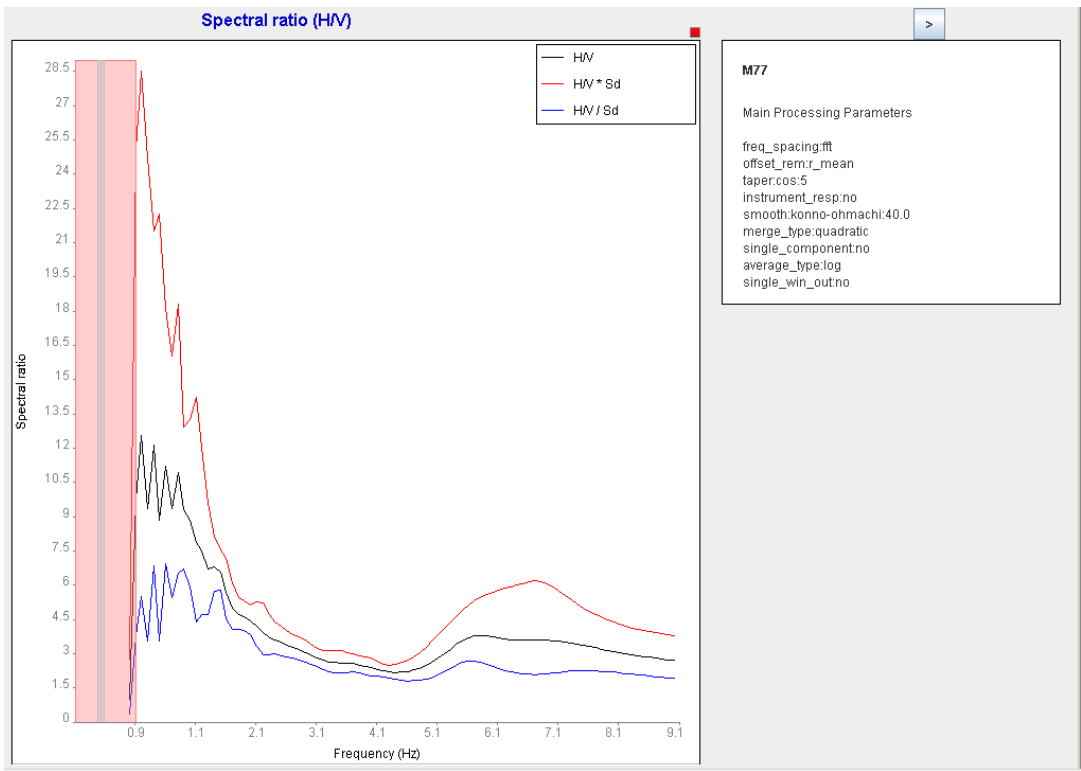
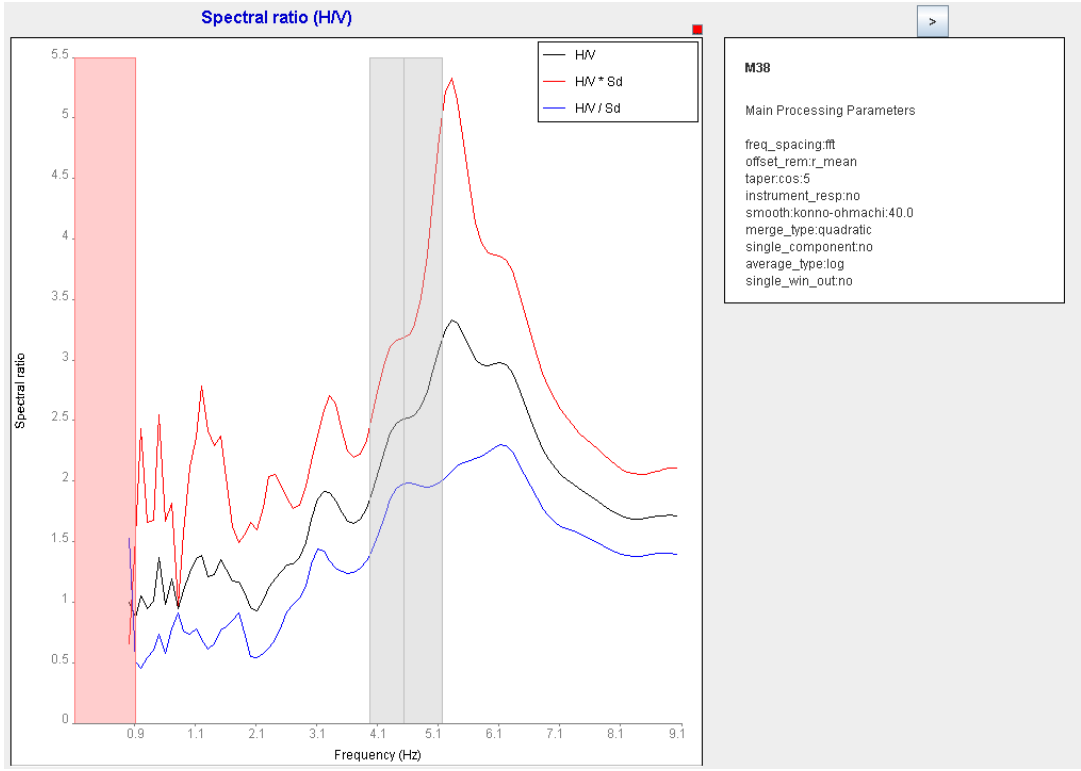


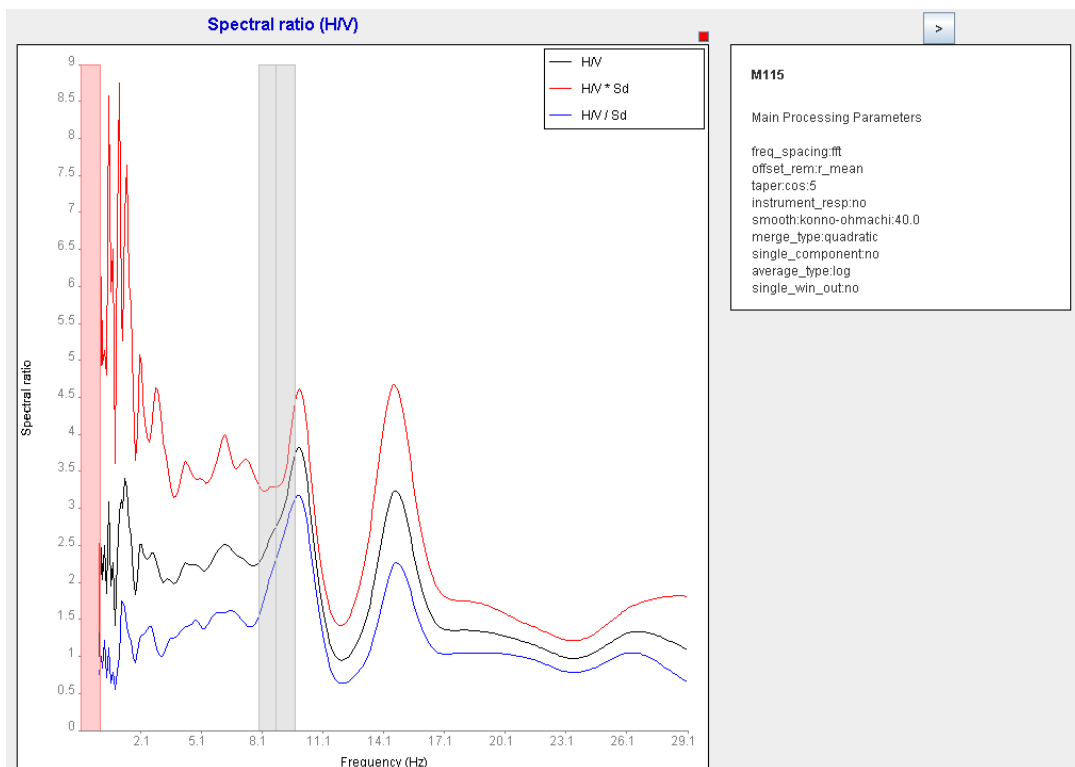
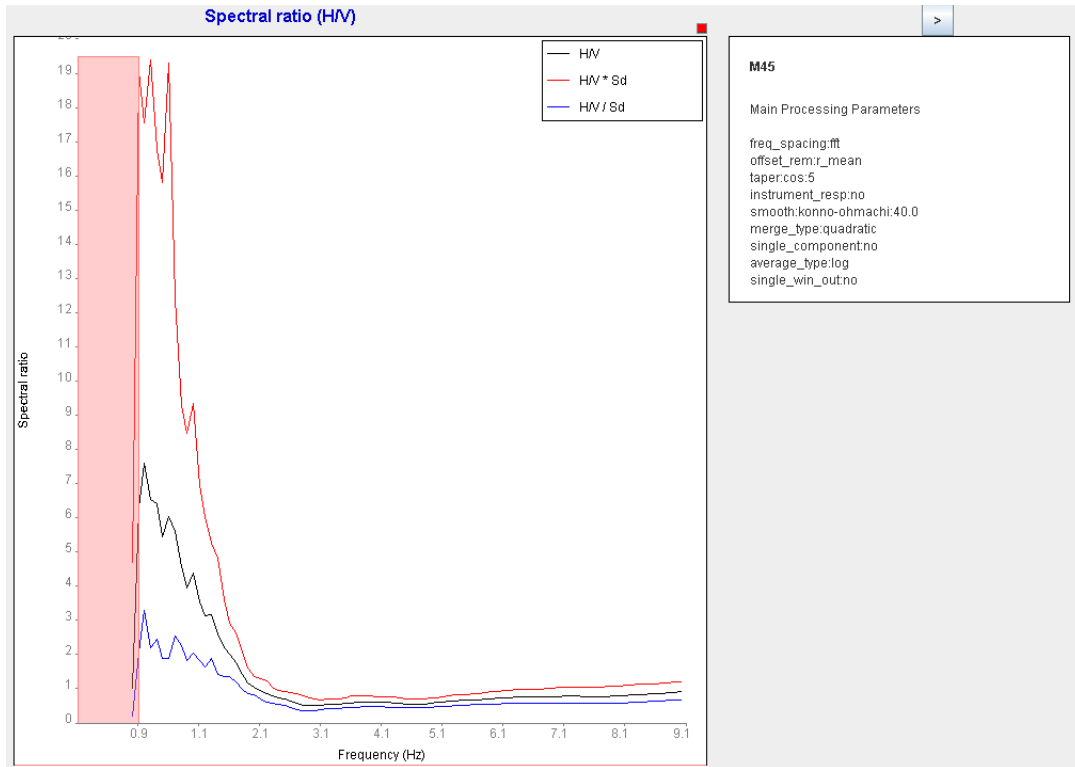
## Cross section C-C1













# Appendix C: Standard Spectral Ratio and H/V ratio using local earthquake records

Table C1: the parameter using for estimated standard spectral ratio and H/V ratio calculation using noise and S- wave part of earthquake data. These parameters are used with The SPEC program (SEISAN software).

Parameters	Noise script	Signal of S - Waves script
Selection criteria 2:S, 3: from S and P , 4:abs	4	2
Start	0.1	1
Windows length	10,1,1	10,1,1
Number of time to smooth	5	5
Gain factor of channel 1	1	1
Noise spectrum 0:no 1:yes	0	1
Make relative spectra 1:yes 0:no	1	1
Plot pics	1	1
Frequency band to use	0.5 10	0.5 10
Response removal: 0:none, 1:displ., 2;velocity ., 3: acceleration	0	0
Rotate: 0:no, 1:yes	0	0
Q0 and qalpha	0,0,0	0,0,0
Distance correction	0	1
Minimum correlation and sn for kappa	0,0	0,0
Velocity and density	0.0 0.0	0.0 0.0
Magnitude spectrum	0	0
Station and components format	MRKH SE/SZ or SN/SZ	MRKH or SLAT

More information about the SPEC program work and specifically parameters used can found in SEISAN (*Version 8.1.3, December, 2006*) manual (Havskov and Ottemöller, 2005) and website [http://www.geo.uib.no/seismo/SOFTWARE/SEISAN/seisan\\_8.1.pdf](http://www.geo.uib.no/seismo/SOFTWARE/SEISAN/seisan_8.1.pdf) .

Table C2: the Standard Spectral Ratio result of group one (two earthquakes records EQ10 and EQ6) using two relative different components.

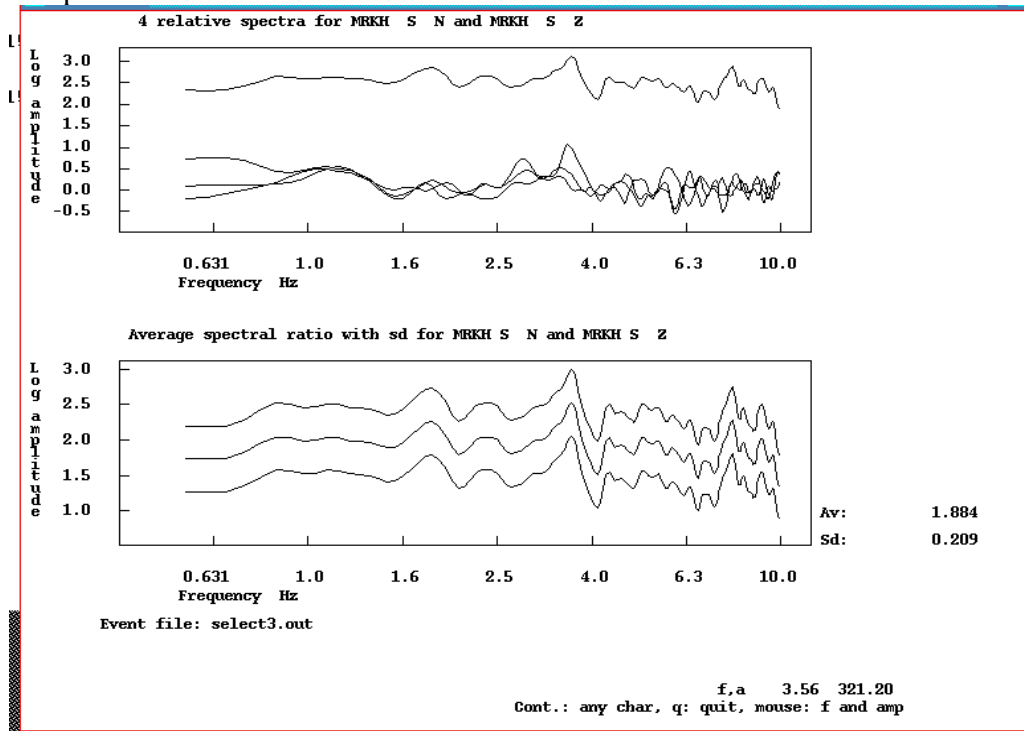
Earthquake	Relative station	Fundamental frequency on spectral ratio	Amplification on spectral ratio
S- wave			
EQU6	S MRKH n-s/S SLAT n-s	1.31	2.33
EQU10	S MRKH n-s/S SLAT n-s	0.97	5,8
EQU10+ EQU6	AVARAGE	0.98	2.88
S- wave			
EQU1	S MRKH e-w/S SLAT e-w	1.34	6.15
EQU2	S MRKH e-w/S SLAT e-w	1,29	6.19
EQU10+EQU6	AVARAGE	1.32	6.12

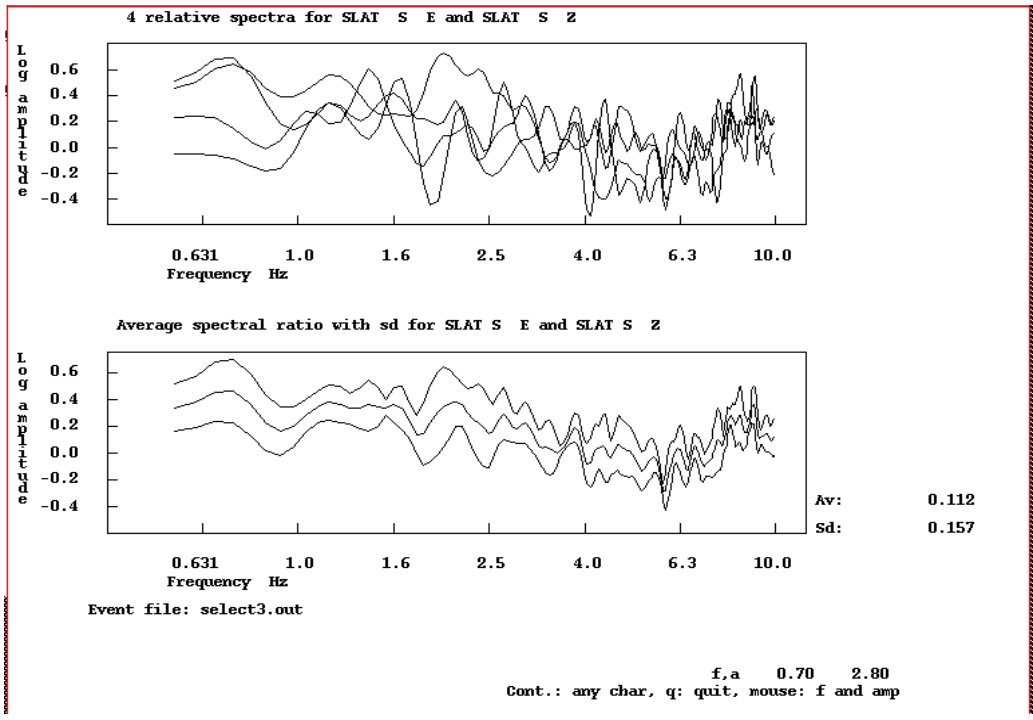
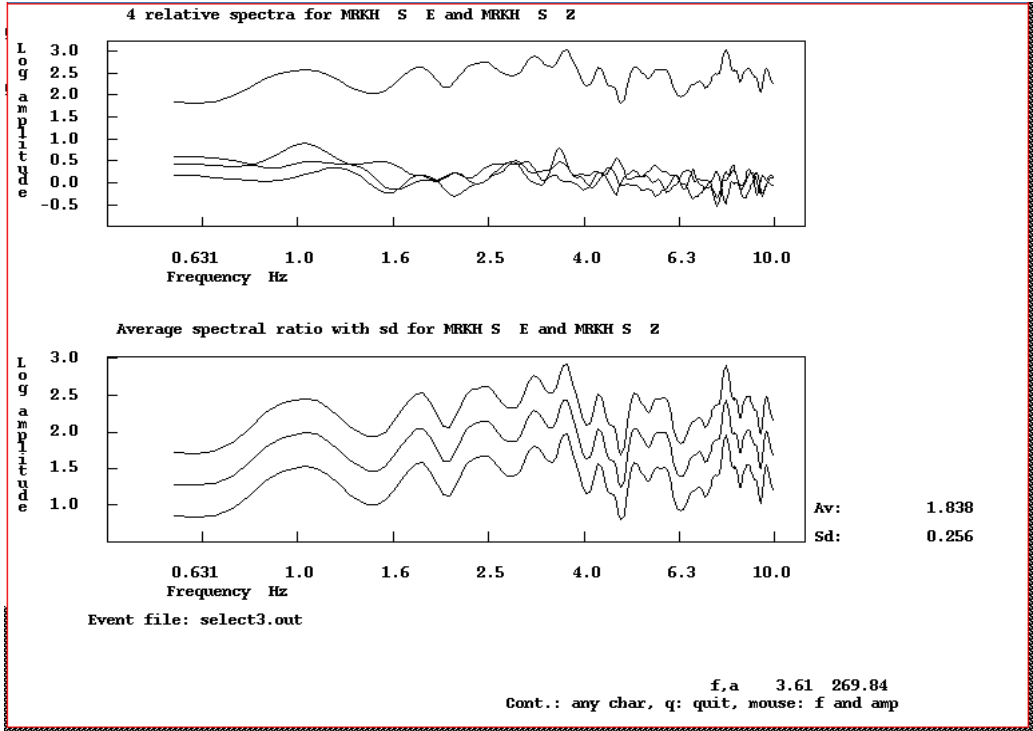
Table C3: H/V ratio result using group one earthquake in two stations (MRKH and SLAT).

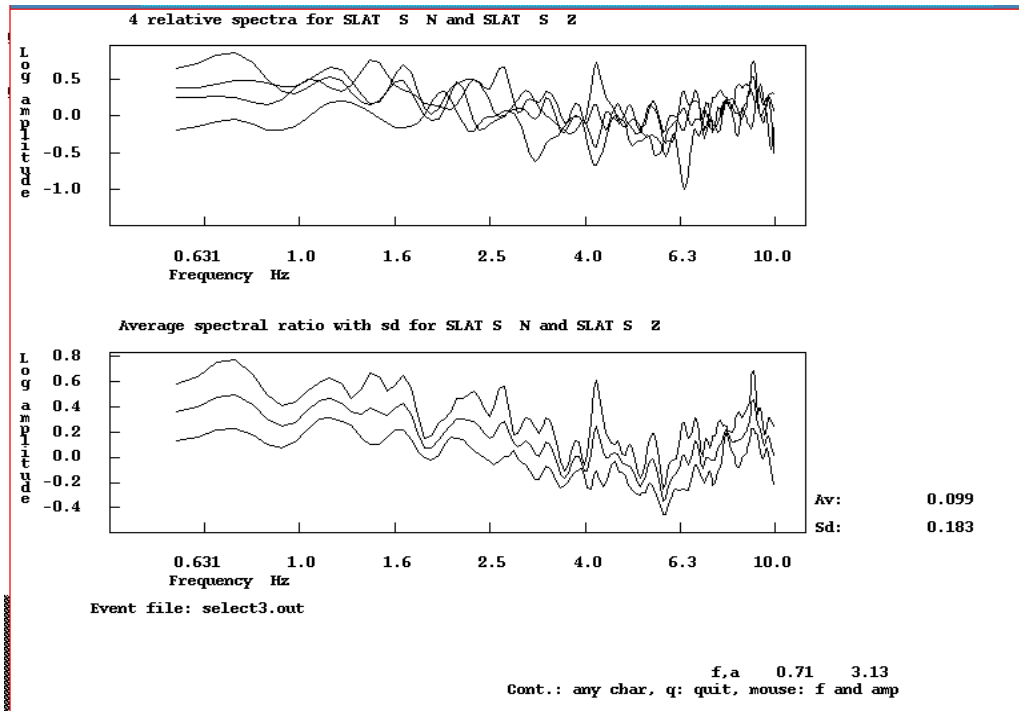
Earthquake	Relative station	H/V ratio of frequency	H/V ratio of amplification
EQU6	S MRKH n-s/S MRKH Z	2.49	3.68
EQU10	S MRKH n-s/S MRKH Z	2.82	4.86
EQU10+EQU6(MRKH)	AVARAGE H/V n-s	2.57	3.69
s wave			
EQU6	S MRKH e-w/S MRKH Z	3.23	3.79
EQU10	S MRKH e-w/S MRKH Z	2.52	5.47
EQU10+EQU6(MRKH s wave)	AVARAGE H/V e-w	2.52	3.54
Noise			
EQU6	S MRKH n-s/S MRKH Z	1.38	2.60
EQU10	S MRKH n-s/S MRKH Z	1.13	4.05
EQU10+EQU6(MRKH) (noise)	AVARAGE H/V n-s	1.10	2.66
Noise			
EQU6	S MRKH e-w/S MRKH Z	1.69	1.62
EQU10	S MRKH e-w/S MRKH Z	0.98	2.67
EQU10+EQU6(MRKH) (noise)	AVARAGE H/V e-w	0.96	1.87
S- wave			
EQU6	S SLAT n-s/S SLAT Z	1.01	7.09
EQU10	S SLAT n-s/S SLAT Z	0.72	4.72
EQU10+EQU6(SLAT) (s wave)	AVARAGE H/V n-s	1.02	4.15
(s -wave)			
EQU6	S SLAT e-w/S SLAT Z	0.99	3.74
EQU10	S SLAT e-w/S SLAT Z	0.98	2.16
EQU10+EQU6(SLAT) (s wave)	AVARAGE H/V e-w	0.98	3.06
noise			
EQU10	S SLAT n-s/S SLAT Z	1.41	1.83
EQU6	S SLAT n-s/S SLAT Z	0.96	2.41

<i>EQU10+EQU6(SLAT)</i> (noise)	<i>AVERAGE H/V n-s</i>	1.12	1.90
noise			
EQU10	S SLAT e-w/S SLAT Z	1.15	3.88
EQU6	S SLAT e-w/S SLAT Z	1.75	2.94
<i>EQU10+EQU6(SLAT)</i> (noise)	<i>AVERAGE H/V e-w</i>	1.16	2.56

Four figures below show the H/V ratio spectral of S-wave part of four earthquakes (*EQ2+EQ3+EQ4+EQ8*) records in two stations (MRKH and SLAT) with two different components.







Four figures below show the H/V ratio spectral of noise wave of four earthquakes computed in two stations (MRKH and SLAT) with different components.

